AFCRL-68-0438
3EPTEMBER 1968
ENVIRONMENTAL RESEARCH PAPERS, NO. 291

AIR FORCE CAMBRIDGE RESEARCH LABORATORIES
L. G. HANSCOM FIELD, BEDFORD, MASSACHUSETTS

Gemini 7 Lunar Measurements

T. P. CONDRON
J. J. LOVETT
W. H. BARNES
L. MARCOTTE
R. NADILE

OFFICE OF AEROSPACE RESEARCH
United States Air Force

93

AFCRL-68-0438
SEPTEMBER 1968
ENVIRONMENTAL RESEARCH PAPERS, NO. 291

OPTICAL PHYSICS LABORATORY PROJECT 8662

AIR FORCE CAMBRIDGE RESEARCH LABORATORIES

L. G. HANSCOM FIELD, BEDFORD, MASSACHUSETTS

Gemini 7 Lunar Measurements

T. P. CONDRON
J. J. LOVETT
W. H. BARNES
L. MARCOTTE
R. NADILE

Supported by SSD 631A and ARPA Order 363

OFFICE OF AEROSPACE RESEARCH

United States Air Force

Abstract

Radiometric and interferometric measurements were made of the lunar surface during a penumbral eclipse from the Gemini 7 spacecraft. Data were obtained in the region from 0.25 to 2.6 microns. The bond albedo of the moon is computed for the spectral regions measured.

Contents

Illustrations

Illustrations

Tables

BLANK PAGE

Gemini 7 Lunar Measurements

1. INTRODUCTION

During the flight of Gemini-7, AFCRL optical instruments mounted on the capsule were aimed at the moon on 5 and 8 December 1965 by Astronauts Frank Borman and James Lovell. The observation on 5 December was designated the "boresight" experiment, since it was designed to check the alignment of the optical instruments with the astronaut's sighting scope. The observation on 8 December was designated the "full moon" experiment.

The primary objective of the lunar observations was to satisfy a NASA-APOLLO requirement for lunar ultraviolet irradiance measurements in five broad spectral bands (200 Å) lying between 2200 and 3000 Å, but lunar data were also obtained in additional filtered regions that had been selected for other experiments. A secondary but very important objective of both lunar observations was to obtain in-flight measurements of a target that is relatively well known in order to check the validity of the data obtained for other targets during the Gemini-7 flight.

Two interferometers and one radiometer manufactured by Block Associates were flown on Gemini-7. The Model 1-14 interferometer, which operates at ambient temperature, was equipped with a PbS detector and a thermistor bolometer; no lunar data were obtained with the bolometer section of this instrument. The Model 1-15 interferometer was equipped with a mercury doped germanium detector

(Received for publication 1 July 1968)

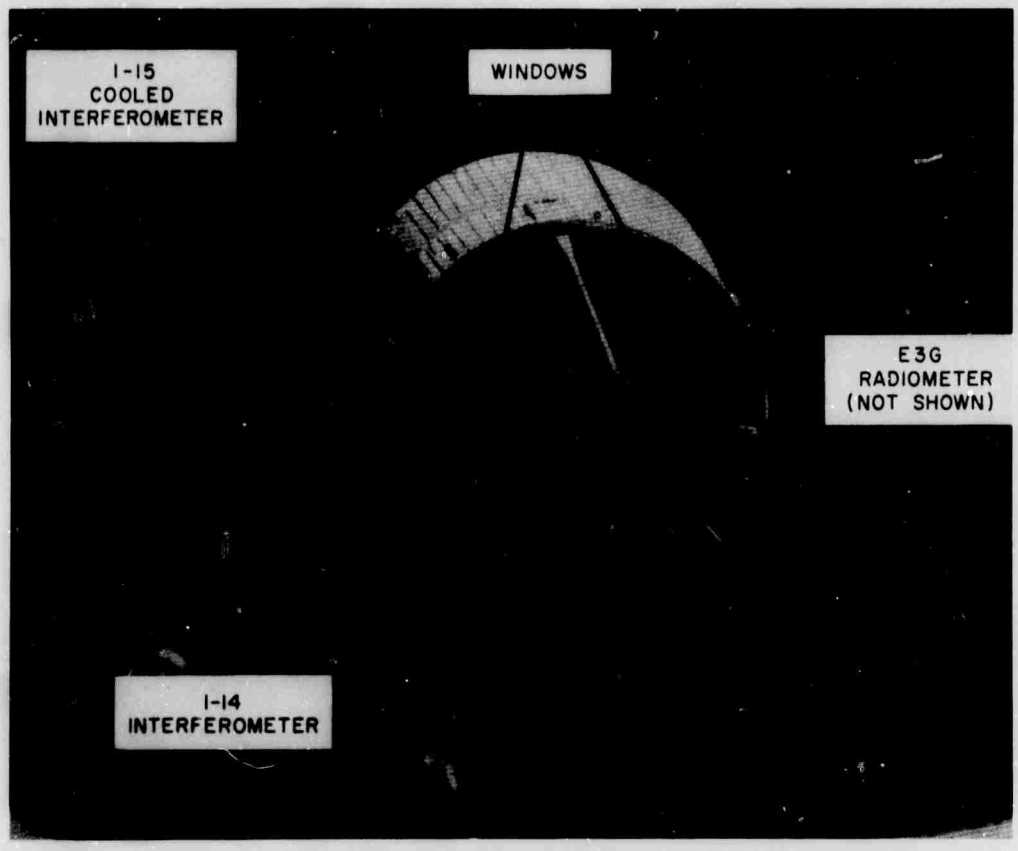

Figure 1. Locations of Instruments

cooled to liquid neon temperature; since the coolant life was 15 hours, no lunar data were obtained with this instrument. The Model E3G radiometer flown on Gemini-7 was equipped with a PbS detector and an EMR solar blind photomultiplier; it had a 20-position filter wheel that allowed for obtaining measurements in 10 filtered spectral bands with each detector.

The locations of the three instruments on the spacecraft are shown in Figure 1, a photograph of the Gemini-7 spacecraft taken from the Gemini-6 craft in flight; all of the instruments were mounted on the aft section which was jettisoned before re-entry. Detailed descriptions of the instruments used for the lunar measurements are given in Appendixes B and C.

2. DATA OBTAINED

The spectral irradiances measured with the radiometer on 5 and 8 December 1965 are given in columns 4 and 6 of Table 1 where L_o is the wavelength above and below which 50 percent of the radiometer output would be contributed by a target having the relative spectral distribution of a 4000°K blackbody and ΔL is the wavelength interval within which 70 percent of the output would be contributed by this blackbody. (See Appendixes A and B.) The angles in parentheses in Table 1 are lunar phase angles and the dashes in columns 4 and 6 indicate that the radiation was above the saturation limit for those channels.

Table 1. Lunar Irradiance Values

Chan No.	L_o microns	ΔL microns	$H_{L_o}(1°5')$ $w\,cm^{-2}\,\mu^{-1}$	Signal to Noise Ratio	$H_{L_o}(38°32')$ $w\,cm^{-2}\,\mu^{-1}$	Signal to Noise Ratio
G-7-1	0.2259	0.0194	1.56-09	1.9+03	6.02-10	7.2+02
-2	0.2418	0.0205	2.30-09	2.9+03	9.25-10	1.2+03
-3	0.2940	0.0191	-------	-------	1.41-08	2.5+03
-4	0.2651	0.0161	1.31-08	3.5+02	7.45-09	2.0+03
-5	0.2797	0.0169	-------	-------	-------	-------
-6	0.2567	0.0274	-------	-------	4.10-10	4.4+02
-7	0.2811	0.0072	2.07-08	1.4+03	1.20-08	8.0+02
-8	0.3047	0.0096	3.86-08	6.8+02	2.01-08	3.6+02
-9	0.2872	0.0093	2.69-08	1.7+03	1.34-08	8.5+02
-10	0.2258	0.0192	1.63-09	1.9+03	5.75-10	6.7+02
G-7-11	1.056	0.109	2.48-07	1.8+02	1.06-07	7.6+01
-12	1.263	0.112	2.33-07	3.1+02	9.29-08	1.2+02
-13	1.559	0.084	1.52-07	2.4+02	6.77-08	1.0+02
-14	1.370	0.099	1.95-07	2.1+02	9.13-08	9.6+01
-15	2.795	0.214	2.37-08	4.0+01	1.63-08	2.8+01
-16	1.895	0.107	8.06-08	1.5+02	4.77-08	8.7+01
-17	2.181	0.092	5.45-08	8.5+01	3.46-08	5.3+01
-18	2.710	0.085	2.72-08	3.2+01	1.83-08	2.2+01
-19	2.774	0.092	2.91-08	2.2+01	1.97-08	1.5+01
-20	2.815	0.099	2.87-08	2.1+01	1.96-08	8.5+00

The irradiances tabulated in Table 1 are plotted vs. wavelength in Figures 2 and 3. Included on Figure 3 are the irradiances obtained with the PbS section of the I-14 interferometer. The scatter in the interferometer data at the shorter wavelengths was caused by low signal-to-noise ratios which in turn were caused by a dichroic filter used in the instrument. (See Appendixes A and C.)

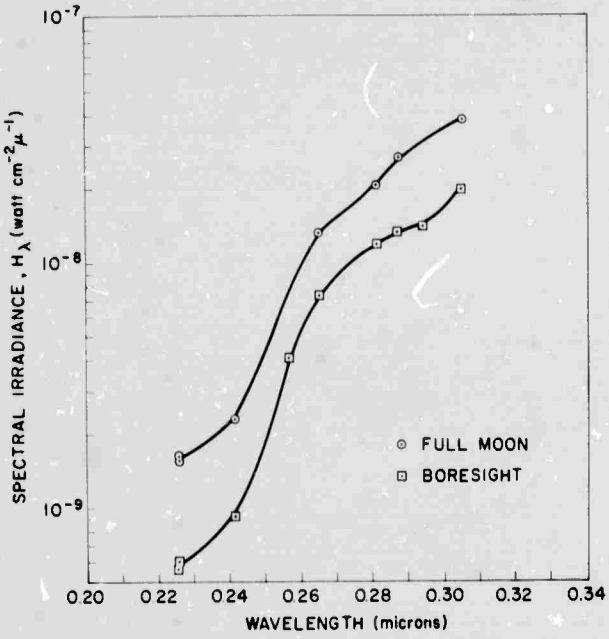

Figure 2. Lunar Spectral Irradiance vs. Wavelength — 2200 to 3050 Å

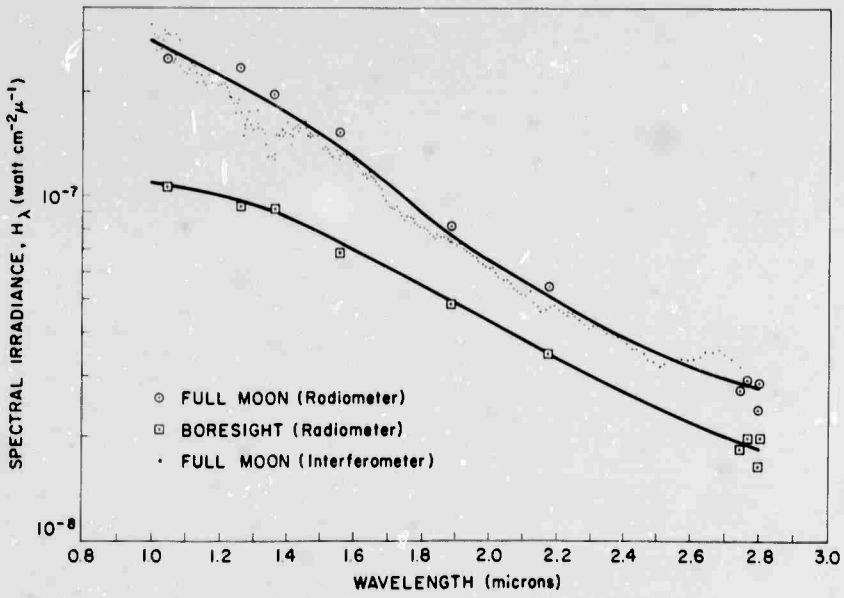

Figure 3. Lunar Spectral Irradiance vs. Wavelength — 1.0 to 2.8 μ

None of the fine spectral structure indicated by the interferometric data in Figure 3 is considered significant; the dips near 1.3 μ were caused by the dichroic filter, and the rise at 2.7 μ is a calibration error caused by water vapor in the optical path during calibration. The radiometer was flushed with nitrogen during calibration and the responsivities were not affected by atmospheric constituents.

No interferometer data for the boresight experiment are given in Figure 3 because the on-board tape recorder was not used during these measurements; the boresight interferometer data were telemetered to the Madagascar telemetry receiving station. A noisy dub of these data was scrutinized but, although the interferograms are well above the continuous telemetry noise, there are many large short-duration transients which make it impossible to reduce the data with the computerized wave analysis system being used for the on-board tape recordings.

3. SOLAR-LUNAR-EARTH GEOMETRY

The 5 December data given in Figures 2 and 3 (Boresight Case) were obtained from approximately 18:28 to 18:32 GMT when the lunar phase angle was $38^{\circ}32'$. The 8 December measurements were made in the interval from 16:45 to 16:50 GMT when the lunar phase angle was approximately $1^{\circ}5'$. Geocentric opposition in right ascension occurred approximately 45 min later at 17:33:37.52 E.T.; at that time, the moon was in a partial penumbral eclipse with a penumbral magnitude of 0.908.

An approximate geometrical representation of the solar-lunar-earth geometry at the time of the 8 December measurements is given in Figure 4 in which distances were greatly reduced for purposes of illustration. At 16:47 GMT approximately eight-tenths of the lunar disk was in the penumbra; if it were not for the double refraction of the earth's atmosphere, an observer on the side of the moon facing the earth would have seen the solar disk in partial eclipse everywhere except in the vicinity of the moon's northern limb. However, since the sun's limb is raised by refraction in the earth's atmosphere 27' beyond that of the earth (Kuiper and Middlehurst, 1961), the entire solar disk would be visible to an observer anywhere on the moon's hemisphere facing the earth. The solar radiation incident on most of the moon's surface, however, would be attenuated by an amount that is dependent upon the altitude at which the sun's rays traversed the earth's atmosphere.

The altitudes involved in the Gemini-7 measurements can be more conveniently discussed in terms of the projected earth's shadow depicted in Figure 5. The large circle on Figure 5 is the projection of the earth's limb onto a plane in the vicinity

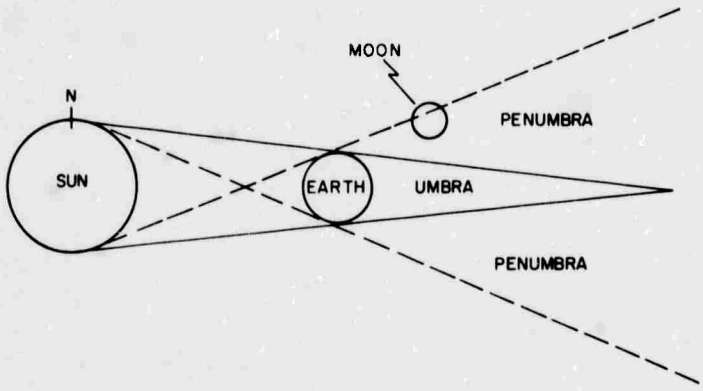

Figure 4. Eclipse Geometry

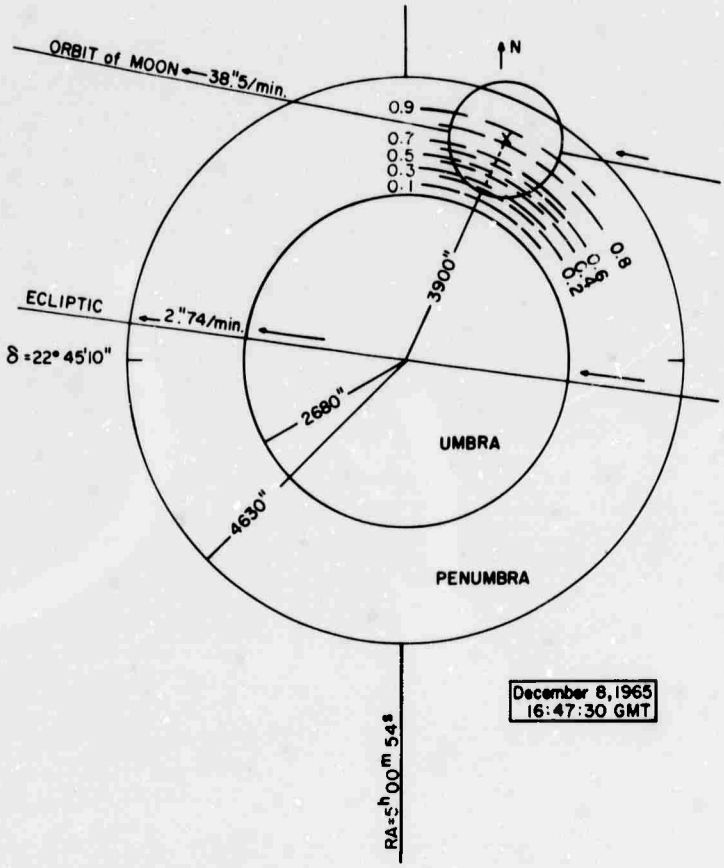

Figure 5. Location of Lunar Disk with Respect to Earth's Shadow

of the moon. The moon is represented by the small circle in the northern portion of the penumbra. At the time of the measurements, the point on the moon's limb closest to the umbra was approximately 5' away from it. Thus, the rays which emanate from the sun's southern limb would pass 27' from the earth's limb and traverse the earth's atmosphere at an altitude of 9 km before irradiating that point on the moon (Table 1, page 250, Vol. 3, ibid).

Radiation incident at that point from all other portions of the sun's disk would traverse the earth's atmosphere at altitudes greater than 9 km; radiation from the center of the sun's disk, for example, would traverse the earth's atmosphere at an altitude of 15 km, and that from the northern solar limb would pass at an altitude greater than 40 km.

The net effect of the earth's atmosphere at the lunar location closest to the umbra during the Gemini-7 measurements would be to reduce the visible radiation by 85 percent; this estimate is based on the curve given in Figure 1, page 252 of Kuiper and Middlehurst. The increase in visible insolation with distance from the umbra based on the Kuiper and Middlehurst curve is depicted by the dashed contours drawn on Figure 5. A rough integration of these contours indicates that the total reduction in visible solar insolation at the time of the Gemini-7 measurements would be approximately 20 percent.

4. ALBEDO EQUATIONS

Most of the material presented in this section is discussed in more detail in Kuiper and Middlehurst. The Bond Albedo, A, is defined as the ratio of the total flux reflected in all directions to the total flux incident on an object and is given for spherical objects illuminated by the sun and viewed from the earth by:

$$A = \frac{2}{\pi F \sigma_1^2} \int_0^{\pi} j(\alpha)\, \sigma_1^2 \sin\alpha \, d\alpha = \frac{j(0)}{\pi F} \times 2 \int_0^{\pi} \Phi(\alpha) \sin\alpha \, d\alpha = pq \qquad (1)$$

where

A = Bond Albedo

$\pi F \sigma_1^2$ = total incident solar flux

σ_1 = apparent diameter of the sphere if it were at unit distance from both the earth and the sun

$j(\alpha)\, \sigma_1^2$ = flux reflected by the sphere in the direction of earth

α = phase angle defined as the angle subtended at the center of the sphere by the earth and the sun

$\Phi(\alpha) = \frac{j(\alpha)}{j(0)}$ = phase variation

$p = \frac{j(0)}{\pi F}$ = geometrical albedo

$q = 2 \int_0^{\pi} \Phi(\alpha) \sin\alpha \, d\alpha$ = phase integral.

The formula for computing the geometrical albedo of the moon is:

$$\log p = 0.4\,[m(\text{sun}) - m(1,0)] - 2 \log \sigma_1 \tag{2}$$

where

$$\sigma_1 = \frac{R}{R_E} \sin 8.''79$$

R/R_E = ratio of moon's mean radius to the earth's mean radius = 0.273

$m(\text{sun})$ = magnitude of the sun

$m(1,0)$ = magnitude of the moon at unit distance from the sun and earth

$8.''79$ = solar parallax

Thus, Eq. (2) becomes

$$\log (p) = 0.4\,[m(\text{sun}) - m(1,0)] + 9.869\,. \tag{3}$$

For the analysis of the Gemini data, it is more convenient to express p in terms of spectral irradiance, H_λ, as follows:

$$P_\lambda = 4.88 \times 10^4 \, \frac{H_\lambda(\text{moon}, 0)}{H_\lambda(\text{sun})} \tag{4}$$

where the zero denotes $\alpha = 0$.

5. GEOMETRICAL ALBEDO

Although the definition of the geometrical albedo given above is convenient from a mathematical standpoint, it is somewhat confusing in that the moon is in total eclipse when $\alpha = 0$; therefore, one must imagine that the earth is replaced by a point observer in order to obtain the correct value for substitution into Eq. (1). In practice the geometric albedo can be computed by extrapolating the phase variation curve. The phase curve most commonly used appears to be that based on Rougier's data which is tabulated on page 214 of Kuiper and Middlehurst. A plot of Rougier's curve which applies to a wavelength of 4450 Å (Figure 6) shows that although the variation is most rapid near full moon, an increase of less than 10 percent is expected in the interval from $\alpha = 0$ to $\alpha = 1.5^{\circ}$, the minimum phase angle at which measurements can be made without some effect from the earth's shadow.

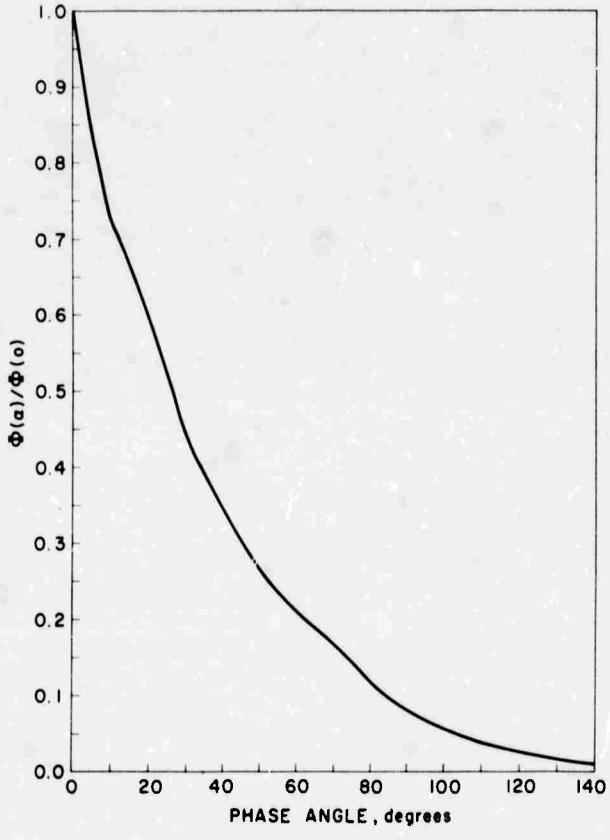

Figure 6. Lunar Phase Variation Curve

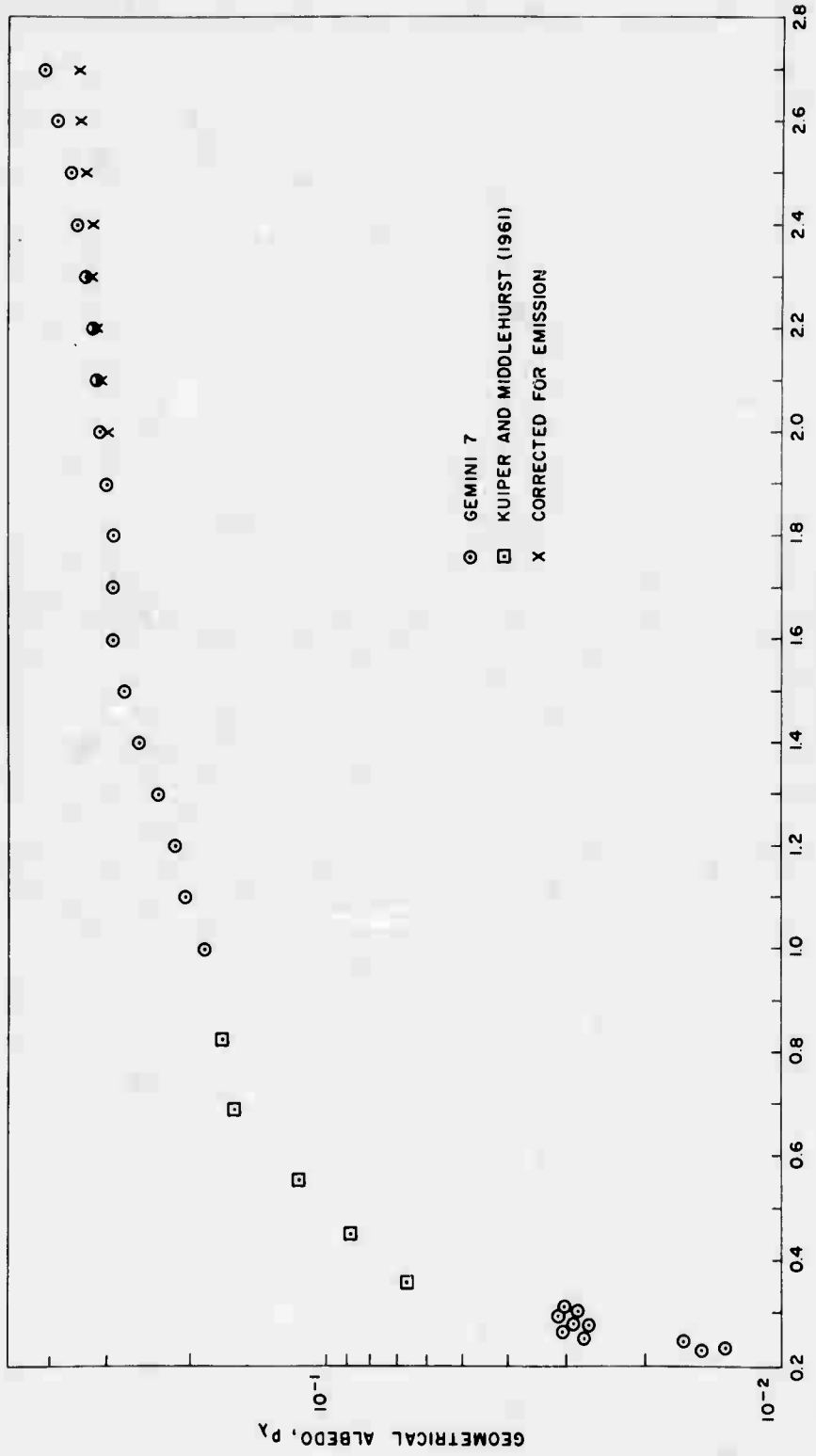

Figure 7. Geometrical Albedo vs. Wavelength

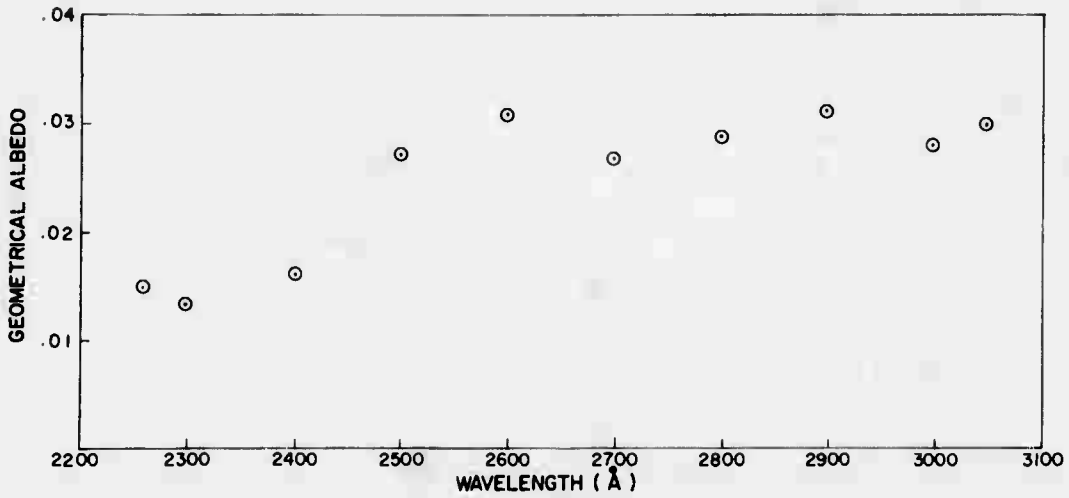

Figure 8. UV Geometrical Albedo vs. Wavelength

Since it is not known whether the contours drawn on Figure 5 would apply at all wavelengths covered by the Gemini-7 data, the geometrical albedo was computed without adding any correction for the penumbral eclipse effects. A plot of the results (Figure 7) shows that there is reasonably good agreement between the Gemini-7 data and the data presented in Table 22, page 310 of Kuiper and Middlehurst. It would appear, however, that the transition from the Kuiper and Middlehurst data to the Gemini data beyond 1.0μ would be smoother if a small correction factor were applied to account for the decreased insolation caused by the penumbral eclipse.

The ultraviolet data given in Figure 7 are presented on an expanded scale in Figure 8 where the albedo levels off to within 15 percent in the 2500 to 3050 Å region. Since there is a large spread in the solar spectral irradiance data used in computing the geometric albedo (Valley, 1965, page 16-11) it is not known whether this trend is real. A value of 0.018 for p at 3050 Å appears reasonable based on an extrapolation of the reflectance measurements reported by Stair and Johnston (1953), and a decrease to 0.008 at 2200 Å also appears reasonable on the basis of their reflectance versus wavelength slope. It would appear that the fraction of the solar insolation which traversed the atmosphere at altitudes above the ozone layer was sufficient to reduce ozone absorption below the level detectable within the precision of the measurements since no large dip at 2500 Å was observed.

6. PHASE VARIATION

The ratios of the irradiances measured on 5 December to those measured on 8 December are plotted versus wavelength in Figure 9, which raises some interesting questions. In the ultraviolet region, the value of the phase function at $\Phi = 38^{\circ}32'$ is as much as 60 percent greater than that indicated by Rougier's curve; in the infrared region at 1.0 μ the value is less than 10 percent greater than Rougier's value, but at 2.4 μ it is nearly twice Rougier's value. There are undoubtedly many possible ways to interpret these results, but we shall not pursue the subject further until time is available for computing the effect of the earth's atmosphere on the observations.

7. BOND ALBEDO

The value of the phase integral, q, is required for the computation of the Bond Albedo. An empirically derived value for q based on visible radiation observations is available (Kuiper and Middlehurst, page 309) but the variation of q with wavelength is not known. Figure 9 indicates that Φ increases with increasing wavelength in the 1.0 to 2.8 μ region; it is also quite possible that this trend will be found to continue down to 2200 Å after corrections for atmospheric absorption, scattering, and refraction have been applied to the full moon irradiances. If Φ increases with wavelength, one would expect q to increase with wavelength also. Since no detailed investigation of atmospheric effects has been performed for this preliminary report, the value of $q = 0.585$ given in Kuiper and Middlehurst was used for all wavelengths in the computation of the Bond albedo; the results are given in Figure 10.

8. ALBEDO TABULAR SUMMARY

To allow other investigators to check our computations without reading the graphs on which the points are plotted, a complete summary of the data used in the computations is given in Table 2. The computations are carried out to three significant figures, but the measured irradiance data are probably good to no more than 5 to 10 percent and the smooth curves drawn in Figures 7 and 10 are subject to the whim of the analyst and draftsman. The use of a mean solar insolation curve could have introduced a small additional error.

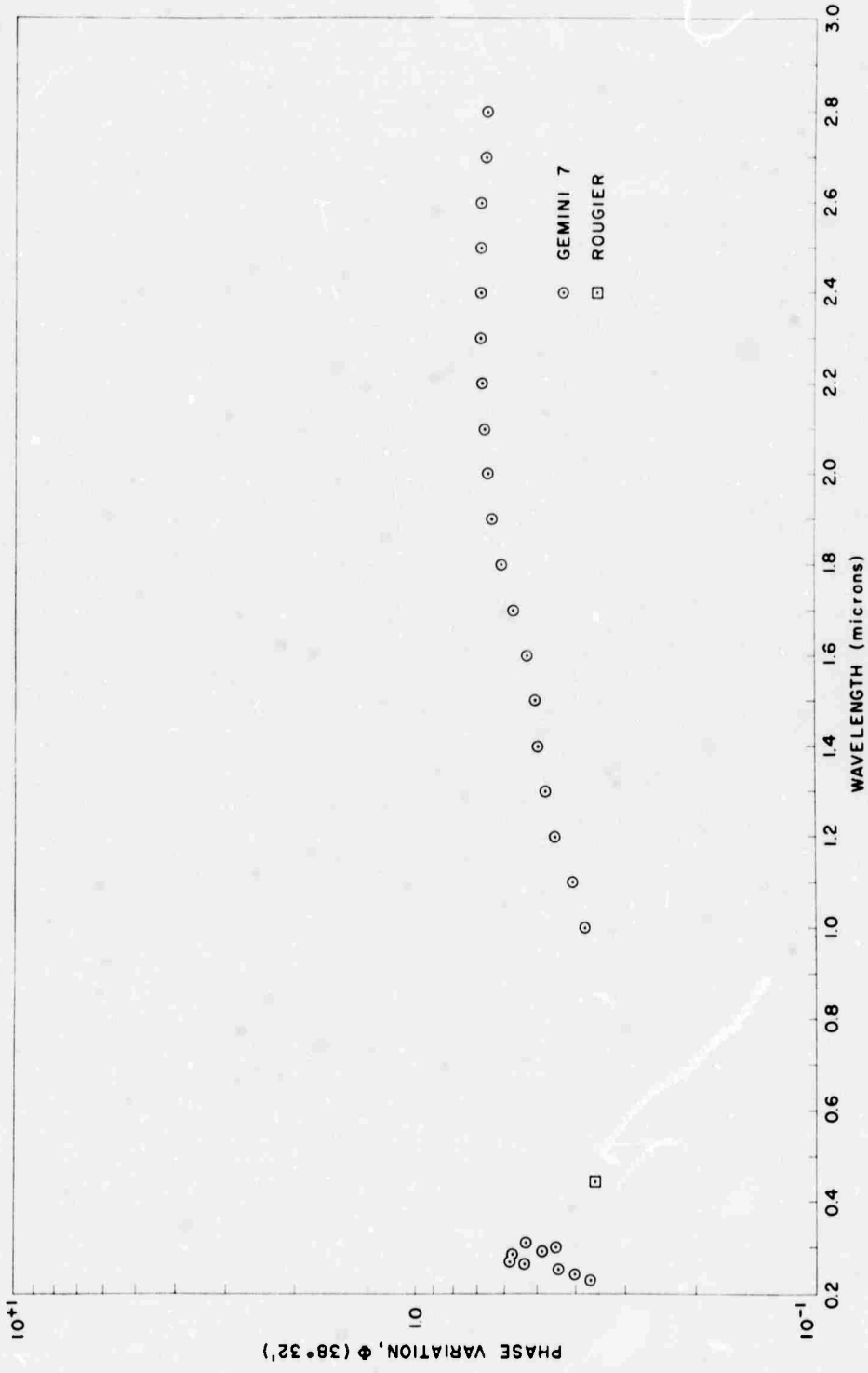

Figure 9. Phase Variations for $38^{o}32'$ Phase Angle vs. Wavelength

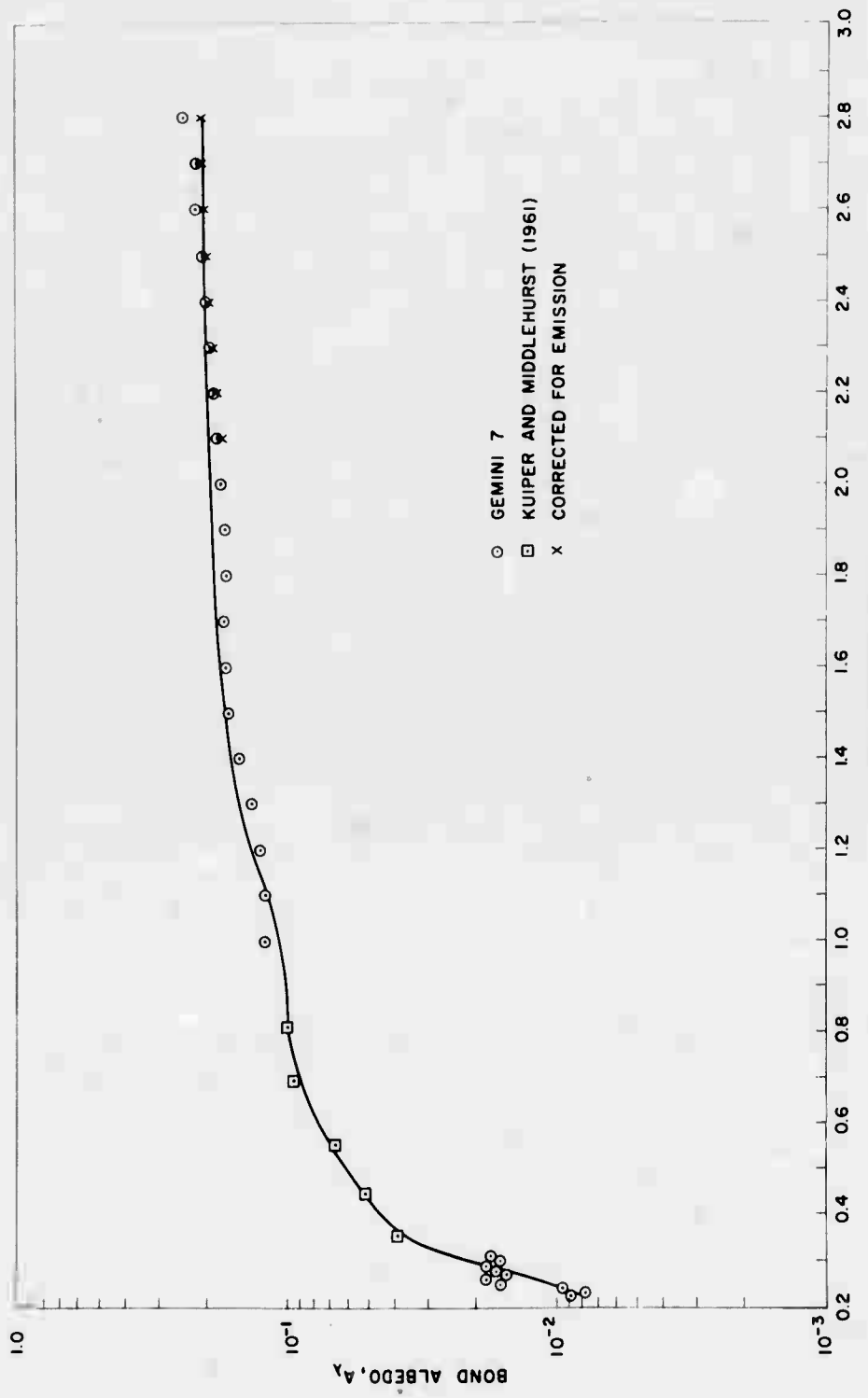

Figure 10. Bond Albedo vs. Wavelength

Table 2. Albedo Computations

λ microns	H_λ(38°32') $wcm^{-2}\mu^{-1}$	H_λ(1°5') $wcm^{-2}\mu^{-1}$	H_λ SUN $wcm^{-2}\mu^{-1}$	p	Φ(38°32')	A
0.2260	5.85-10	1.59-09	5.20-03	1.49-02	3.68-01	8.71-03
0.2300	6.40-10	1.70-09	6.20-03	1.34-02	3.76-01	7.84-03
0.2400	8.90-10	2.20-09	6.60-03	1.63-02	4.05-01	9.54-03
0.2500	1.92-09	4.30-09	7.70-03	2.72-02	4.47-01	1.59-02
0.2600	5.15-09	9.50-09	1.50-02	3.09-02	5.42-01	1.81-02
0.2700	8.80-09	1.51-08	2.75-02	2.68-02	5.83-01	1.57-02
0.2800	1.15-08	2.00-08	3.40-02	2.87-02	5.75-01	1.68-02
0.2900	1.37-08	2.80-08	4.40-02	3.10-02	4.89-01	1.81-02
0.3000	1.58-08	3.50-08	6.10-02	2.80-02	4.51-01	1.64-02
0.3050	2.05-08	3.85-08	6.30-02	2.99-02	5.32-01	1.75-02
1.00	1.08-07	2.80-07	7.26-02	1.88-01	3.86-01	1.10-01
1.10	1.05-07	2.52-07	6.00-02	2.05-01	4.16-01	1.20-01
1.20	1.01-07	2.22-07	5.02-02	2.16-01	4.55-01	1.26-01
1.30	9.40-08	1.96-07	4.08-02	2.34-01	4.80-01	1.37-01
1.40	8.65-08	1.73-07	3.29-02	2.57-01	5.00-01	1.50-01
1.50	7.75-08	1.52-07	2.66-02	2.79-01	5.09-01	1.63-01
1.60	6.90-08	1.30-07	2.18-02	2.91-01	5.31-01	1.70-01
1.70	6.15-08	1.07-07	1.79-02	2.92-01	5.75-01	1.71-01
1.80	5.45-08	8.85-08	1.49-02	2.90-01	6.16-01	1.70-01
1.90	4.82-08	7.45-08	1.25-02	2.91-01	6.47-01	1.70-01
2.00	4.31-08	6.45-08	1.05-02	3.00-01	6.68-01	1.76-01
2.10	3.82-08	5.65-08	8.90-03	3.10-01	6.76-01	1.81-01
2.20	3.37-08	4.95-08	7.59-03	3.18-01	6.81-01	1.86-01
2.30	3.00-08	4.35-08	6.51-03	3.26-01	6.90-01	1.91-01
2.40	2.69-08	3.88-08	5.61-03	3.38-01	6.93-01	1.98-01
2.50	2.42-08	3.48-08	4.87-03	3.49-01	6.95-01	2.04-01
2.60	2.19-08	3.19-08	4.24-03	3.67-01	6.87-01	2.15-01
2.70	1.99-08	2.95-08	3.71-03	3.88-01	6.75-01	2.27-01
2.80	1.84-08	2.76-08	3.26-03	4.13-01	6.67-01	2.42-01

9. LUNAR TEMPERATURE AND EMISSION

The self emission of the moon was neglected in the albedo computations reported above since it was not considered to be of sufficient magnitude to affect the results except at the long wavelength extremity of the curve. It is apropos, however, to compute the average lunar surface temperature during the eclipse as a further check on the validity of the data obtained.

The lunar surface temperature based on an albedo of 7 percent yields a temperature of 385°K if Stefan's equation is used (Kuiper and Middlehurst, page 413). Thus, the temperature during the eclipse T_E can be computed as follows:

Table 3. Average Albedo Computation

λ	$H_{\Delta\lambda}$	$H_{\Delta\lambda}A_{\lambda}$
.001-.225	0.90	-------
.225-.250	1.77	1.71-02
.250-.275	4.25	5.51-02
.275-.300	10.73	2.01-01
.300-.325	19.09	4.84-01
.325-.350	28.28	9.21-01
.350-.375	31.22	1.19-00
.375-.400	31.05	1.31-00
.400-.425	47.48	2.20-00
.425-.450	47.41	2.39-00
.450-.475	53.18	2.88-00
.475-.500	52.00	3.03-00
.500-.525	48.50	3.01-00
.525-.550	49.15	3.24-00
.550-.575	47.91	3.35-00
.575-.600	47.44	3.51-00
.600-.650	85.95	6.85-00
.650-.700	76.70	6.63-00
.700-.750	67.92	6.25-00
.750-.800	59.90	5.77-00
.800-.850	53.19	5.21-00
.850-.900	47.40	4.71-00
.900-.950	42.39	4.28-00
.950-1.00	38.14	3.95-00
1.00-1.05	34.71	3.76-00
1.05-1.10	31.74	3.62-00
1.10-1.50	166.11	2.39+01
1.50-2.00	84.63	1.53+01
2.00-2.50	36.02	7.07-00
2.50-3.30	17.71	3.56-00
3.00-3.50	9.65	1.95-00
3.50-4.00	5.69	1.15-00
4.00-4.50	3.45	6.97-01
4.50-5.00	2.24	4.52-01
5.0 -6.0	2.55	5.15-01
6.0 -7.0	1.34	2.71-01
7.0-11.0	1.75	6.24-01
11.0-30.0	0.73	1.47-01
	Σ = 1390	134.45

$$\frac{T_E}{385} = \left(\frac{1 - A}{0.93}\right)^{\frac{1}{4}} . \qquad (1)$$

The A in Eq. (1) was determined by taking the product of the smooth curve in Figure 10 and the mean solar spectral irradiance curve in Valley (1965) to obtain the sum given at the bottom of Table 3. Taking the ratio of this integrated product

to the solar constant gives an average albedo of 0.0967. Substituting this value into Eq. (1) yields:

$$T_E = 385 \left(\frac{1-0.0967}{0.93}\right)^{\frac{1}{4}} = 0.97 \times 385 - 373.8^{\circ}K \, . \qquad (2)$$

If the albedos given in Figure 10 were increased to account for the eclipse and a variation of q with wavelength, the value of A in Eq. (2) would be increased and a lower temperature would result for an uneclipsed full moon. The lunar emission based on the assumption of a 374°K blackbody was computed and the results are given in Table 4; these values were used for the computation of the points plotted as crosses on Figures 7 and 10.

Table 4. Lunar Emission Irradiance

λ	Irradiance Due To Emission $w cm^{-2} \mu$	$HL_o(1°5')$ Corrected For Emission $w cm^{-2} \mu$	p	A
2.0	9.59-11	6.44-08	2.99-01	1.75-01
2.1	1.88-10	5.63-08	3.09-01	1.81-01
2.2	4.50-10	4.90-08	3.15-01	1.84-01
2.3	5.87-10	4.29-08	3.22-01	1.88-01
2.4	9.47-10	3.79-08	3.30-01	1.93-01
2.5	1.47-09	3.33-08	3.34-01	1.95-01
2.6	2.18-09	2.97-08	3.42-01	2.00-01
2.7	3.13-09	2.64-08	3.47-01	2.03-01
2.8	4.34-09	2.33-08	3.49-01	2.04-01

10. CONCLUSIONS AND RECOMMENDATIONS

The primary purpose of the Gemini-7 lunar measurements was accomplished. Measurements in the 2200 to 3000 Å region were made with sufficient accuracy to establish sensitivity and dynamic range criteria for the UV spectrometer to be flown by NASA on Gemina-12. It appears that the dynamic range of film is sufficient to obtain measurements throughout most of the spectrum. There are many Fraunhofer lines in the solar spectrum in this region, however, which could be masked, particularly if radiation outside the band is not blocked sufficiently to reduce film

fogging. An estimate of the effect of scattered radiation can be obtained if spectra of a Bureau of Standards Lamp are taken with and without Schott glasses WG1 through WG8; also, the spare Gemini-7 broad UV filters could be useful in checking out the spectrometer. It is possible that an analyst would interpret the strength of the lunar Fraunhofer lines on the basis of lunar fluorescence; if scattered radiation is a problem his conclusions could be misleading.

The reduction and analysis of the Gemini-7 data would have been simplified if continuous motion picture coverage were available and if the spacecraft inertial system were erected during the measurements to obtain accurate orientation and angular rate information; if possible, these two types of information should be sought during the Gemini-12 lunar measurements.

The secondary objective of the lunar observations was also accomplished. Although the agreement with other lunar observation is not perfect in all respects, we can proceed to reduce data obtained on other Gemini-7 targets, confident that no large errors will be introduced by unpredictable changes in instrument responsivity due to the environment in which the data were taken.

Although neither the instrument nor the experiment was designed specifically for the purpose, reasonably accurate lunar geometrical albedos were determined in the 2000 to 3000 Å region (where the earth's atmosphere is practically opaque) and in the 1.0 to 2.8 μ region (where the earth's atmosphere selectivity absorbs and or attenuates radiation).

It is recommended that detailed computations be performed to arrive at an estimate of the reduction in solar insolation caused by the penumbral eclipse, particularly in the UV region. It is also recommended that the 36 motion picture frames taken with the spacecraft camera during the full moon measurements be densitometered.

Acknowledgments

We are particularly indebted to the following organizations and personnel:

USAF Space Systems Division for their financial support and for the assignment of Major B. Brentnall to the project.

NASA personnel at Houston, St. Louis, and Cape Kennedy whose excellent support and cooperation are sincerely appreciated.

ARPA for support in the reduction and analysis of the Gemini optical data.

We also acknowledge the following personnel who contributed a great deal of their time, effort, and skill to make the program a success: Warren Howell of Block Engineering Co. for supervising the development and fabrication of the optical instruments; James Powers, David Newell, and Vernon Turner of Concord Radiance Laboratory for their excellent field engineering.

A special note of thanks is also due Prof. G. Mumford of Tufts University for his guidance in the computation of solar-lunar-earth geometry.

Last but not least, to Gemini-5 Astronauts Gordon Cooper and Peter Conrad and to Gemini-7 Astronauts Frank Borman and James Lovell goes our sincere appreciation for their cooperation before, during, and after the flights and for their accurate recording of personal observations which contributed significantly to the interpretation of the data.

References

Kuiper, G.P. and Middlehurst, B.M. (1961) Planets and Satellites - The Solar System--Vol. 111.

Stair, R., and Johnston, R. (1953) Ultraviolet spectral radiant energy reflected from the moon, Journal of the National Bureau of Standards, 51 (No. 2):81.

Valley, Shea L. (1965) Handbook of Geophysics and Space Environments, AFCRL, CAR, USAF.

Appendix A

Measurement Systems

1. MEASURING EQUIPMENT CHARACTERISTICS

A complete description of the instruments used for the lunar measurements is given in Appendixes B and C where the calibration procedures are discussed and complete calibration data are presented. A summary of the more important equipment characteristics is given below.

The characteristics of the 20 Gemini-7 radiometer channels are given in Table A-1 where λ_s is the wavelength of peak system response; $\Delta\lambda_s$ is the wavelength interval for which the system response is greater than or equal to one-half the peak response; H_{Neff} is the effective irradiance equivalent to the system noise; and H_{Meff} is the effective irradiance above which saturation occurs.

The spectral response curve for the PbS section of the I-14 interferometer is given in Figure A-1, while the noise equivalent irradiance curve and the saturation irradiance curve obtained for the 2100°C blackbody source used during calibration are given in Figure A-2. The peak to peak output of the interferometer is the voltage produced by the target in the entire wavelength region to which the instrument responds; thus, narrow bands of much higher irradiance than those given in Figure A-2 will not saturate it.

The field of view curves for the two radiometer sections and the interferometer PbS section are given in Figures A-3 through A-5. These were measured by placing the instrument in collimated radiation and rotating it while the collimator remained fixed; the target subtended an angle of approximately 0.005 radian.

2. EQUIPMENT OPERATING MODES

The astronauts had a choice of one of three possible operating modes for each experiment. In MODE 1 the radiometer filter wheel cycled repeatedly through the last four positions, completing a cycle in 40 sec, while the output of the cooled I-15 interferometer was fed to a meter on the capsule instrument panel. In MODE 2 the radiometer cycled repeatedly through all 10 filter positions, completing each cycle in 100 sec, while the output of the I-14 interferometer was fed to the panel meter. In MODE 3 the filter wheel was locked in position number 3 and the output of radiometer channel 13 was fed to the panel meter.

In all three modes the outputs of all instruments that were turned on were fed to the capsule telemetry transmitting system and could be transmitted in real time to a ground based receiving station if the spacecraft were near one. In all three modes the radiometer outputs could be recorded on an on-board PCM tape recorder that could be "dumped" when the capsule was near a receiving station. The interferometer outputs were recorded only on an on-board FM tape recorder that could not be "dumped". This FM recorder had a total recording capacity of only 1 hr and was, therefore, used sparingly during the flight.

3. THE BORESIGHT EXPERIMENT

At the beginning of the boresight experiment the instruments were operated in MODE 3 to check the alignment of the radiometer with the sighting scope. Astronaut Borman maneuvered the spacecraft so that the moon would appear at various locations in his scope, while Astronaut Lovell read the meter (monitoring radiometer channel 13) and reported the values to him. When the position of peak signal had been determined the equipment was switched to MODE 2 and the PbS section of the I-14 interferometer was monitored for peak signal. The results are given in Figure A-6, which was taken from the flight log book and shows that the two instruments peaked within 0.5 deg of the reticle cross-hairs; the I-15 interferometer had been checked earlier on a different target.

The lunar irradiances obtained with the radiometer during MODE 3 are given in Figures A-7(a) and A-7(b). The peak to peak output voltage of the I-14 interferometer PbS section is plotted versus time in Figure A-7(c). The UV irradiances measured during MODE 2 when the filter wheel was cycling are given in Figure A-8(a). These data are replotted in Figure A-8(b), which was normalized to the peak that occurred at 18:28:50 GMT. The Figure A-8(b) plot represents our best estimate of the variation that would have occurred in the measuring interval if the filter wheel were locked in one position. Three versions of Figure A-8(b) were

made (by three independent analysts) and the three plots agreed to within 5 percent. The series of small tick marks at the top of Figure A-8 indicate the times when the filter wheel position changed.

The PbS irradiance values given in Figure A-9(a) were also measured when the filter wheel was cycling in MODE 2. The PbS data varied much more in a 10-sec interval than did the UV data, and the three analysts' versions of Figure A-9(b) agreed to within only 10 percent. The larger variation is probably due to the smaller and more variable field of view of the PbS section of the radiometer. The behavior of the interferometer output with time during the MODE 2 measurements is shown in Figure A-9(c). The filter position marks on the figure have no significance, since there was no filter wheel in the interferometer; they are drawn as a visual aid in comparing the variation of the measurements with time for the two instruments.

The variation in signal during the 100-sec interval required for a complete cycle presented a serious problem in the data reduction. For example, only two measurements were obtained for filter position 19, and our best estimate of the temporal (actually sighting) variation with time indicates that the signals measured at those times were lower than would have been measured if position 19 occurred at 18:28:50 GMT when the optical axis was more nearly aligned with the moon. The data tabulated in Table 1 of the main body of this report were obtained by correcting the irradiances for all filter wheel positions on the basis of the sighting variation curves given in Figures A-8(b) and A-9(b) and, thus, contain an uncertainty factor of ±2.5 percent in the UV and ±5 percent in the IR.

4. THE FULL MOON MEASUREMENT

The planned program for the 8 December full moon measurement was to orient the capsule so that the moon would initially appear at the location of peak radiometer response and then to maneuver the craft until the moon appeared at the location of peak interferometer response. MODE 2 was used and, thus, the filter wheel was cycling during the entire measuring period. The radiometric data for the full moon measurements (Figures A-10 and A-11) varied as much with time as those obtained during the bore-sighting measurement, and the procedure described for the 5 December measurements was used for removing sighting variations from the full moon data; the results are given in Figures A-10(b) and A-11(b).

The interferometer irradiance vs. time behavior is given for a wavelength of 2.4 μ in Figure A-11(c), where the data have been normalized to an irradiance of 3.83×10^{-8} watt $cm^{-2}\ \mu^{-1}$ occurring at 16:46:08 GMT. An interferometric spectrum taken from a 2-sec magnetic tape loop commencing at 16:46:06 GMT is

given in Figure A-12; the fluctuations at the shorter wavelengths are due to low signal-to-noise ratios which in turn were caused by a dichroic interference filter used in the instrument.

A tabulation of the irradiances for both lunar measurements was presented in Table 1 in the main body of the report where it was mentioned that L_o is the wavelength above and below which 50 percent of the radiometer output would be contributed by a target having a given normalized spectral distribution.* The normalized spectral distribution used for converting the lunar effective irradiances to spectral irradiances was determined by first reducing the data using the normalized solar spectral distribution as a target and then comparing the results with the spectral distribution of blackbodies at various temperatures. It was found that a 4000°K blackbody produced the spectrum that most nearly matched the lunar data (Figure A-13). The spectral irradiances were then recomputed using a normalized 4000°K blackbody curve to compute the responsivities that were used in the final conversion of effective irradiance to spectral irradiance. Incidentally, although it has no physical significance, the 4000°K source would have an emissivity of 0.0017 percent if it were a disk having the diameter of the moon and possessing Lambertian properties.

*See Appendix B for a detailed discussion of the method used to convert effective irradiance to spectral irradiance.

Table A-1. Gemini-7 Radiometer Characteristics

Chan No.	λ_s microns	$\Delta\lambda_s$ microns	H_{Neff_2}* w cm^{-2}	H_{Meff_2}* w cm^{-2}
G-7-1	0.2180	0.0219	2.03-14	7.26-11
-2	0.2340	0.0228	2.03-14	7.25-11
-3	0.2940	0.0157	1.06-13	3.77-10
-4	0.2600	0.0187	7.95-14	2.84-10
-5	0.2760	0.0168	3.47-14	1.24-10
-6	0.2475	0.0258	3.15-14	1.12-10
-7	0.2810	0.0068	1.19-13	4.25-10
-8	0.3050	0.0075	5.45-13	1.95-09
-9	0.2870	0.0082	1.60-13	5.69-10
-10	0.2190	0.0217	2.09-14	7.46-11
G-7-11	1.110	0.137	3.30-10	2.42-06
-12	1.275	0.118	1.56-10	1.14-06
-13	1.575	0.109	1.07-10	7.81-07
-14	1.400	0.124	1.81-10	1.32-06
-15	2.800	0.171	2.41-10	1.76-06
-16	1.930	0.135	1.11-10	8.14-07
-17	2.175	0.111	1.14-10	8.36-07
-18	2.735	0.082	1.59-10	1.17-06
-19	2.750	0.111	3.30-10	2.42-06
-20	2.800	0.119	5.94-10	4.36-06

*These values apply for an instrument temperature of 85°F.

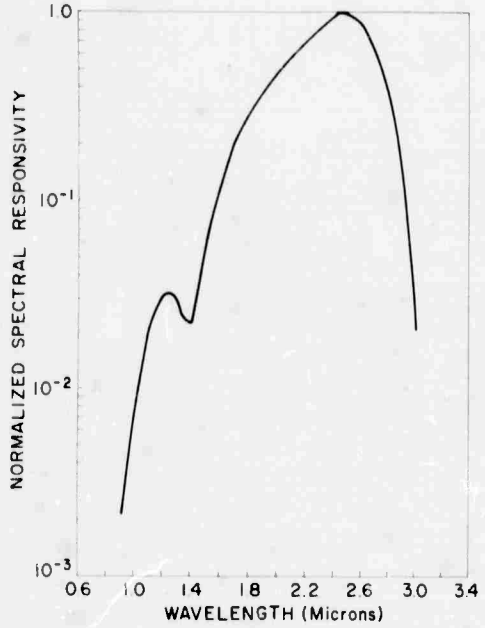

Figure A-1. Spectral Response of the I-14 Interferometer — PbS Section

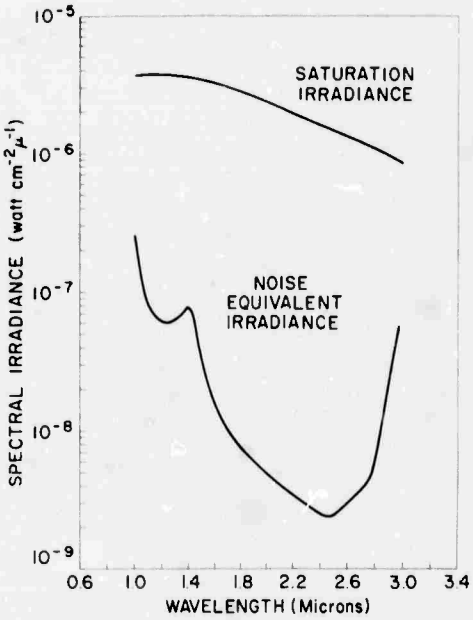

Figure A-2. Saturation and Noise Equivalent Irradiance Curves for I-14 Interferometer — PbS Section

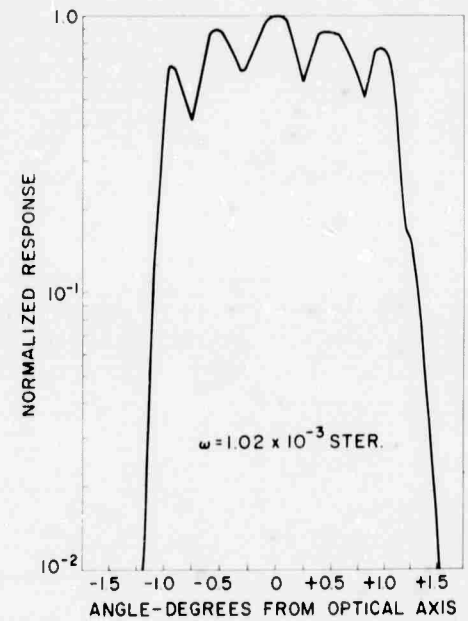

Figure A-3. Radiometer Field of View — Photomultiplier Section

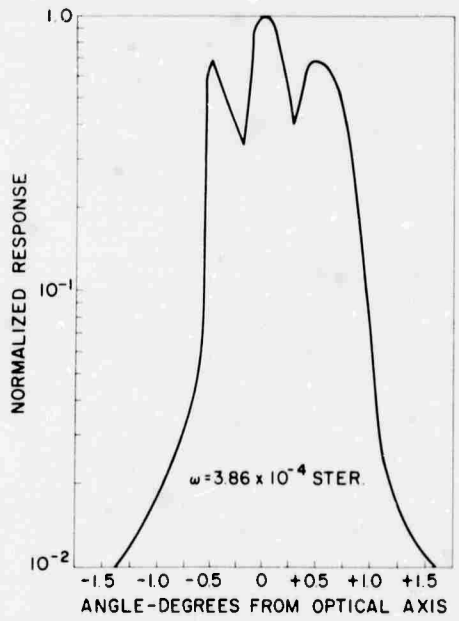

Figure A-4. Radiometer Field of View — PbS Section

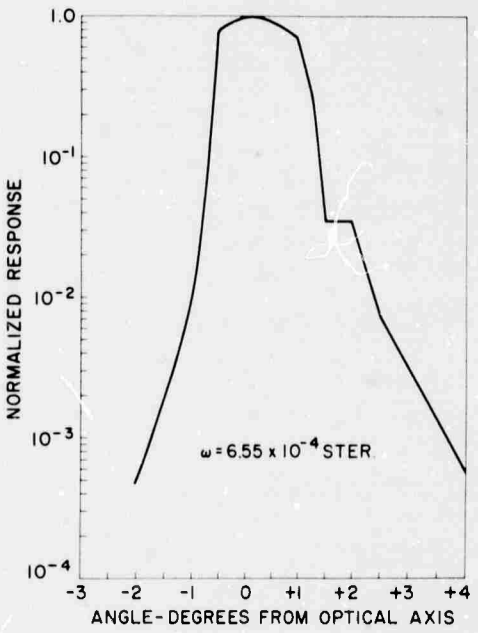

Figure A-5. Interferometer Field of View — PbS Section

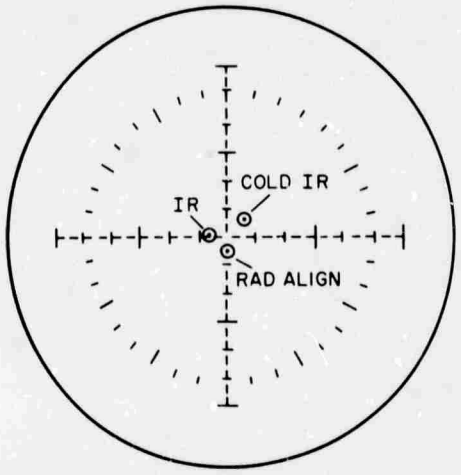

IR SPECT – 1/2° X AXIS

RAD. – 1/2° Y AXIS

I-15 + 9/16° Y AXIS, + 9/16° X AXIS

Figure A-6. Instrument Alignment Pattern

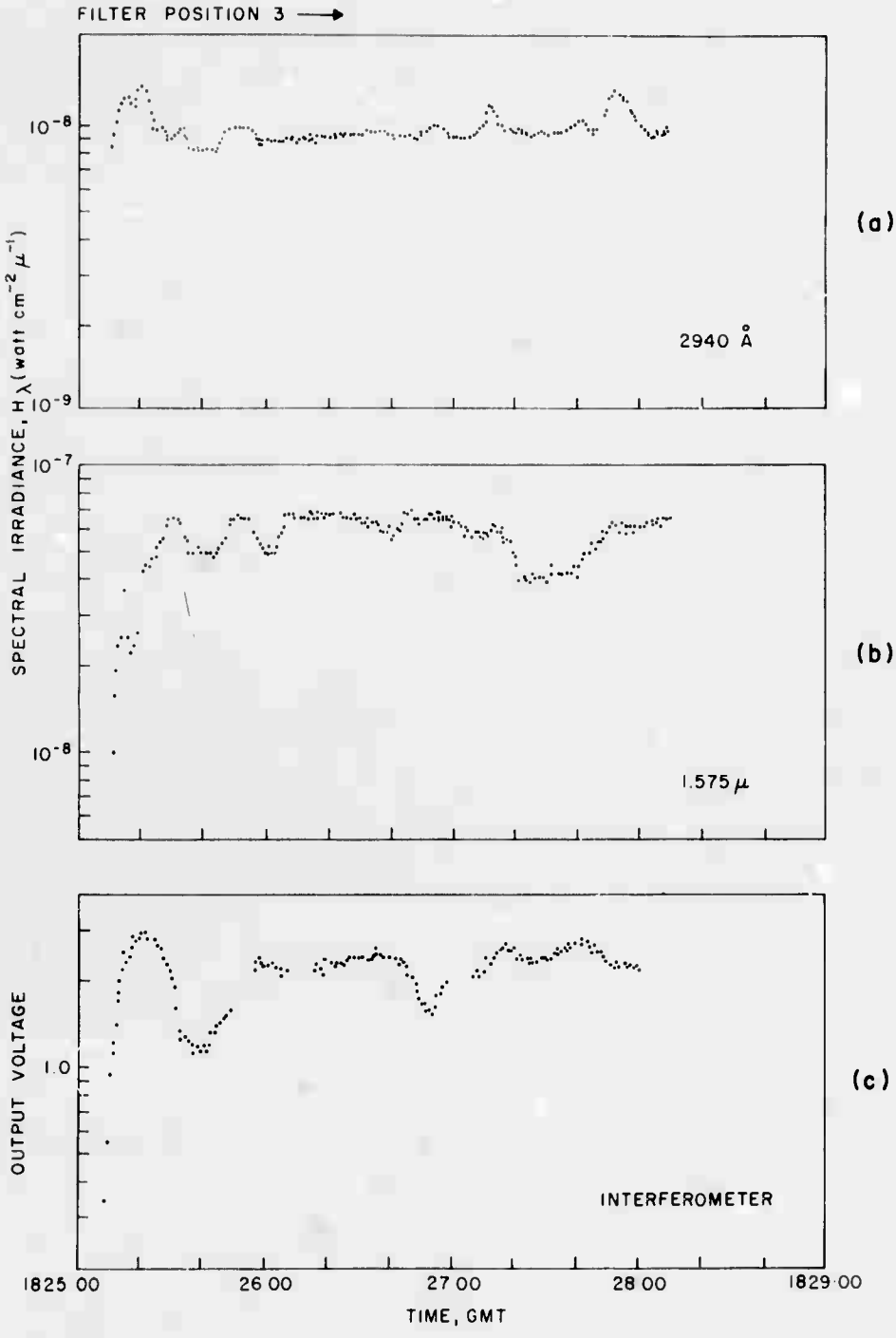

Figure A-7. MODE 3 Radiometer and Interferometer Data — Boresight Experiment

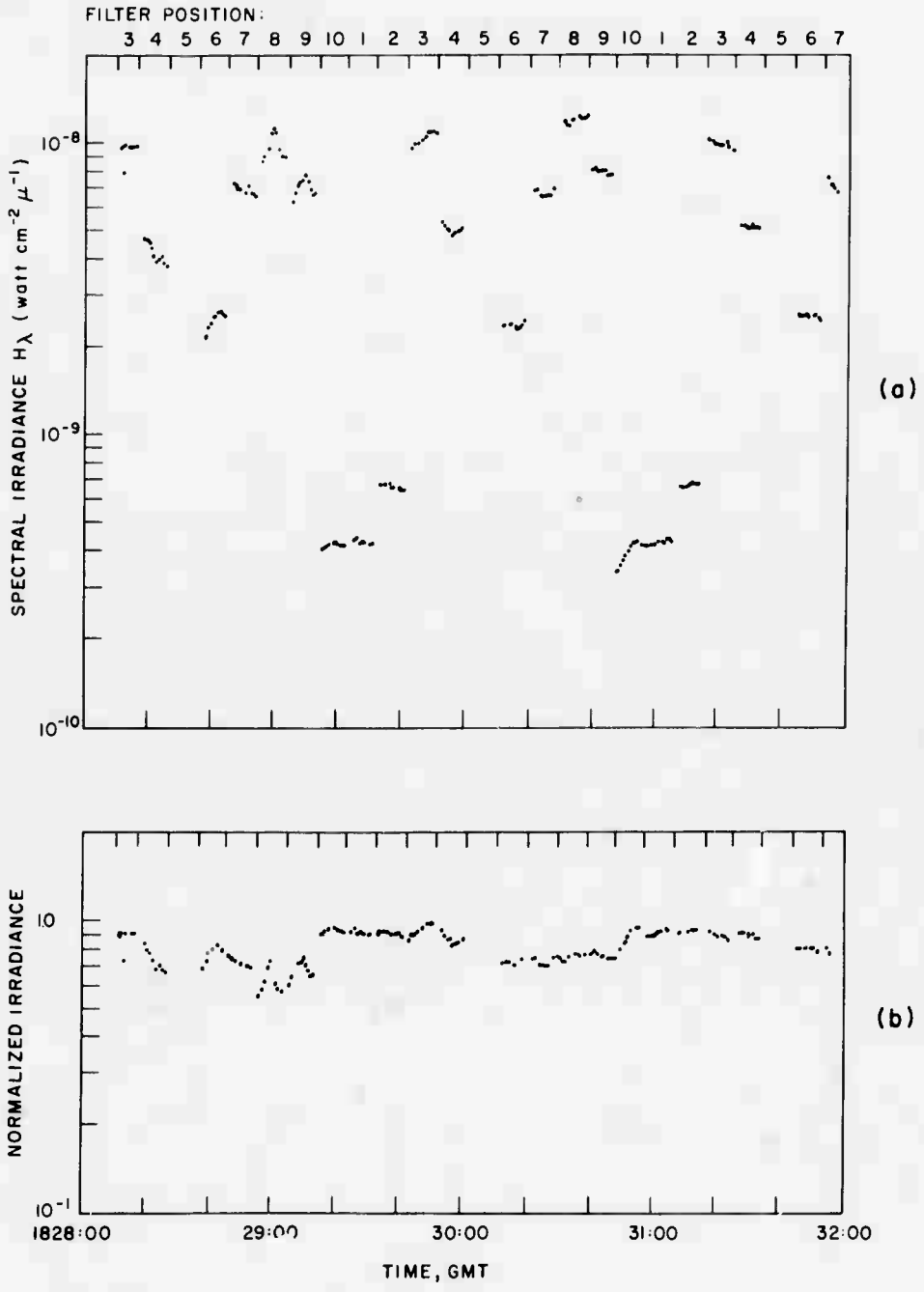

Figure A-8. MODE 2 Photomultiplier Data — Boresight Experiment

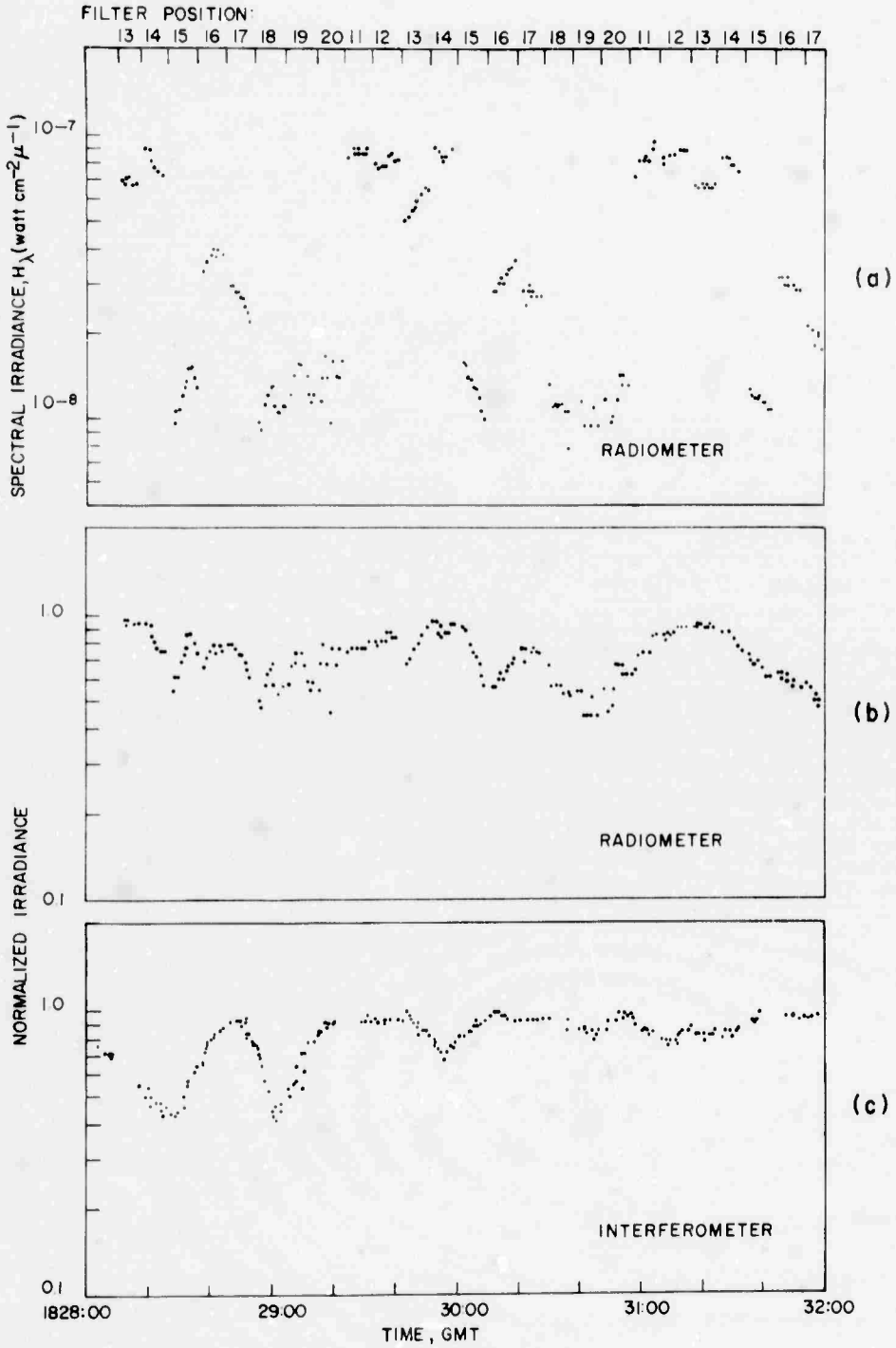

Figure A-9. MODE 2 PbS Radiometer and Interferometer Data — Boresight Experiment

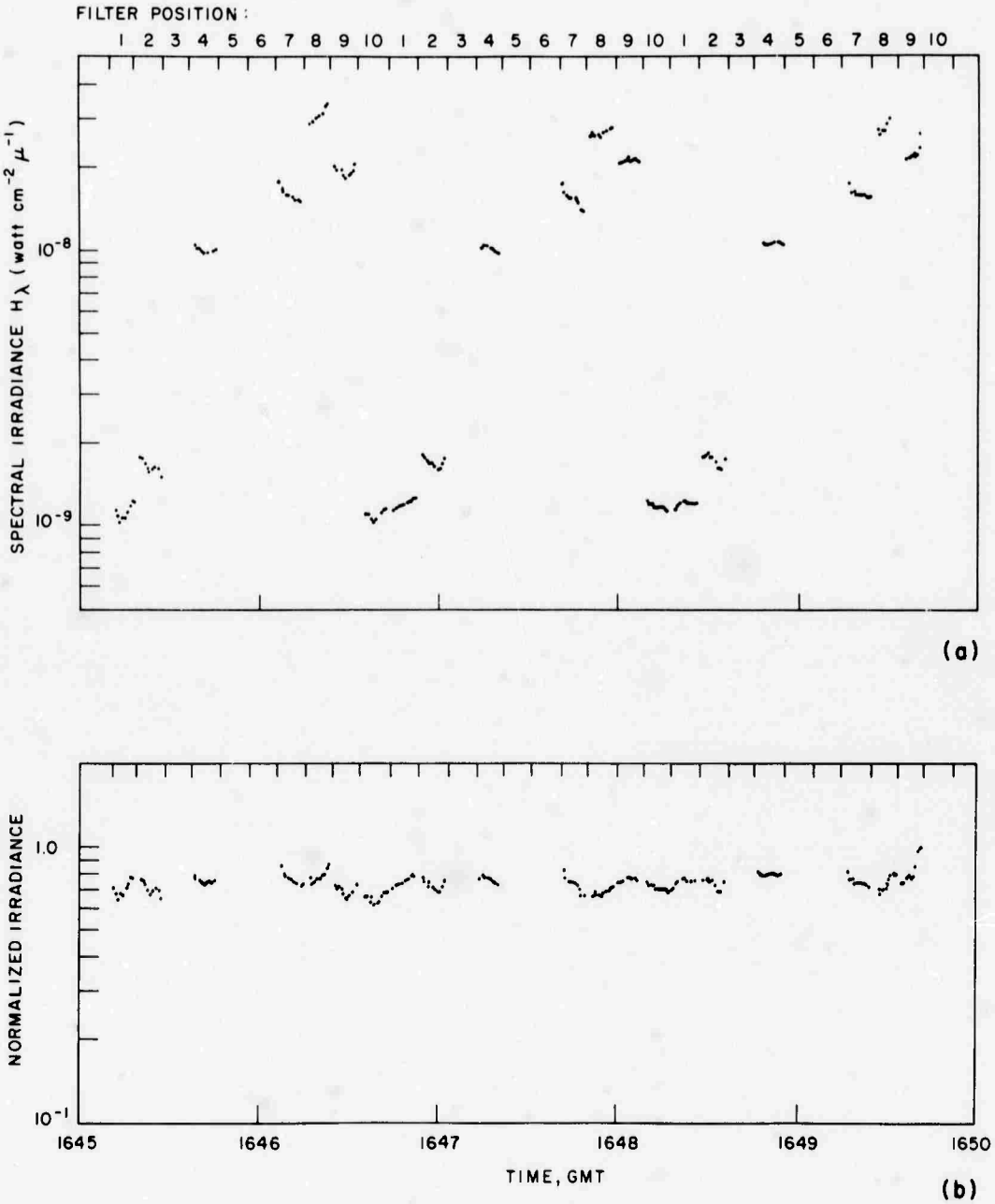

Figure A-10. Full Moon Photomultiplier Data

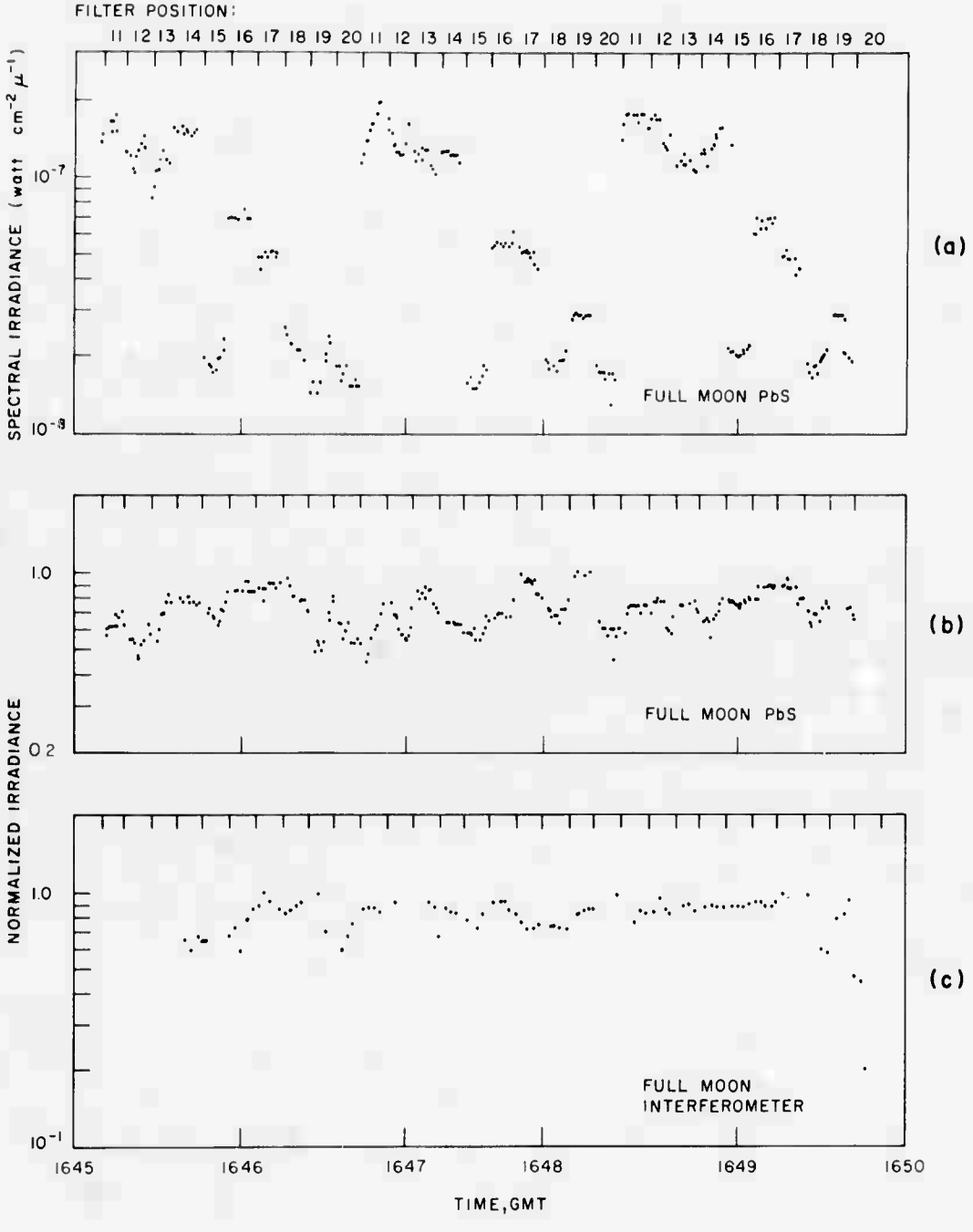

Figure A-11. Full Moon PbS Radiometer and Interferometer Data

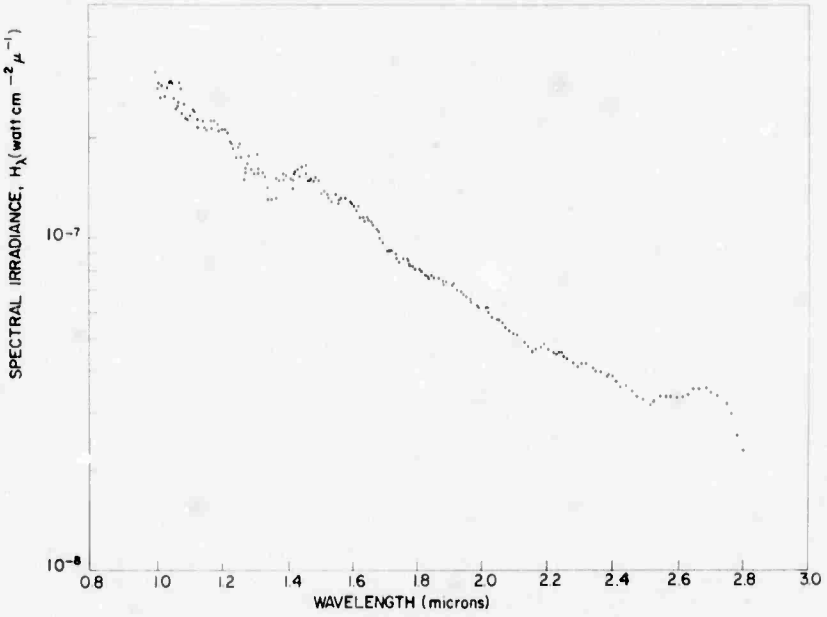

Figure A-12. Full Moon Interferometer Spectrum

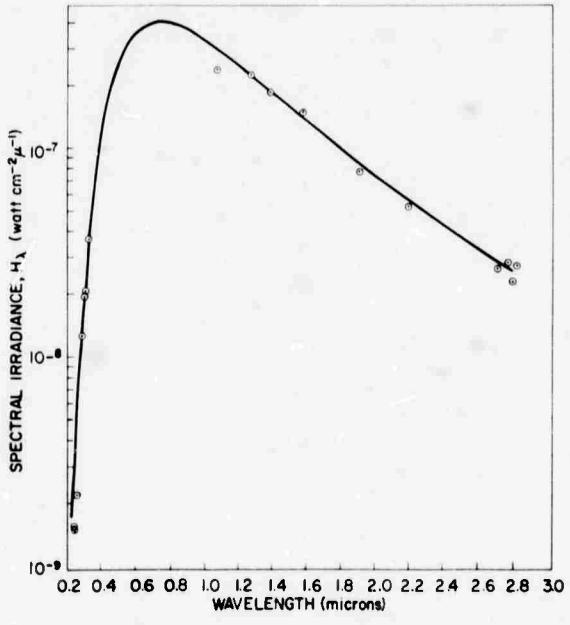

Figure A-13. Full Moon Data Compared With 4000°K Blackbody

BLANK PAGE

Appendix B

Gemini 7 Radiometer Calibrations

1. DESCRIPTION OF THE E3G RADIOMETER

The E3G Radiometer flown on Gemini-7 (Figure B-1) was a modified version of the E3G Radiometer flown on Gemini-5. In the original configuration, one-half of the power collected by the 4-in. Cassegrain fore-optics was diverted to a bolometer, and the other half was divided between a PbS detector and a IP28 photomultiplier. Since it was impossible to obtain filters for wavelengths shorter than 2800 Å having sufficient long wave rejection to be used reliably with the IP28 photomultiplier, the IP28 was replaced by an EMR type 541-05-08 solar blind photomultiplier for the Gemini-7 flight. Because of the modification, the bolometer had to be removed; thus, one-half of the incident radiation was directed to a void in the Gemini-7 radiometer.

The other half of the incident radiation was chopped at a frequency of 150 Hz by vibrating chopper beamsplitter and transmitted to a front-surfaced, striped-aluminum mirror. This mirror transmitted one-quarter of the originally available power to a front-surfaced, aluminum mirror that reflected it to the PbS detector through one of ten possible filter wheel apertures. The remaining 25 percent was reflected by the striped mirror through one of the photomultiplier filter wheel apertures to a front-surfaced, aluminum mirror that reflected it to the solar blind photomultiplier. The outputs of both detectors were amplified, commutated, and fed to a PCM recorder and to the telemetry transmitting system.

The photomultiplier section of the Gemini-7 radiometer was equipped with an automatic four-step attenuator that allowed linear operation over most of its

dynamic range, the attenuation factors being 1, 3, 10, and 30. The PbS section of the radiometer was equipped with a logarithmic amplifier designed to compress four decades of incident irradiance into a 4-volt output. An off-set of 1 volt was provided to allow measurement of targets that were colder than the radiometer chopper and to raise the output voltage for small signals to a level well above telemetry noise.

2. DYNAMIC RANGE CALIBRATION

The first step in the calibration of the two radiometer sections was to drive the output slightly above the 5-volt telemetry limit, using a 2000°C blackbody source, and then to reduce the irradiance in known steps with neutral density filters until no drop in voltage was observed with a further decrease in irradiance; this threshold voltage, V_N, was then subtracted from the voltages obtained with each neutral density filter, V_{T+N}, to arrive at the target voltage, V_T. Plots of V_T vs. neutral density filter transmission were then made. These plots showed that the photomultiplier section had a linear response for the three lowest attenuator settings but was non linear for outputs above 4.6 volts on the highest attenuator setting; during this calibration the attenuator factors were also determined. Thus for all voltages on attenuator settings 1, 2, and 3 the conversion of target voltage to irradiance could be accomplished by an equation of the form

$$H_{eff} = B_{eff} V_T G \tag{1}$$

where

H_{eff} = effective irradiance (watt cm^{-2})

B_{eff} = inverse effective irradiance responsivity (watt cm^{-2} $volt^{-1}$)

G = attenuator factor.

This equation could also be used for attenuator setting 4 for output voltages less than 4.6 volts; for larger output voltages a quantity V_E was substituted for V_T. A plot of V_E vs V_T is given in Figure B-2.

The PbS section was non linear by design, and the equation which applied is

$$H_{eff} = B_{eff} f(P) \tag{2}$$

where B_{eff} is the effective irradiance corresponding to an $f(P)$ value of unity and is the effective irradiance required to produce a V_T of 4.5 volts. A plot of V_T vs $f(P)$ based on the neutral density filter run is given in Figure B-3.

3. ABSOLUTE RESPONSIVITY CALIBRATION

The 20 radiometer channels were calibrated absolutely by placing the instrument in the collimated beam of a 25-inch-focal-length, 6-inch-diameter, off-axis collimator manufactured by Infrared Industries, Inc. . The radiation source was a one-quarter-inch circular aperture 2000°C blackbody manufactured by Rocketdyne. The radiometer was oriented to obtain maximum output and the system was then flushed with nitrogen. Calibration points were obtained by rotating the precision aperture plate provided with the collimator and by varying the source temperature; a Leeds and Northrup optical pyrometer was used to set and monitor the blackbody temperature. Plots of $V_T G$ vs. effective irradiance for channels 1 to 10 are given in Figures B-4 to B-13, and plots of V_T vs. effective irradiance for PbS channels 11 to 20 are given in Figures B-14 to B-23. The effective irradiance values were computed using the equation:

$$H_{eff} = \int_0^\infty H(\lambda) \frac{s(\lambda)}{s(\lambda_s)} \, d\lambda \tag{3}$$

where

$H(\lambda)$ = spectral irradiance incident at the radiometer aperture (watt $cm^{-2} \mu^{-1}$)

$s(\lambda)$ = system spectral response

λ_s = wavelength of peak system response.

These integrations were performed on an IBM computor over the wavelength region to which the detector responded significantly.

4. VARIATION OF RESPONSIVITY WITH TEMPERATURE

A summary of the data presented in Figures B-4 through B-23 is given in Table A-1 of Appendix A. Past experience has shown that the responsivity of a PbS radiometer varies considerably with temperature; thus, the values given in Table A-1 apply only for calibration ambient conditions. The magnitude of the increase in sensitivity accompanying a decrease in temperature is usually independent of wavelength, except at the long wavelength cut off. Thus the responsivity as a function of temperature was determined both at 1.55 μ and at 2.7 μ by placing the instrument in an environmental chamber and varying the temperature while the instrument was irradiated with a constant source.

Plots of responsivity vs. temperature as determined by reading the output voltage from a thermistor bead located in the radiometer near the detector are given in Figure B-24. These plots were normalized to the response at 85°F, the temperature indicated by the radiometer thermistor during the absolute calibration described earlier.

It is interesting that the response in both wavelength regions goes through a maximum; the only explanation we can offer for this behavior is that changes in the characteristics of log amplifier with temperature eventually cause an overall decrease in system gain which counteracts the increased detector sensitivity as the temperature is decreased. All three E3G radiometers tested exhibited this type of behavior. The change in the photomultiplier section responsivity with temperature is considered insignificant and no correction was applied to the data obtained with this section of the radiometer.

5. RADIOMETER FIELD OF VIEW

The field of view curves for the two radiometer sections are given in Figures B-25 and B-26. These were measured by placing the instrument in collimated radiation and rotating it while the collimator remained fixed; the target used subtended an angle of approximately 0.005 radian.

6. RADIOMETER DATA REDUCTION METHODS

Equations (1) and (2) were used to reduce the telemetered voltages to effective irradiances. Since the effective irradiance by itself does not describe the spectral distribution of the target, the spectral irradiance was also computed. The procedure used for converting effective irradiance to spectral irradiance was to assume a target having an unknown absolute radiance but having the spectral distribution $H(\lambda)$. Thus

$$H_{eff} = \int_0^\infty H(\lambda) \frac{s(\lambda)}{s(\lambda_s)} \, d\lambda \tag{4}$$

for the assumed target, and

$$H_{Teff} = \int_0^\infty H_T(\lambda) \frac{s(\lambda)}{s(\lambda_s)} \, d\lambda \tag{5}$$

for the measured target. Since both targets have the same spectral distribution,

$$\frac{H_T(\lambda)}{H_{Teff}} = \frac{H(\lambda)}{H_{eff}} \quad \text{or} \quad H_T(\lambda) = \frac{H(\lambda)}{H_{eff}} H_{Teff} . \tag{6}$$

Combining Eqs. (1) and (6) and substituting B for $\frac{H(\lambda)B_{eff}}{H_{eff}}$ gives

$$H_T(\lambda) = B\,G\,V_T \tag{7}$$

and Eq. (2) becomes

$$H_T(\lambda) = B\,f(P) . \tag{8}$$

In order to determine how critically the conversion of effective irradiance to spectral irradiance depended on the target spectral distribution for the various channel system spectral responses, computations were performed for blackbodies at temperatures of 1500 to 6000°K in 500° increments. In addition, computations were performed for the 1700°, 2000°, 2100°, and 2200°C blackbodies used during calibration for a spectrally flat source and for the mean solar spectrum. The results are given in the second column on the lower half of Tables B-1 to B-20.

By way of illustration, the values of B for channel 1 given in Table B-1 vary only slightly with target spectral distribution, except for a temperature of 1500°C. At that temperature a significant contribution to the channel output voltage would be made by radiation at wavelengths far removed from the nominal pass band.

In order to assign the computed spectral irradiance to a particular wavelength region, a wavelength L_o was computed such that

$$\int_0^{L_o} H(\lambda)\,\frac{s(\lambda)}{s(\lambda_s)}\,d\lambda = \int_{L_o}^{\infty} H(\lambda)\,\frac{s(\lambda)}{s(\lambda_s)}\,d\lambda = \frac{H_{eff}}{2} . \tag{9}$$

Thus, one-half of the radiometer output would be contributed by irradiance in the wavelength region below L_o and the other half by irradiance at wavelengths longer than L_o. A wavelength interval $\Delta L = L_2 - L_1$ was also computed such that

$$\int_0^{L_1} H(\lambda)\,\frac{s(\lambda)}{s(\lambda_s)}\,d\lambda = 0.15\,H_{eff} \quad \text{and} \quad \int_0^{L_2} H(\lambda)\,\frac{s(\lambda)}{s(\lambda_s)}\,d\lambda = 0.85\,H_{eff} . \tag{10}$$

Thus, 70 percent of the radiometer output would be contributed by irradiance in the wavelength interval ΔL. The values of L_o, L_1, L_2, ΔL, $H(L_o)$, and H_{eff} are given in the top portion of Tables B-1 to B-20. The $T(L_o)$ given in the tables is the transmittance of the channel filter at wavelength L_o. The quantity labeled "C" on the lower tables is the factor used to convert H_{eff} to spectral radiance for a target filling the field of view of the radiometer. The other quantities given in the tables are:

T - LAMBDA (o) = peak filter transmittance

LAMBDA (o) = wavelength of peak filter transmittance, (μ)

LAMBDA (A) and LAMBDA (B) = wavelengths at which filter transmittance is one-half the peak transmittance, (μ)

LAMBDA (C) = (LAMBDA (A) + LAMBDA (B)) ÷ 2, (μ)

LAMBDA (S) = wavelength of peak system response, (μ)

W = Field of View (ster)

A_{eff} = Inverse effective irradiance responsivity for an auxiliary filter used in calibration. $A_{eff} = B_{eff}$ if instrument is calibrated with flight filter installed, as was the case for all Gemini-7 channels.

The system response curves used for the IBM computations are shown on an expanded scale in Figures B-27 through B-46. All UV filters were measured on a Cary 14 spectrophotometer and had off band rejection of 5.5 or more orders of magnitude. All infrared filters were measured with a Beckman DK2A spectrophotometer and exhibited off band rejection of 4 or more orders of magnitude. As a further check on off band rejection, all channels were tested against the blackbody set at 2200°C after the filters were installed, using various blocking filters to test for "leaks"; all channels behaved well and exhibited no off band leaks.

7. PRECISION AND ACCURACY OF CALIBRATION

The spread in the calibration data is shown in Figures B-4 to B-23. The spread is caused by many factors such as source temperature setting, meter reading, aperture area, neutral density filter calibration, etc.; in some cases the products of errors are involved, e.g., when the target voltage is multiplied by the attenuator factor. One could compute the responsivity based on each calibration point and compute standard deviations but there are not enough points to warrant this approach.

However, using the equipment and methods employed for the Gemini-7 instruments, the smallest spread in a large number of calibration points we ever observed on an absolute basis was ±5 percent. This was a very carefully controlled calibration

of an excellent radiometer equipped with a narrow interference filter and a PbS detector. The radiometer was a Model R4K, built by Barnes Engineering Co.; it operated linearly over 4 decades, was provided with a total radiation chopper, was state-of-the-art when purchased 5 years ago, and is probably still better than most radiometers one can buy today. Approximately 100 calibration points were obtained during the calibration, and approximately one-half of the data spread was traced to the voltage level recorder. The spread in the calibration data for the Gemini-7 instruments appears to be approximately twice that obtained during the Barnes radiometer calibration on the average.

Since one-half of the filters used on Gemini-7 peaked in the ultraviolet region where accurate absolute responsivities are not easy to measure, an investigation of UV calibration methods was undertaken. The main cause for concern was the rapid decrease in blackbody radiance with decreasing wavelengths and temperature in the 2000°C temperature range; another cause for concern was whether the Rocketdyne source was actually black in the ultraviolet region. A solar blind photomultiplier system that could be operated linearly over a range of 4 orders of magnitude was used for the tests to compare the blackbody with a Bureau of Standards Spectral Irradiance Standard.

The instrument was first calibrated absolutely at one wavelength, using both sources, and then relative spectral calibrations were performed with the two sources. A 2850 Å filter 200 Å wide was used for the absolute responsivity comparison, and points were taken at distances of 25, 50, and 100 inches from each source. It was found that although the spread in the responsivity values obtained with each source was 5 percent, the average responsivity value obtained with the blackbody differed from that obtained with the standard by only 1.2 percent.

The radiation from each source was then fed to a Leiss monochrometer, using the Leed's and Northrup optical pyrometer to set the blackbody temperature. The output voltages obtained with the Standard Lamp at 10 wavelengths in the interval 2500 and 3200 Å were divided by the irradiance values provided by the Bureau of Standards to determine the relative spectral response of the Leiss-photomultiplier system.

The relative spectral response was also determined, using the blackbody set at 2100°C. Several runs were made with each source and various Schott glasses were used to check for scattered radiation effects. The ratios of the relative spectral responsivity values obtained with the two sources were then taken. The ratios were constant to within ±3.5 percent; thus, it was concluded that the blackbody was in fact behaving according to Plank's law. Since there is no standard for wavelengths shorter than 2500 Å, it is necessary to assume that the blackbody source remains black down to 2200 Å where the shortest wavelength Gemini-7 filter peaked.

Table B-1. CHANNEL GT7-1, CURVE NO. 1

T-LAMBDA(C)	1.800E-01	LAMBDA(A)	0.2108	W	1.020E-03
LAMBDA(C)	0.2180	LAMBDA(B)	0.2322	1/W	9.804E 02
LAMBDA(C)	0.2215	DELTA LAMBDA	0.0214	A(EFF)	4.070E-13
LAMBDA(S)	0.2180			B(EFF)	4.070E-13
				C(EFF)	3.990E-10

TEMP K	L1	LO	L2	DELTA L	T(LO)	H(LO)	H(EFF)
1500	0.2297	0.2457	0.3806	0.1509	6.44E-03	7.73E-17	6.23E-18
2000	0.2225	0.2326	0.2436	0.0211	8.78E-02	4.60E-12	1.11E-13
2373	0.2204	0.2304	0.2404	0.0200	1.09E-01	6.03E-10	1.45E-11
2473	0.2200	0.2300	0.2399	0.0199	1.13E-01	1.75E-09	4.21E-11
2500	0.2199	0.2298	0.2398	0.0199	1.15E-01	2.29E-09	5.53E-11
3000	0.2183	0.2281	0.2380	0.0197	1.29E-01	1.49E-07	3.65E-09
3500	0.2172	0.2268	0.2368	0.0196	1.41E-01	3.03E-06	7.44E-08
4000	0.2165	0.2259	0.2359	0.0194	1.50E-01	2.97E-05	7.21E-07
4500	0.2159	0.2252	0.2352	0.0193	1.54E-01	1.74E-04	4.24E-06
5000	0.2154	0.2246	0.2346	0.0192	1.58E-01	7.22E-04	1.76E-05
5500	0.2150	0.2242	0.2342	0.0192	1.61E-01	2.33E-03	5.65E-05
6000	0.2147	0.2238	0.2338	0.0191	1.63E-01	6.18E-03	1.50E-04
FLAT	0.2125	0.2213	0.2315	0.0190	1.75E-01	9.77E-01	2.32E-02
SUN	0.2152	0.2244	0.2338	0.0186	1.59E-01	4.50E-03	1.05E-04

TEMP K	B	C
1500	5.05E-12	4.95E-09
2000	1.69E-11	1.65E-08
2373	1.69E-11	1.66E-08
2473	1.69E-11	1.66E-08
2500	1.69E-11	1.65E-08
3000	1.66E-11	1.62E-08
3500	1.66E-11	1.63E-08
4000	1.68E-11	1.64E-08
4500	1.67E-11	1.64E-08
5000	1.67E-11	1.64E-08
5500	1.68E-11	1.64E-08
6000	1.68E-11	1.65E-08
FLAT	1.71E-11	1.68E-08
SUN	1.75E-11	1.71E-08

Table B-2. CHANNEL GT7-2, CURVE NO. 2

T-LAMBDA(0)	2.080E-01	LAMBDA(A)	0.2265	W	1.020E-03
LAMBDA(0)	0.2340	LAMBDA(B)	0.2485	1/W	9.804E 02
LAMBDA(C)	0.2375	DELTA LAMBDA	0.0220	A(EFF)	4.060E-13
LAMBDA(S)	0.2340			B(EFF)	4.060E-13
				C(EFF)	3.980E-10

TEMP K	L1	L0	L2	DELTA L	T(L0)	H(L0)	H(EFF)
1500	0.2420	0.2531	0.2670	0.0250	6.58E-02	1.77E-15	4.72E-17
2000	0.2376	0.2483	0.2588	0.0212	1.10E-01	2.50E-11	6.50E-13
2373	0.2357	0.2462	0.2568	0.0211	1.28E-01	2.35E-09	6.32E-11
2473	0.2353	0.2458	0.2564	0.0211	1.32E-01	6.36E-09	1.71E-10
2500	0.2353	0.2457	0.2563	0.0210	1.33E-01	8.21E-09	2.21E-10
3000	0.2338	0.2439	0.2547	0.0209	1.51E-01	4.15E-07	1.11E-08
3500	0.2329	0.2427	0.2536	0.0207	1.63E-01	7.01E-06	1.86E-07
4000	0.2322	0.2418	0.2527	0.0205	1.73E-01	5.97E-05	1.55E-06
4500	0.2317	0.2411	0.2520	0.0203	1.84E-01	3.25E-04	8.12E-06
5000	0.2312	0.2406	0.2515	0.0203	1.93E-01	1.26E-03	3.06E-05
5500	0.2309	0.2402	0.2510	0.0201	2.00E-01	3.84E-03	9.08E-05
6000	0.2306	0.2398	0.2507	0.0201	2.03E-01	9.58E-03	2.25E-04
FLAT	0.2289	0.2378	0.2486	0.0197	1.98E-01	9.54E-01	2.36E-02
SUN	0.2304	0.2396	0.2519	0.0215	2.02E-01	6.34E-03	1.61E-04

TEMP K	B	C
1500	1.52E-11	1.49E-08
2000	1.56E-11	1.53E-08
2373	1.51E-11	1.48E-08
2473	1.51E-11	1.48E-08
2500	1.51E-11	1.48E-08
3000	1.51E-11	1.48E-08
3500	1.53E-11	1.50E-08
4000	1.56E-11	1.53E-08
4500	1.62E-11	1.59E-08
5000	1.67E-11	1.64E-08
5500	1.72E-11	1.68E-08
6000	1.73E-11	1.69E-08
FLAT	1.64E-11	1.61E-08
SUN	1.60E-11	1.57E-08

Table B-3. CHANNEL GT7-3, CURVE NO. 3

T-LAMBDA(0)	1.430E-01	LAMBDA(A)	0.2900	W	1.020E-03
LAMBDA(0)	0.2970	LAMBDA(B)	0.3180	1/W	9.804E 02
LAMBDA(C)	0.3040	DELTA LAMBDA	0.0280	A(EFF)	2.110E-12
LAMBDA(S)	0.2940			B(EFF)	2.110E-12
				C(EFF)	2.069E-09

TEMP K	L1	L0	L2	DELTA L	T(L0)	H(L0)	H(EFF)
1500	0.2910	0.3000	0.3118	0.0208	1.41E-01	4.58E-13	1.24E-14
2000	0.2888	0.2972	0.3082	0.0194	1.43E-01	1.62E-09	3.73E-11
2373	0.2877	0.2961	0.3068	0.0191	1.41E-01	7.73E-08	1.68E-09
2473	0.2874	0.2959	0.3065	0.0191	1.40E-01	1.79E-07	3.83E-09
2500	0.2874	0.2958	0.3064	0.0190	1.40E-01	2.22E-07	4.74E-09
3000	0.2863	0.2950	0.3053	0.0190	1.38E-01	6.00E-06	1.22E-07
3500	0.2854	0.2944	0.3044	0.0190	1.36E-01	6.39E-05	1.25E-06
4000	0.2847	0.2940	0.3038	0.0191	1.35E-01	3.78E-04	7.16E-06
4500	0.2841	0.2936	0.3033	0.0192	1.27E-01	1.44E-03	2.80E-05
5000	0.2836	0.2933	0.3029	0.0193	1.22E-01	4.23E-03	8.33E-05
5500	0.2832	0.2931	0.3026	0.0194	1.18E-01	1.02E-02	2.04E-04
6000	0.2828	0.2929	0.3023	0.0195	1.14E-01	2.14E-02	4.30E-04
FLAT	0.2806	0.2919	0.3011	0.0205	9.85E-02	9.44E-01	2.00E-02
SUN	0.2849	0.2942	0.3039	0.0190	1.36E-01	4.99E-02	9.62E-04

TEMP K	B	C
1500	7.80E-11	7.64E-08
2000	9.15E-11	8.97E-08
2373	9.73E-11	9.54E-08
2473	9.84E-11	9.65E-08
2500	9.89E-11	9.70E-08
3000	1.04E-10	1.02E-07
3500	1.08E-10	1.06E-07
4000	1.11E-10	1.09E-07
4500	1.09E-10	1.07E-07
5000	1.07E-10	1.05E-07
5500	1.06E-10	1.04E-07
6000	1.05E-10	1.03E-07
FLAT	9.94E-11	9.74E-08
SUN	1.10E-10	1.07E-07

Table B-4. CHANNEL GT7-4, CURVE NO. 4

T-LAMBDA(O)	7.900E-02	LAMBDA(A)	0.2540	W	1.020E-03
LAMBDA(O)	0.2620	LAMBDA(B)	0.2745	1/W	9.804E 02
LAMBDA(C)	0.2642	DELTA LAMBDA	0.0205	A(EFF)	1.590E-12
LAMBDA(S)	0.2600			B(EFF)	1.590E-12
				C(EFF)	1.559E-09

TEMP K	L1	LO	L2	DELTA L	T(LO)	H(LO)	H(EFF)
1500	0.2621	0.2707	0.2796	0.0175	6.64E-02	2.95E-14	5.85E-16
2000	0.2600	0.2685	0.2768	0.0168	7.26E-02	2.07E-10	4.26E-12
2373	0.2591	0.2674	0.2756	0.0165	7.45E-02	1.38E-08	2.90E-10
2473	0.2590	0.2672	0.2754	0.0164	7.47E-02	3.43E-08	7.26E-10
2500	0.2589	0.2672	0.2753	0.0164	7.47E-02	4.34E-08	9.18E-10
3000	0.2582	0.2662	0.2745	0.0163	7.57E-02	1.57E-06	3.35E-08
3500	0.2578	0.2656	0.2739	0.0161	7.63E-02	2.06E-05	4.41E-07
4000	0.2574	0.2651	0.2735	0.0161	7.68E-02	1.43E-04	3.06E-06
4500	0.2572	0.2647	0.2731	0.0159	7.72E-02	6.51E-04	1.38E-05
5000	0.2570	0.2644	0.2729	0.0159	7.75E-02	2.19E-03	4.62E-05
5500	0.2568	0.2642	0.2727	0.0159	7.77E-02	5.93E-03	1.24E-04
6000	0.2566	0.2640	0.2725	0.0159	7.79E-02	1.36E-02	2.83E-04
FLAT	0.2560	0.2630	0.2716	0.0156	7.84E-02	9.33E-01	1.89E-02
SUN	0.2588	0.2665	0.2741	0.0153	7.54E-02	1.77E-02	3.56E-04

TEMP K	B	C
1500	8.03E-11	7.88E-08
2000	7.74E-11	7.59E-08
2373	7.56E-11	7.41E-08
2473	7.52E-11	7.37E-08
2500	7.52E-11	7.37E-08
3000	7.42E-11	7.28E-08
3500	7.42E-11	7.28E-08
4000	7.45E-11	7.31E-08
4500	7.50E-11	7.35E-08
5000	7.55E-11	7.40E-08
5500	7.59E-11	7.44E-08
6000	7.63E-11	7.48E-08
FLAT	7.86E-11	7.71E-08
SUN	7.89E-11	7.74E-08

Table B-5. CHANNEL GT7-5, CURVE NO. 5

T-LAMBDA(O)	1.940E-01	LAMBDA(A)	0.2720	W	1.020E-03
LAMBOA(O)	0.2820	LAMBOA(B)	0.2860	1/W	9.804E 02
LAMBOA(C)	0.2790	OELTA LAMBDA	0.0140	A(EFF)	6.940E-13
LAMBDA(S)	0.2760			B(EFF)	6.940E-13
				C(EFF)	6.804E-10

TEMP K	L1	LO	L2	DELTA L	T(LO)	H(LO)	H(EFF)
1500	0.2767	0.2855	0.2968	0.0201	1.86E-01	1.26E-13	3.00E-15
2000	0.2747	0.2830	0.2932	0.0185	1.93E-01	6.15E-10	1.36E-11
2373	0.2739	0.2819	0.2918	0.0179	1.94E-01	3.49E-08	7.42E-10
2473	0.2737	0.2816	0.2915	0.0178	1.94E-01	8.40E-08	1.77E-09
2500	0.2736	0.2816	0.2914	0.0178	1.94E-01	1.05E-07	2.21E-09
3000	0.2729	0.2807	0.2902	0.0173	1.93E-01	3.30E-06	6.67E-08
3500	0.2724	0.2801	0.2895	0.0171	1.92E-01	3.91E-05	7.66E-07
4000	0.2720	0.2797	0.2889	0.0169	1.89E-01	2.45E-04	4.79E-06
4500	0.2717	0.2794	0.2884	0.0167	1.87E-01	1.02E-03	2.00E-05
5000	0.2714	0.2791	0.2881	0.0167	1.84E-01	3.19E-03	6.28E-05
5500	0.2712	0.2789	0.2878	0.0166	1.82E-01	8.13E-03	1.60E-04
6000	0.2710	0.2787	0.2875	0.0165	1.81E-01	1.78E-02	3.51E-04
FLAT	0.2701	0.2778	0.2865	0.0164	1.74E-01	9.63E-01	1.90E-02
SUN	0.2721	0.2797	0.2890	0.0169	1.89E-01	3.23E-02	6.33E-04

TEMP K	B	C
1500	2.92E-11	2.86E-08
2000	3.13E-11	3.07E-08
2373	3.26E-11	3.20E-08
2473	3.30E-11	3.23E-08
2500	3.30E-11	3.23E-08
3000	3.43E-11	3.36E-08
3500	3.54E-11	3.47E-08
4000	3.54E-11	3.47E-08
4500	3.53E-11	3.46E-08
5000	3.52E-11	3.45E-08
5500	3.52E-11	3.45E-08
6000	3.51E-11	3.44E-08
FLAT	3.52E-11	3.45E-08
SUN	3.55E-11	3.48E-08

Table B-6. CHANNEL GT7-6, CURVE NO. 6

T-LAMBDA(O)	1.590E-01	LAMBDA(A)	0.2370	W	1.020E-03
LAMBDA(O)	0.2475	LAMBDA(B)	0.2660	1/W	9.804E 02
LAMBDA(C)	0.2515	DELTA LAMBDA	0.0290	A(EFF)	6.300E-13
LAMBDA(S)	0.2475			B(EFF)	6.300E-13
				C(EFF)	6.170E-10

TEMP K	L1	LO	L2	DELTA L	T(LO)	H(LO)	H(EFF)
1500	0.2618	0.2810	0.3028	0.1010	3.54E-02	1.15E-14	6.47E-16
2000	0.2528	0.2680	0.2861	0.0333	7.34E-02	9.09E-11	3.62E-12
2373	0.2497	0.2640	0.2807	0.0310	9.12E-02	6.62E-09	2.51E-10
2473	0.2491	0.2632	0.2798	0.0307	9.47E-02	1.69E-08	6.34E-10
2500	0.2490	0.2630	0.2795	0.0305	9.56E-02	2.16E-08	8.05E-10
3000	0.2469	0.2601	0.2760	0.0291	1.08E-01	8.75E-07	3.13E-08
3500	0.2455	0.2581	0.2736	0.0281	1.18E-01	1.25E-05	4.37E-07
4000	0.2445	0.2567	0.2719	0.0274	1.25E-01	9.39E-05	3.20E-06
4500	0.2438	0.2556	0.2706	0.0268	1.31E-01	4.57E-04	1.52E-05
5000	0.2432	0.2548	0.2697	0.0265	1.36E-01	1.62E-03	5.30E-05
5500	0.2428	0.2542	0.2689	0.0261	1.38E-01	4.57E-03	1.48E-04
6000	0.2424	0.2536	0.2682	0.0258	1.40E-01	1.09E-02	3.48E-04
FLAT	0.2402	0.2509	0.2648	0.0246	1.52E-01	9.46E-01	2.80E-02
SUN	0.2447	0.2598	0.2744	0.0297	1.09E-01	9.29E-03	3.31E-04

TEMP K	B	C
1500	1.12E-11	1.10E-08
2000	1.58E-11	1.55E-08
2373	1.66E-11	1.63E-08
2473	1.68E-11	1.65E-08
2500	1.69E-11	1.66E-08
3000	1.76E-11	1.73E-08
3500	1.80E-11	1.77E-08
4000	1.85E-11	1.81E-08
4500	1.89E-11	1.86E-08
5000	1.93E-11	1.89E-08
5500	1.95E-11	1.91E-08
6000	1.97E-11	1.93E-08
FLAT	2.13E-11	2.09E-08
SUN	1.77E-11	1.73E-08

Table B-7. CHANNEL GT7-7, CURVE NO. 7

T-LAMBDA(O)	7.520E-02	LAMBDA(A)	0.2780	W	1.020E-03
LAMBDA(O)	0.2815	LAMBDA(B)	0.2852	1/W	9.804E 02
LAMBDA(C)	0.2816	DELTA LAMBDA	0.0072	A(EFF)	2.380E-12
LAMBDA(S)	0.2810			B(EFF)	2.380E-12
				C(EFF)	2.335E-09

TEMP K	L1	LO	L2	DELTA L	T(LO)	H(LO)	H(EFF)
1500	0.2787	0.2820	0.2860	0.0073	7.30E-02	1.46E-13	1.21E-15
2000	0.2783	0.2816	0.2854	0.0071	7.48E-02	7.41E-10	5.95E-12
2373	0.2781	0.2815	0.2851	0.0070	7.52E-02	4.15E-08	3.30E-10
2473	0.2780	0.2814	0.2851	0.0071	7.50E-02	9.91E-08	7.89E-10
2500	0.2780	0.2814	0.2851	0.0071	7.50E-02	1.24E-07	9.87E-10
3000	0.2778	0.2813	0.2849	0.0071	7.47E-02	3.75E-06	2.99E-08
3500	0.2777	0.2812	0.2847	0.0070	7.45E-02	4.30E-05	3.42E-07
4000	0.2775	0.2811	0.2847	0.0072	7.42E-02	2.68E-04	2.13E-06
4500	0.2774	0.2810	0.2846	0.0072	7.40E-02	1.12E-03	8.85E-06
5000	0.2774	0.2810	0.2845	0.0071	7.40E-02	3.48E-03	2.77E-05
5500	0.2773	0.2809	0.2845	0.0072	7.30E-02	8.78E-03	7.05E-05
6000	0.2772	0.2809	0.2844	0.0072	7.30E-02	1.91E-02	1.53E-04
FLAT	0.2767	0.2807	0.2842	0.0075	7.12E-02	9.89E-01	8.12E-03
SUN	0.2775	0.2811	0.2846	0.0071	7.42E-02	3.52E-02	2.80E-04

TEMP K	B	C
1500	2.85E-10	2.80E-07
2000	2.96E-10	2.90E-07
2373	2.99E-10	2.93E-07
2473	2.99E-10	2.93E-07
2500	2.99E-10	2.93E-07
3000	2.99E-10	2.93E-07
3500	2.99E-10	2.93E-07
4000	2.99E-10	2.93E-07
4500	3.00E-10	2.94E-07
5000	2.99E-10	2.94E-07
5500	2.97E-10	2.92E-07
6000	2.97E-10	2.91E-07
FLAT	2.90E-10	2.84E-07
SUN	2.99E-10	2.93E-07

Table B-8. CHANNEL GT7-8, CURVE NO. 8

T-LAMBDA(0)	8.180E-02	LAMBDA(A)	0.3022	W	1.020E-03
LAMBDA(0)	0.3055	LAMBDA(B)	0.3102	1/W	9.804E 02
LAMBDA(C)	0.3062	DELTA LAMBDA	0.0080	A(EFF)	1.090E-11
LAMBDA(S)	0.3050			B(EFF)	1.090E-11
				C(EFF)	1.069E-08

TEMP K	L1	LO	L2	DELTA L	T(LO)	H(LO)	H(EFF)
1500	0.3020	0.3059	0.3102	0.0082	8.15E-02	1.41E-12	1.30E-14
2000	0.3013	0.3055	0.3096	0.0083	8.18E-02	3.65E-09	3.32E-11
2373	0.3009	0.3053	0.3093	0.0084	8.15E-02	1.49E-07	1.36E-09
2473	0.3008	0.3052	0.3093	0.0085	8.13E-02	3.34E-07	3.04E-09
2500	0.3008	0.3052	0.3092	0.0084	8.13E-02	4.10E-07	3.73E-09
3000	0.3002	0.3050	0.3090	0.0088	8.10E-02	9.59E-06	8.76E-08
3500	0.2997	0.3048	0.3089	0.0092	7.84E-02	8.91E-05	8.39E-07
4000	0.2991	0.3047	0.3087	0.0096	7.72E-02	4.77E-04	4.58E-06
4500	0.2986	0.3046	0.3086	0.0100	7.59E-02	1.76E-03	1.72E-05
5000	0.2979	0.3044	0.3085	0.0106	7.35E-02	4.95E-03	4.99E-05
5500	0.2971	0.3043	0.3084	0.0113	7.24E-02	1.16E-02	1.19E-04
6000	0.2961	0.3042	0.3084	0.0123	7.12E-02	2.36E-02	2.48E-04
FLAT	0.2557	0.3032	0.3078	0.0521	5.75E-02	8.54E-01	1.16E-02
SUN	0.2994	0.3047	0.3087	0.0093	7.72E-02	6.70E-02	6.35E-04

TEMP K	B	C
1500	1.18E-09	1.16E-06
2000	1.20E-09	1.18E-06
2373	1.20E-09	1.17E-06
2473	1.20E-09	1.17E-06
2500	1.20E-09	1.17E-06
3000	1.19E-09	1.17E-06
3500	1.16E-09	1.14E-06
4000	1.13E-09	1.11E-06
4500	1.11E-09	1.09E-06
5000	1.08E-09	1.06E-06
5500	1.06E-09	1.04E-06
6000	1.04E-09	1.02E-06
FLAT	7.99E-10	7.84E-07
SUN	1.15E-09	1.13E-06

Table B-9. CHANNEL GT7-9, CURVE NO. 9

T-LAMBDA(O)	7.560E-02	LAMBDA(A)	0.2840	W	1.020E-03
LAMBDA(O)	0.2880	LAMBDA(B)	0.2930	1/W	9.804E 02
LAMBDA(C)	0.2885	DELTA LAMBDA	0.0090	A(EFF)	3.190E-12
LAMBDA(S)	0.2870			B(EFF)	3.190E-12
				C(EFF)	3.127E-09

TEMP K	L1	LO	L2	DELTA L	T(LO)	H(LO)	H(EFF)
1500	0.2845	0.2888	0.2940	0.0095	7.35E-02	2.71E-13	2.89E-15
2000	0.2838	0.2881	0.2929	0.0091	7.53E-02	1.14E-09	1.16E-11
2373	0.2834	0.2879	0.2925	0.0091	7.54E-02	5.82E-08	5.91E-10
2473	0.2833	0.2878	0.2924	0.0091	7.52E-02	1.37E-07	1.39E-09
2500	0.2833	0.2878	0.2924	0.0091	7.52E-02	1.70E-07	1.72E-09
3000	0.2830	0.2875	0.2921	0.0091	7.45E-02	4.80E-06	4.85E-08
3500	0.2827	0.2874	0.2919	0.0092	7.43E-02	5.21E-05	5.28E-07
4000	0.2824	0.2872	0.2917	0.0093	7.38E-02	3.14E-04	3.17E-06
4500	0.2822	0.2871	0.2916	0.0094	7.36E-02	1.27E-03	1.28E-05
5000	0.2820	0.2871	0.2915	0.0095	7.36E-02	3.86E-03	3.91E-05
5500	0.2818	0.2870	0.2914	0.0096	7.34E-02	9.65E-03	9.77E-05
6000	0.2817	0.2869	0.2914	0.0097	7.23E-02	2.05E-02	2.09E-04
FLAT	0.2802	0.2865	0.2910	0.0108	6.80E-02	9.70E-01	1.05E-02
SUN	0.2824	0.2873	0.2918	0.0094	7.41E-02	4.04E-02	4.14E-04

TEMP K	B	C
1500	2.99E-10	2.94E-07
2000	3.13E-10	3.06E-07
2373	3.14E-10	3.08E-07
2473	3.15E-10	3.08E-07
2500	3.14E-10	3.08E-07
3000	3.15E-10	3.09E-07
3500	3.15E-10	3.09E-07
4000	3.16E-10	3.10E-07
4500	3.16E-10	3.10E-07
5000	3.15E-10	3.09E-07
5500	3.15E-10	3.09E-07
6000	3.12E-10	3.06E-07
FLAT	2.94E-10	2.88E-07
SUN	3.12E-10	3.06E-07

Table B-10. CHANNEL GT7-10, CURVE NO. 10

T-LAMBDA(O)	1.700E-01	LAMBDA(A)	0.2110	W	1.020E-03
LAMBDA(O)	0.2190	LAMBDA(B)	0.2320	1/W	9.804E 02
LAMBDA(C)	0.2215	DELTA LAMBDA	0.0210	A(EFF)	4.180E-13
LAMBDA(S)	0.2190			B(EFF)	4.180E-13
				C(EFF)	4.098E-10

TEMP K	L1	LO	L2	DELTA L	T(LO)	H(LO)	H(EFF)
1500	0.2299	0.2486	0.3815	0.1516	2.80E-03	5.29E-17	6.36E-18
2000	0.2224	0.2325	0.2440	0.0216	8.14E-02	4.46E-12	1.09E-13
2373	0.2203	0.2302	0.2402	0.0199	1.05E-01	6.00E-10	1.42E-11
2473	0.2199	0.2298	0.2397	0.0198	1.09E-01	1.74E-09	4.13E-11
2500	0.2198	0.2297	0.2395	0.0197	1.09E-01	2.29E-09	5.42E-11
3000	0.2182	0.2280	0.2377	0.0195	1.25E-01	1.51E-07	3.59E-09
3500	0.2172	0.2267	0.2365	0.0193	1.34E-01	3.04E-06	7.31E-08
4000	0.2164	0.2258	0.2356	0.0192	1.41E-01	2.94E-05	7.09E-07
4500	0.2159	0.2251	0.2349	0.0190	1.45E-01	1.73E-04	4.18E-06
5000	0.2154	0.2246	0.2344	0.0190	1.48E-01	7.16E-04	1.73E-05
5500	0.2150	0.2241	0.2340	0.0190	1.51E-01	2.31E-03	5.57E-05
6000	0.2147	0.2237	0.2336	0.0189	1.53E-01	6.12E-03	1.48E-04
FLAT	0.2124	0.2212	0.2313	0.0189	1.64E-01	9.68E-01	2.31E-02
SUN	0.2152	0.2244	0.2336	0.0184	1.49E-01	4.46E-03	1.03E-04

TEMP K	B	C
1500	3.48E-12	3.41E-09
2000	1.71E-11	1.67E-08
2373	1.76E-11	1.73E-08
2473	1.77E-11	1.73E-08
2500	1.77E-11	1.73E-08
3000	1.76E-11	1.72E-08
3500	1.74E-11	1.70E-08
4000	1.73E-11	1.70E-08
4500	1.73E-11	1.69E-08
5000	1.73E-11	1.69E-08
5500	1.73E-11	1.70E-08
6000	1.73E-11	1.70E-08
FLAT	1.75E-11	1.72E-08
SUN	1.80E-11	1.77E-08

Table B-11. CHANNEL GT7-11, CURVE NO. 11

1-LAMBDA(O)	4.070E-01	LAMBDA(A)	0.9870	W	3.860E-04
LAMBDA(O)	1.1100	LAMBDA(B)	1.1490	1/W	2.591E 03
LAMBDA(O)	1.0680	DELTA LAMBDA	0.1620	A(EFF)	1.100E-05
LAMBDA(S)	1.1100			B(EFF)	1.100E-05
				C(EFF)	2.850E-02

TEMP K	LI	LO	L2	DELTA L	T(LO)	H(LO)	H(EFF)
1500	1.0110	1.0720	1.1150	0.1040	3.15E-01	1.17E-05	1.80E-06
1923	1.0070	1.0670	1.1130	0.1060	3.17E-01	8.37E-05	1.32E-05
2000	1.0060	1.0660	1.1130	0.1070	3.18E-01	1.10E-04	1.73E-05
2273	1.0050	1.0630	1.1120	0.1070	3.20E-01	2.47E-04	3.91E-05
2373	1.0040	1.0630	1.1120	0.1080	3.20E-01	3.18E-04	5.04E-05
2500	1.0040	1.0620	1.1110	0.1070	3.20E-01	4.25E-04	6.75E-05
3000	1.0020	1.0590	1.1100	0.1080	3.22E-01	1.06E-03	1.69E-04
3500	1.0010	1.0570	1.1100	0.1090	3.23E-01	2.05E-03	3.27E-04
4000	1.0000	1.0560	1.1090	0.1090	3.23E-01	3.39E-03	5.39E-04
4500	1.0000	1.0550	1.1090	0.1090	3.24E-01	5.04E-03	8.01E-04
5000	0.9990	1.0540	0.1080	0.1090	3.25E-01	6.97E-03	1.11E-03
5500	0.9990	1.0530	1.1080	0.1090	3.25E-01	9.14E-03	1.45E-03
6000	0.9990	1.0530	1.1080	0.1090	3.25E-01	1.15E-02	1.82E-03
FLAT	1.0030	1.0600	1.1110	0.1080	3.21E-01	7.57E-01	1.21E-01
SUN	1.0000	1.0540	1.1080	0.1080	3.25E-01	5.01E-02	7.96E-03

TEMP K	B	C
1500	7.16E-05	1.86E-01
1923	7.00E-05	1.81E-01
2000	6.98E-05	1.81E-01
2273	6.94E-05	1.80E-01
2373	6.93E-05	1.80E-01
2500	6.92E-05	1.79E-01
3000	6.91E-05	1.79E-01
3500	6.91E-05	1.79E-01
4000	6.91E-05	1.79E-01
4500	6.92E-05	1.79E-01
5000	6.93E-05	1.80E-01
5500	6.94E-05	1.80E-01
6000	6.94E-05	1.80E-01
FLAT	6.88E-05	1.78E-01
SUN	6.93E-05	1.80E-01

Table B-12. CHANNEL GT7-12, CURVE NO. 12

T-LAMBDA(0)	5.710E-01	LAMBDA(A)	1.1990	W	3.860E-04
LAMBDA(0)	1.2750	LAMBDA(B)	1.3210	1/W	2.591E 03
LAMBDA(C)	1.2600	DELTA LAMBDA	0.1220	A(EFF)	5.200E-06
LAMBDA(S)	1.2750			B(EFF)	5.200E-06
				C(EFF)	1.347E-02

TEMP K	LI	LO	L2	DELTA L	T(LO)	H(LO)	H(EFF)
1500	1.2170	1.2740	1.3300	0.1130	5.68E-01	2.72E-05	3.43E-06
1923	1.2130	1.2700	1.3260	0.1130	5.58E-01	1.39E-04	1.81E-05
2000	1.2120	1.2890	1.3250	0.1130	5.58E-01	1.74E-04	2.28E-05
2273	1.2110	1.2680	1.3230	0.1120	5.53E-01	3.43E-04	4.52E-05
2373	1.2100	1.2670	1.3230	0.1130	5.51E-01	4.22E-04	5.59E-05
2500	1.2100	1.2670	1.3220	0.1120	5.51E-01	5.39E-04	7.15E-05
3000	1.2080	1.2650	1.3200	0.1120	5.46E-01	1.15E-03	1.55E-04
3500	1.2070	1.2640	1.3190	0.1120	5.43E-01	2.01E-03	2.71E-04
4000	1.2060	1.2630	1.3180	0.1120	5.41E-01	3.07E-03	4.15E-04
4500	1.2050	1.2630	1.3170	0.1120	5.41E-01	4.31E-03	5.84E-04
5000	1.2050	1.2620	1.3170	0.1120	5.38E-01	5.67E-03	7.72E-04
5500	1.2040	1.2620	1.3160	0.1120	5.38E-01	7.16E-03	9.76E-04
6000	1.2040	1.2610	1.3160	0.1120	5.36E-01	8.72E-03	1.19E-03
FLAT	1.2100	1.2680	1.3230	0.1130	5.53E-01	9.63E-01	1.28E-01
SUN	1.2040	1.2620	1.3160	0.1120	5.38E-01	4.11E-02	5.57E-03

TEMP K	B	C
1500	4.12E-05	1.07E-01
1923	4.00E-05	1.04E-01
2000	3.98E-05	1.03E-01
2273	3.95E-05	1.02E-01
2373	3.92E-05	1.02E-01
2500	3.92E-05	1.02E-01
3000	3.88E-05	1.00E-01
3500	3.86E-05	9.99E-02
4000	3.84E-05	9.94E-02
4500	3.83E-05	9.93E-02
5000	3.82E-05	9.89E-02
5500	3.82E-05	9.89E-02
6000	3.80E-05	9.85E-02
FLAT	3.93E-05	1.02E-01
SUN	3.83E-05	9.93E-02

Table B-13. CHANNEL GT7-13, CURVE NO. 13

T-LAMBDA(0)	5.300E-01	LAMBDA(A)	1.5000	W	3.860E-04
LAMBDA(0)	1.5750	LAMBDA(B)	1.6080	1/W	2.591E 03
LAMBDA(0)	1.5540	DELTA LAMBDA	0.1080	A(EFF)	3.550E-06
LAMBDA(S)	1.5750			B(EFF)	3.550E-06
				C(EFF)	9.197E-03

TEMP K	LI	LO	L2	DELTA L	T(LO)	H(LO)	H(EFF)
1500	1.5170	1.5630	1.5990	0.0820	5.00E-01	3.72E-05	3.97E-06
1923	1.5150	1.5610	1.5990	0.0840	4.96E-01	1.43E-04	1.55E-05
2000	1.5150	1.5610	1.5980	0.0850	4.96E-01	1.72E-04	1.86E-05
2273	1.5140	1.5610	1.5980	0.0840	4.96E-01	3.02E-04	3.27E-05
2373	1.5140	1.5600	1.5980	0.0840	4.93E-01	3.57E-04	3.90E-05
2500	1.5140	1.5600	1.5980	0.0840	4.93E-01	4.37E-04	4.77E-05
3000	1.5140	1.5600	1.5980	0.0840	4.93E-01	8.27E-04	9.04E-05
3500	1.5130	1.5590	1.5970	0.0840	4.91E-01	1.31E-03	1.44E-04
4000	1.5130	1.5590	1.5970	0.0840	4.91E-01	1.88E-03	2.07E-04
4500	1.5150	1.5590	1.5970	0.0840	4.91E-01	2.51E-03	2.76E-04
5000	1.5120	1.5580	1.5970	0.0850	4.88E-01	3.18E-03	3.51E-04
5500	1.5120	1.5580	1.5970	0.0850	4.88E-01	3.89E-03	4.30E-04
6000	1.5120	1.5580	1.5970	0.0850	4.88E-01	4.64E-03	5.13E-04
FLAT	1.5150	1.5610	1.5990	0.0840	4.96E-01	9.28E-01	1.01E-01
SUN	1.5120	1.5580	1.5970	0.0650	4.88E-01	2.15E-02	2.37E-03

TEMP K	B	C
1500	3.33E-05	8.62E-02
1923	3.28E-05	8.49E-02
2000	3.28E-05	8.49E-02
2273	3.27E-05	8.48E-02
2373	3.25E-05	8.43E-02
2500	3.25E-05	8.43E-02
3000	3.25E-05	8.41E-02
3500	3.23E-05	8.37E-02
4000	3.23E-05	8.36E-02
4500	3.23E-05	8.36E-02
5000	3.21E-05	8.33E-02
5500	3.21E-05	8.32E-02
6000	3.21E-05	8.32E-02
FLAT	3.27E-05	8.48E-02
SUN	3.21E-05	8.32E-02

Table B-14. CHANNEL GT7-14, CURVE NO. 14

T-LAMBDA(0)	4.060E-01	LAMBDA(A)	1.3020	W	3.860E-04
LAMBDA(0)	1.3750	LAMBDA(B)	1.4300	1/W	2.591E 03
LAMBDA(C)	1.3660	DELTA LAMBDA	0.1280	A(EFF)	6.020E-06
LAMBDA(S)	1.4000			B(EFF)	6.020E-06
				C(EFF)	1.560E-02

TEMP K	L1	LO	L2	DELTA L	T(LO)	H(LO)	H(EFF)
1500	1.3240	1.3760	1.4210	0.0970	4.05E-01	3.22E-05	3.92E-08
1923	1.3210	1.3750	1.4190	0.0980	4.06E-01	1.49E-04	1.83E-05
2000	1.3210	1.3750	1.4190	0.0980	4.06E-01	1.84E-04	2.26E-05
2273	1.3200	1.3740	1.4180	0.0980	4.04E-01	3.45E-04	4.28E-05
2372	1.3200	1.3730	1.4180	0.0980	4.01E-01	4.17E-04	5.21E-05
2500	1.3190	1.3730	1.4180	0.0990	4.01E-01	5.24E-04	6.54E-05
3000	1.3180	1.3720	1.4170	0.0990	3.99E-01	1.06E-03	1.34E-04
3500	1.3170	1.3710	1.4170	0.1000	3.96E-01	1.78E-03	2.26E-04
4000	1.3170	1.3700	1.4160	0.0990	3.94E-01	2.64E-03	3.37E-04
4500	1.3160	1.3700	1.4160	0.1000	3.94E-01	3.63E-03	4.63E-04
5000	1.3160	1.3700	1.4160	0.1000	3.94E-01	4.71E-03	6.02E-04
5500	1.3160	1.3690	1.4160	0.1000	3.92E-01	5.85E-03	7.52E-04
6000	1.3160	1.3690	1.4150	0.0990	3.92E-01	7.07E-03	9.09E-04
FLAT	1.3200	1.3740	1.4190	0.0990	4.04E-01	9.81E-01	1.22E-01
SUN	1.3150	1.3690	1.4150	0.1000	3.92E-01	3.31E-02	4.25E-03

TEMP K	B	C
1500	4.94E-05	1.28E-01
1923	4.90E-05	1.27E-01
2000	4.90E-05	1.27E-01
2273	4.86E-05	1.26E-01
2373	4.82E-05	1.25E-01
2500	4.82E-05	1.25E-01
3000	4.78E-05	1.24E-01
3500	4.75E-05	1.23E-01
4000	4.72E-05	1.22E-01
4500	4.71E-05	1.22E-01
5000	4.71E-05	1.22E-01
5500	4.69E-05	1.21E-01
6000	4.68E-05	1.21E-01
FLAT	4.85E-05	1.26E-01
SUN	4.69E-05	1.21E-01

Table B-15. CHANNEL GT7-15, CURVE NO. 15

T-LAMBDA(0)	7.240E-01	LAMBDA(A)	2.7450	W	3.860E-04
LAMBDA(0)	2.8750	LAMBDA(B)	3.1290	1/W	2.591E 03
LAMBDA(0)	2.9370	DELTA LAMBDA	0.3840	A(EFF)	8.020E-06
LAMBDA(S)	2.8000			B(EFF)	8.020E-06
				C(EFF)	2.078E-02

TEMP K	L1	LO	L2	DELTA L	T(LO)	H(LO)	H(EFF)
1550	2.7190	2.8030	2.9350	0.2160	6.54E-01	3.25E-05	7.02E-06
1923	2.7160	2.8010	2.9290	0.2130	6.52E-01	7.30E-05	1.55E-05
2000	2.7150	2.8000	2.9280	0.2130	6.51E-01	8.23E-05	1.73E-05
2273	2.7140	2.7990	2.9260	0.2120	6.45E-01	1.15E-04	2.44E-05
2373	2.7130	2.7990	2.9250	0.2120	6.45E-01	1.28E-04	2.71E-05
2500	2.7120	2.7990	2.9240	0.2120	6.45E-01	1.46E-04	3.08E-05
3000	2.7090	2.7970	2.9210	0.2120	6.33E-01	2.17E-04	4.64E-05
3500	2.7060	2.7960	2.9190	0.2130	6.27E-01	2.95E-04	6.34E-05
4000	2.7030	2.7950	2.9178	0.2140	6.22E-01	3.77E-04	8.16E-05
4500	2.7000	2.7940	2.9160	0.2160	6.16E-01	4.62E-04	1.01E-04
5000	2.6970	2.7930	2.9150	0.2160	6.11E-01	5.48E-04	1.20E-04
5500	2.6940	2.7920	2.9140	0.2200	6.65E-01	6.36E-04	1.41E-04
6000	2.6910	2.7910	2.9120	0.2210	5.99E-01	7.24E-04	1.61E-04
FLAT	2.7230	2.8080	2.9500	0.2270	6.60E-01	9.37E-01	2.14E-01
SUN	2.6920	2.7910	2.9120	0.2200	5.99E-01	3.22E-03	7.16E-04

TEMP K	B	C
1500	3.71E-05	9.62E-02
1923	3.78E-05	9.78E-02
2000	3.81E-05	9.87E-02
2273	3.80E-05	9.84E-02
2373	3.79E-05	9.83E-02
2500	3.79E-05	9.82E-02
3000	3.76E-05	9.74E-02
3500	3.76E-05	9.67E-02
4000	3.71E-05	9.60E-02
4500	3.68E-05	9.53E-02
5000	5.65E-05	9.46E-02
5500	3.63E-05	9.39E-02
6000	3.60E-05	9.33E-02
FLAT	3.52E-05	9.11E-02
SUN	3.61E-05	9.34E-02

Table B-16. CHANNEL GT8-16, CURVE NO. 16

T-LAMBDA(O)	4.600E-01	LAMBDA(A)	1.8180	W	3.860E-04
LAMBDA(O)	1.9300	LAMBDA(B)	1.9540	1/W	2.591E 03
LAMBDA(O)	1.8860	DELTA LAMBDA	0.1360	A(EFF)	3.700E-06
LAMBDA(S)	1.9300			B(EFF)	3.700E-06
				C(EFF)	9.585E-03

TEMP K	L1	LO	L2	DELTA L	T(LO)	H(LO)	H(EFF)
1500	1.8360	1.8980	1.9420	0.1060	4.11E-01	3.99E-05	5.20E-06
1923	1.8350	1.8970	1.9410	0.1060	4.07E-01	1.22E-04	1.61E-05
2000	1.8350	1.8970	1.9410	0.1060	4.07E-01	1.42E-04	1.88E-05
2273	1.8350	1.8960	1.9410	0.1060	4.02E-01	2.25E-04	3.01E-05
2373	1.8340	1.8960	1.9410	0.1070	4.02E-01	2.60E-04	3.48E-05
2500	1.8340	1.8960	1.9410	0.1070	4.02E-01	3.08E-04	4.13E-05
3000	1.8340	1.8950	1.9400	0.1060	3.98E-01	5.24E-04	7.09E-05
3500	1.8353	1.8950	1.9400	0.1070	3.98E-01	7.81E-04	1.06E-04
4000	1.8330	1.8950	1.9400	0.1070	3.98E-01	1.07E-03	1.45E-04
4500	1.8330	1.8940	1.9400	0.1070	3.93E-01	1.36E-03	1.87E-04
5000	1.8330	1.8940	1.9400	0.1070	3.93E-01	1.68E-03	2.31E-04
5500	1.8330	1.8940	1.9390	0.1060	3.93E-01	2.02E-03	2.76E-04
6000	1.8330	1.8940	1.9390	0.1060	3.93E-01	2.36E-03	3.23E-04
FLAT	1.8360	1.8980	1.9420	0.1060	4.11E-01	8.95E-01	1.17E-01
SUN	1.8330	1.8940	1.9390	0.1060	3.93E-01	1.07E-02	1.47E-03

TEMP K	B	C
1500	2.84E-05	7.35E-02
1923	2.80E-05	7.25E-02
2000	2.80E-05	7.25E-02
2273	2.77E-05	7.16E-02
2373	2.76E-05	7.16E-02
2500	2.76E-05	7.16E-02
3000	2.73E-05	7.08E-02
3500	2.73E-05	7.07E-02
4000	2.73E-05	7.07E-02
4500	2.70E-05	7.00E-02
5000	2.70E-05	6.99E-02
5500	2.70E-05	6.99E-02
6000	2.70E-05	6.99E-02
FLAT	2.83E-05	7.34E-02
SUN	2.70E-05	6.99E-02

Table B-17. CHANNEL GT7-17, CURVE NO. 17

T-LAMBDA(O)	4.500E-01	LAMBDA(A)	2.1280	W	3.860E-04
LAMBDA(O)	2.1750	LAMBDA(B)	2.2400	1/W	2.591E 03
LAMBDA(O)	2.1840	DELTA LAMBDA	0.1120	A(EFF)	3.800E-06
LAMBDA(S)	2.1750			B(EFF)	3.800E-06
				C(EFF)	9.845E-03

TEMP K	L1	LO	L2	DELTA L	T(LO)	H(LO)	H(EFF)
1500	2.1400	2.1830	2.2320	0.0920	4.06E-01	3.89E-05	4.67E-06
1923	2.1390	2.1820	2.2310	0.0920	4.11E-01	1.06E-04	1.25E-05
2000	2.1390	2.1820	2.2310	0.0920	4.11E-01	1.21E-04	1.44E-05
2273	2.1390	2.1820	2.2310	0.0920	4.11E-01	1.83E-04	2.18E-05
2373	2.1380	2.1810	2.2310	0.0930	4.16E-01	2.12E-04	2.48E-05
2500	2.1380	2.1810	2.2310	0.0930	4.16E-01	2.46E-04	2.88E-05
3000	2.1380	2.1810	2.2300	0.0920	4.16E-01	3.99E-04	4.68E-05
3500	2.1380	2.1810	2.2300	0.0920	4.16E-01	5.73E-04	6.71E-05
4000	2.1380	2.1810	2.2300	0.0920	4.16E-01	7.62E-04	8.92E-05
4500	2.1380	2.1800	2.2300	0.0920	4.22E-01	9.75E-04	1.13E-04
5000	2.1370	2.1800	2.2300	0.0930	4.22E-01	1.18E-03	1.37E-04
5500	2.1370	2.1800	2.2300	0.0930	4.22E-01	1.40E-03	1.62E-04
6000	2.1370	2.1800	2.2300	0.0930	4.22E-01	1.62E-03	1.87E-04
FLAT	2.1400	2.1830	2.2330	0.0930	4.06E-01	9.02E-01	1.09E-01
SUN	2.1370	2.1800	2.2300	0.0930	4.22E-01	7.31E-03	8.44E-04

TEMP K	B	C
1500	3.16E-05	8.19E-02
1923	3.20E-05	8.30E-03
2000	3.20E-05	8.30E-02
2273	3.20E-05	8.30E-02
2373	3.25E-05	8.41E-02
2500	3.25E-05	8.41E-02
3000	3.25E-05	8.41E-02
3500	3.25E-05	8.41E-02
4000	3.25E-05	8.41E-02
4500	3.29E-05	8.53E-02
5000	3.29E-05	8.53E-02
5500	3.29E-05	8.52E-02
6000	3.29E-05	8.52E-02
FLAT	3.16E-05	8.18E-02
SUN	3.29E-05	8.53E-02

Table B-18. CHANNEL GT7-18, CURVE NO. 18

T-LAMBDA(0)	5.050E-01	LAMBDA(A)	2.6710	W	3.860E-04
LAMBDA(0)	2.7200	LAMBDA(B)	2.7750	1/W	2.591E 03
LAMBDA(0)	2.7230	DELTA LAMBDA	0.1040	A(EFF)	5.300E-06
LAMBDA(S)	2.7000			B(EFF)	5.300E-06
				C(EFF)	1.373E-02

TEMP K	L1	L0	L2	DELTA L	T(LO)	H(LO)	H(EFF)
1500	2.6720	2.7110	2.7580	0.0860	4.75E-01	3.10E-05	3.10E-06
1923	2.6720	2.7100	2.7570	0.0850	4.72E-01	7.00E-05	7.00E-06
2000	2.6720	2.7100	2.7570	0.0850	4.72E-01	7.84E-05	7.85E-06
2273	2.6710	2.7100	2.7570	0.0860	4.72E-01	1.11E-04	1.11E-05
2373	2.6710	2.7100	2.7570	0.0860	4.72E-01	1.24E-04	1.24E-05
2500	2.6710	2.7100	2.7570	0.0860	4.72E-01	1.41E-04	1.41E-05
3000	2.6710	2.7100	2.7570	0.0860	4.72E-01	2.13E-04	2.13E-05
3500	2.6710	2.7100	2.7560	0.0850	4.72E-01	2.91E-04	2.92E-05
4000	2.6710	2.7100	2.7560	0.0850	4.72E-01	3.74E-04	3.75E-05
4500	2.6700	2.7100	2.7560	0.0860	4.72E-01	4.60E-04	4.61E-05
5000	2.6700	2.7090	2.7560	0.0860	4.75E-01	5.55E-04	5.50E-05
5500	2.6700	2.7090	2.7560	0.0860	4.75E-01	6.46E-04	6.40E-05
6000	2.6700	2.7090	2.7560	0.0860	4.75E-01	7.39E-04	7.32E-05
FLAT	2.6730	2.7120	2.7590	0.0860	4.79E-01	8.88E-01	8.89E-02
SUN	2.6700	2.7090	2.7560	0.0860	4.75E-01	3.29E-03	3.25E-04

TEMP K	B	C
1500	5.30E-05	1.37E-01
1923	5.30E-05	1.37E-01
2000	5.30E-05	1.37E-01
2273	5.30E-05	1.37E-01
2373	5.30E-05	1.37E-01
2500	5.30E-05	1.37E-01
3000	5.29L-05	1.37E-01
3500	5.29E-05	1.37E-01
4000	5.29E-05	1.37E-01
4500	5.29E-05	1.37E-01
5000	5.35E-05	1.39E-01
5500	5.35E-05	1.39E-01
6000	5.35E-05	1.39E-01
FLAT	5.29E-05	1.37E-01
SUN	5.35E-05	1.39E-01

Table B-19. CHANNEL GT7-19, CURVE NO. 19

T-LAMBDA(0)	4.810E-01	LAMBDA(A)	2.7310	W	3.860E-04
LAMBDA(0)	2.8250	LAMBDA(B)	2.8550	1/W	2.591E 03
LAMBDA(C)	2.7930	DELTA LAMBDA	0.1240	A(EFF)	1.100E-05
LAMBDA(S)	2.7500			B(EFF)	1.100E-05
				C(EFF)	2.850E-02

TEMP K	L1	LO	L2	DELTA L	T(LO)	H(LO)	H(EFF)
1500	2.7340	2.7760	2.8270	0.0930	3.90E-01	2.72E-05	3.58E-06
1923	2.7340	2.7750	2.8260	0.0920	3.88E-01	6.05E-05	7.94E-06
2000	2.7340	2.7750	2.8260	0.0920	3.88E-01	6.77E-05	8.88E-06
2273	2.7340	2.7750	2.8260	0.0920	3.88E-01	9.52E-05	1.25E-05
2373	2.7330	2.7750	2.8260	0.0930	3.88E-01	1.06E-04	1.39E-05
2500	2.7330	2.7750	2.8260	0.0930	3.88E-01	1.20E-04	1.58E-05
3000	2.7330	2.7750	2.8260	0.0930	3.88E-01	1.81E-04	2.37E-05
3500	2.7330	2.7740	2.8260	0.0930	3.89E-01	2.49E-04	3.24E-05
4000	2.7330	2.7740	2.8250	0.0920	3.89E-01	3.18E-04	4.14E-05
4500	2.7330	2.7740	2.8250	0.0920	3.89E-01	3.90E-04	5.09E-05
5000	2.7330	2.7740	2.8250	0.0920	3.89E-01	4.64E-04	6.05E-05
5500	2.7320	2.7740	2.8250	0.0930	3.89E-01	5.39E-04	7.04E-05
6000	2.7320	2.7740	2.8250	0.0930	3.89E-01	6.16E-04	8.04E-05
FLAT	2.7350	2.7770	2.8280	0.0930	3.91E-01	8.02E-01	1.06E-01
SUN	2.7320	2.7740	2.8250	0.0930	3.89E-01	2.74E-03	3.57E-04

TEMP K	B	C
1500	8.36E-05	2.17E-01
1923	8.39E-05	2.17E-01
2000	8.39E-05	2.17E-01
2273	8.38E-05	2.17E-01
2373	8.38E-05	2.17E-01
2500	8.38E-05	2.17E-01
3000	8.38E-05	2.17E-01
3500	8.45E-05	2.19E-01
4000	8.45E-05	2.19E-01
4500	8.44E-05	2.19E-01
5000	8.44E-05	2.19E-01
5500	8.43E-05	2.18E-01
6000	8.42E-05	2.18E-01
FLAT	8.32E-05	2.16E-01
SUN	8.43E-05	2.18E-01

Table B-20. CHANNEL GT7-20, CURVE NO. 20

T-LAMBDA(0)	5.120E-01	LAMBDA(A)	2.7930	W	3.860E-04
LAMBDA(0)	2.8750	LAMBDA(B)	2.8870	1/W	2.591E 03
LAMBDA(0)	2.8400	DELTA LAMBDA	0.0940	A(EFF)	1.980E-05
LAMBDA(S)	2.8000			B(EFF)	1.980E-05
				C(EFF)	5.130E-02

TEMP K	L1	LO	L2	DELTA L	T(LO)	H(LO)	H(EFF)
1500	2.7700	2.8170	2.8680	0.0980	2.99E-01	2.88E-05	3.98E-06
1923	2.7690	2.8160	2.8670	0.0980	3.01E-01	6.44E-05	8.76E-06
2000	2.7690	2.8160	2.8670	0.0980	3.01E-01	7.19E-05	9.78E-06
2273	2.7690	2.8160	2.8670	0.0980	3.01E-01	1.01E-04	1.37E-05
2373	2.7690	2.8160	2.8670	0.0980	3.01E-01	1.12E-04	1.53E-05
2500	2.7690	2.8160	2.8670	0.0980	3.01E-01	1.27E-04	1.73E-05
3000	2.7680	2.8150	2.8670	0.0990	3.02E-01	1.93E-04	2.59E-05
3500	2.7680	2.8150	2.8670	0.0990	3.02E-01	2.62E-04	3.53E-05
4000	2.7680	2.8150	2.8670	0.0990	3.02E-01	3.35E-04	4.52E-05
4500	2.7670	2.8150	2.8670	0.1000	3.02E-01	4.10E-04	5.54E-05
5000	2.7670	2.8150	2.8670	0.1000	3.02E-01	4.87E-04	6.59E-05
5500	2.7670	2.8140	2.8660	0.0990	3.04E-01	5.75E-04	7.66E-05
6000	2.7660	2.8140	2.8660	0.1000	3.04E-01	6.56E-04	8.75E-05
FLAT	2.7710	2.8180	2.8690	0.0980	2.98E-01	8.58E-01	1.20E-01
SUN	2.7660	2.8140	2.8660	0.1000	3.04E-01	2.91E-03	3.88E-04

TEMP K	B	C
1500	1.43E-04	3.72E-01
1923	1.45E-04	3.77E-01
2000	1.45E-04	3.77E-01
2273	1.45E-04	3.77E-01
2373	1.45E-04	3.76E-01
2500	1.45E-04	3.76E-01
3000	1.47E-04	3.82E-01
3500	1.47E-04	3.81E-01
4000	1.47E-04	3.81E-01
4500	1.47E-04	3.80E-01
5000	1.46E-04	3.79E-01
5500	1.49E-04	3.85E-01
6000	1.48E-04	3.85E-01
FLAT	1.41E-04	3.66E-01
SUN	1.48E-04	3.85E-01

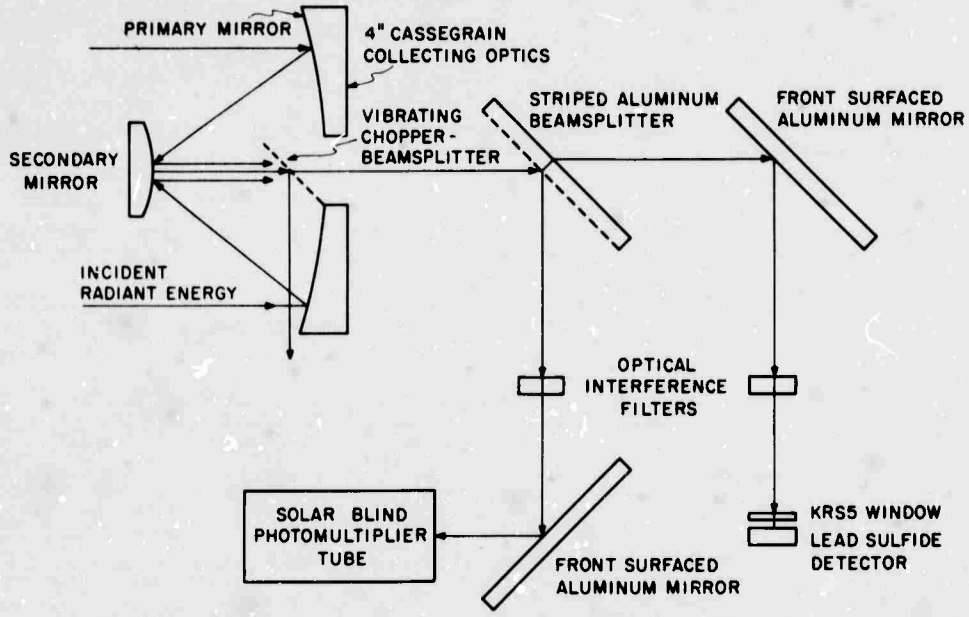

Figure B-1. Radiometer Schematic Diagram

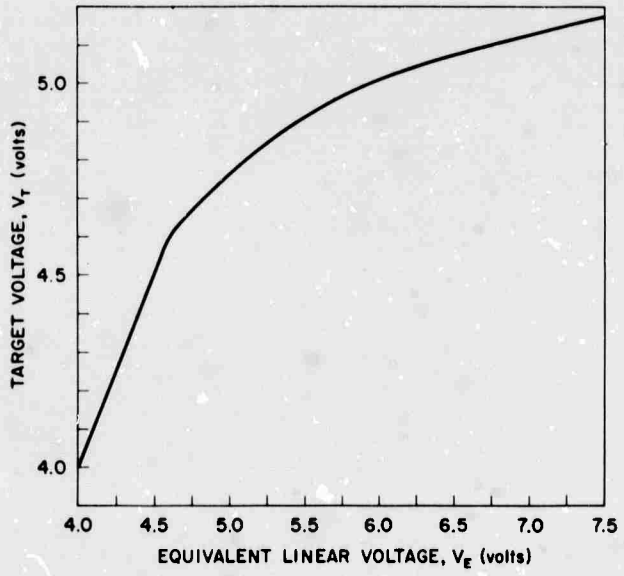

Figure B-2. V_T vs. V_E

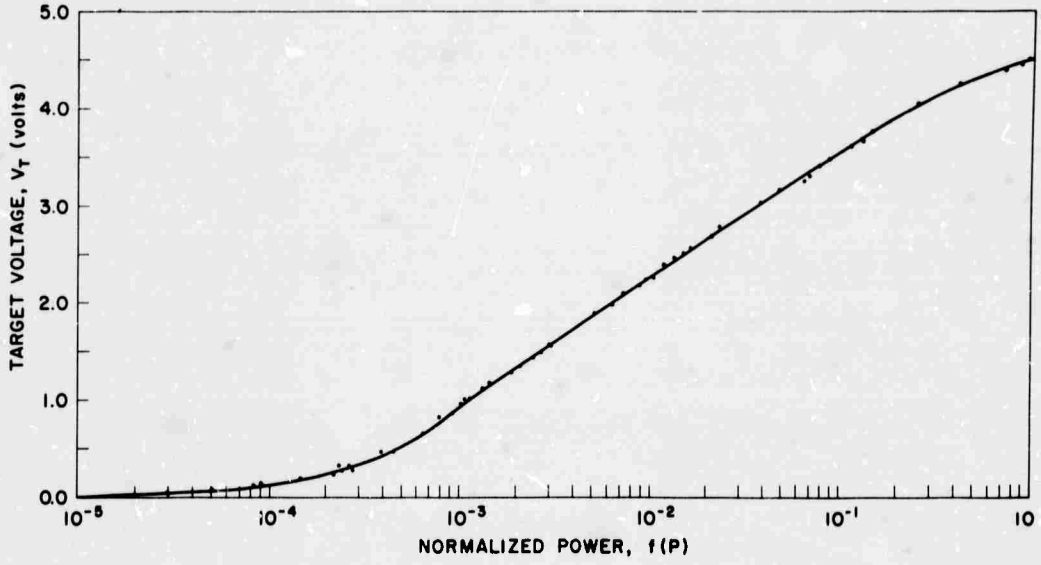

Figure B-3. V_T vs. f(P)

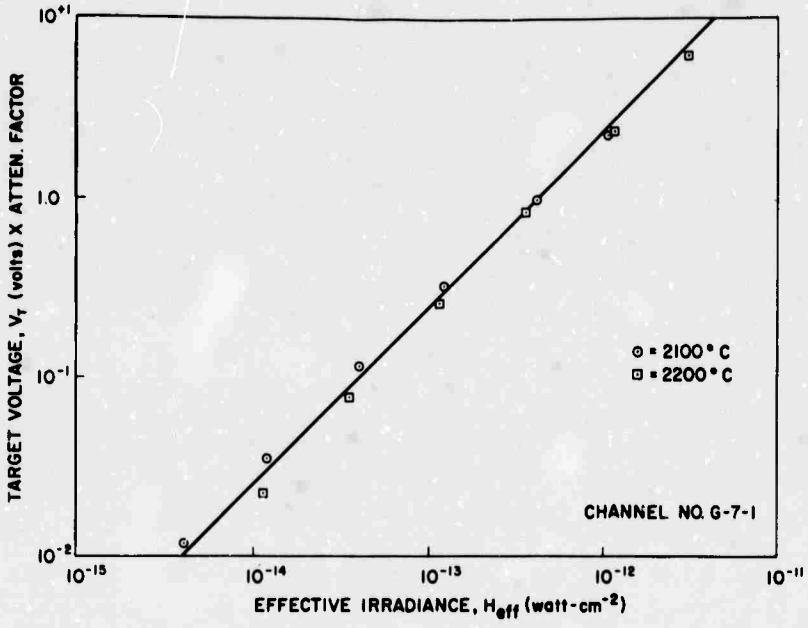

Figure B-4. $V_T G$ vs. Effective Irradiance

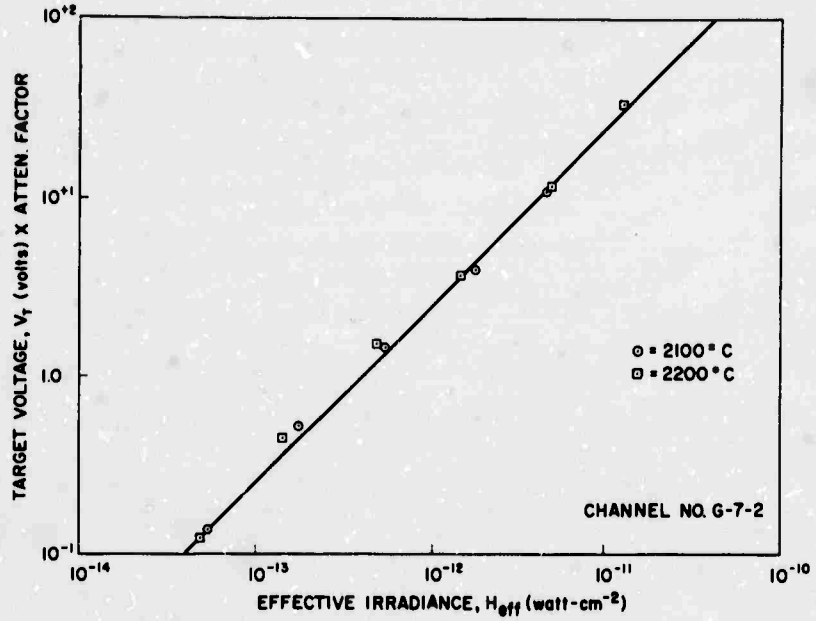

Figure B-5. $V_T G$ vs. Effective Irradiance

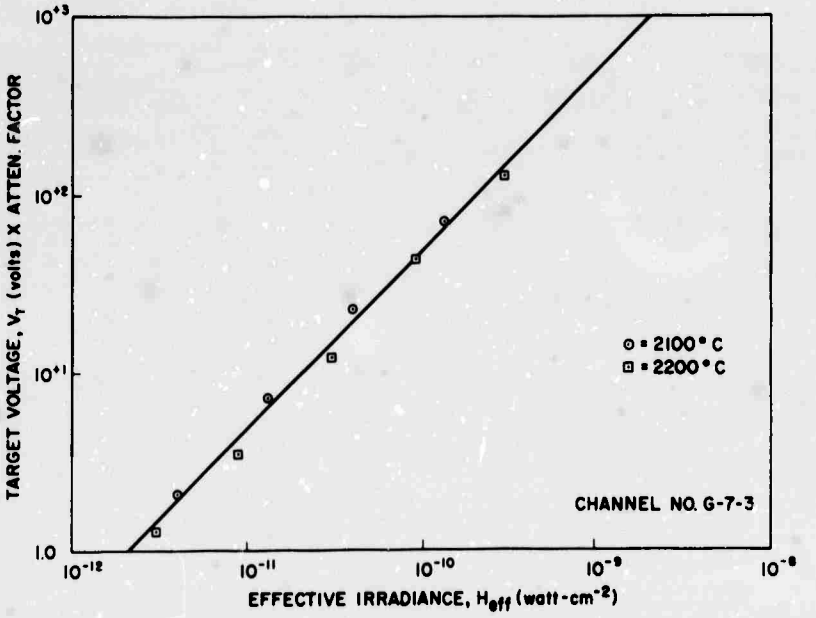

Figure B-6. $V_T G$ vs. Effective Irradiance

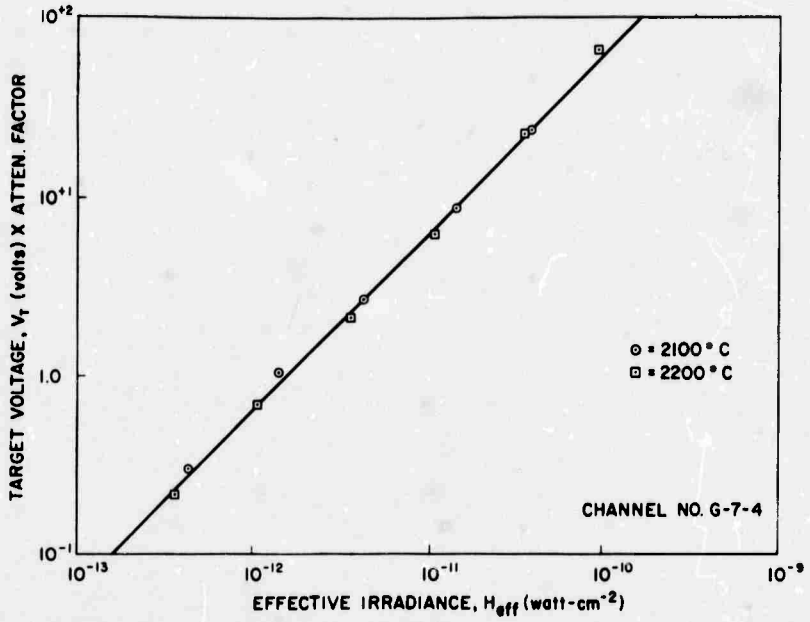

Figure B-7. $V_T G$ vs. Effective Irradiance

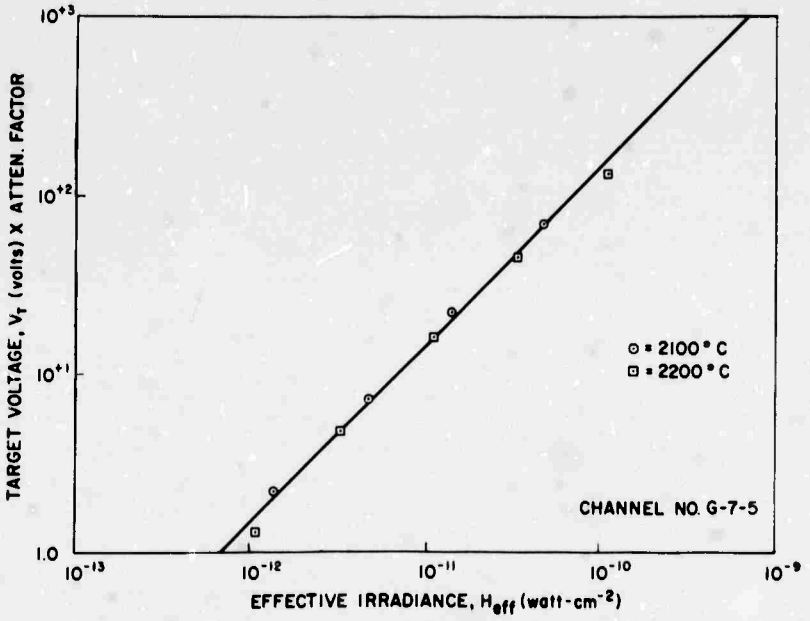

Figure B-8. $V_T G$ vs. Effective Irradiance

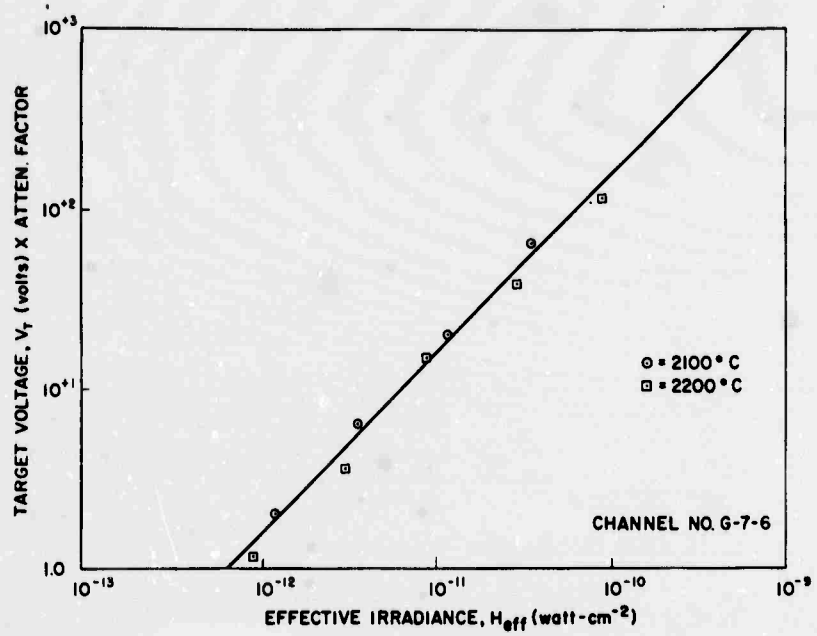

Figure B-9. $V_T G$ vs. Effective Irradiance

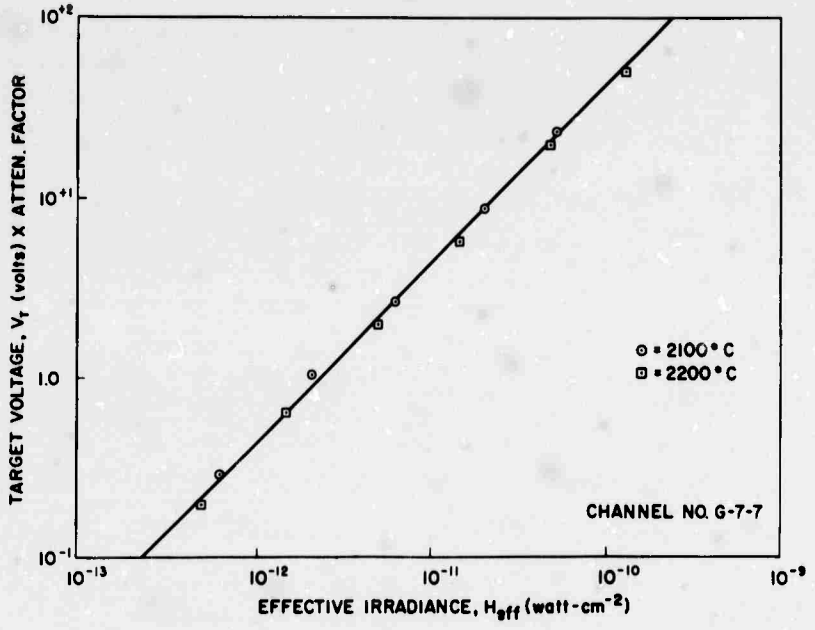

Figure B-10. $V_T G$ vs. Effective Irradiance

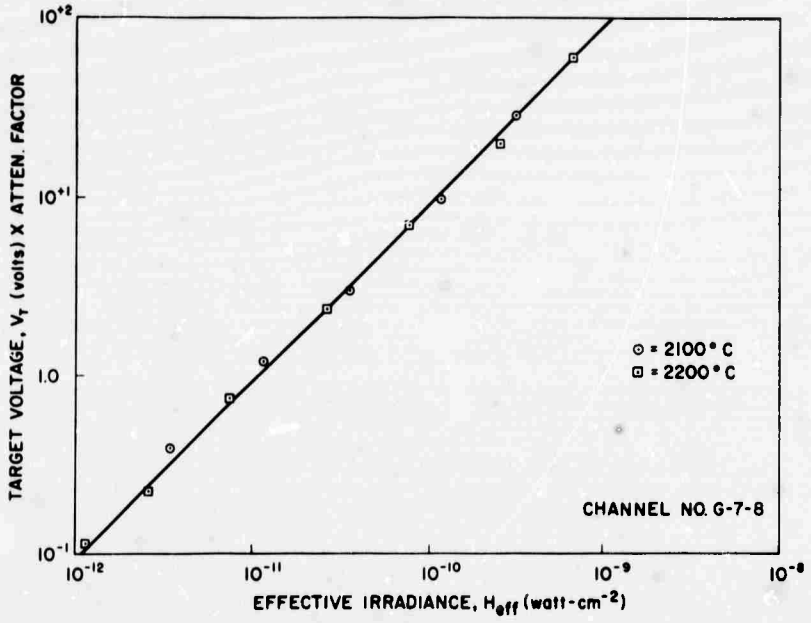

Figure B-11. $V_T G$ vs. Effective Irradiance

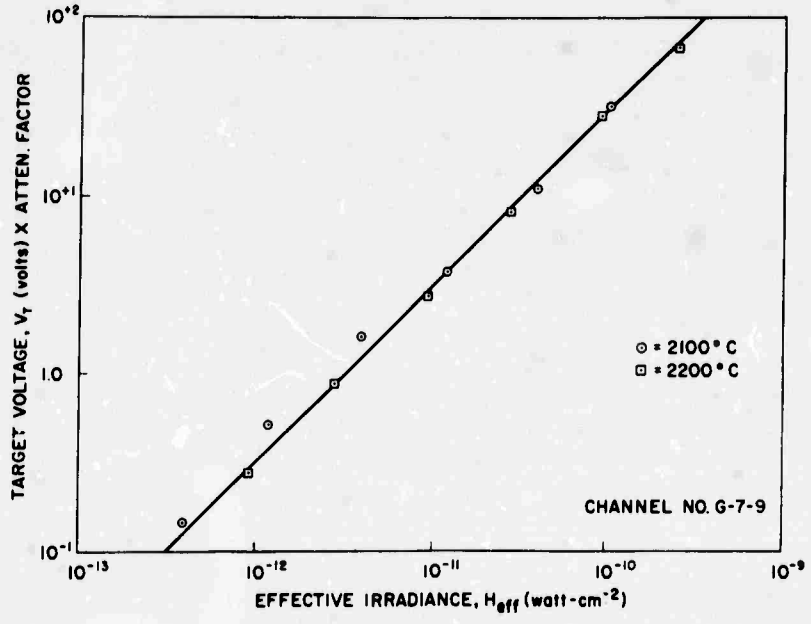

Figure B-12. $V_T G$ vs. Effective Irradiance

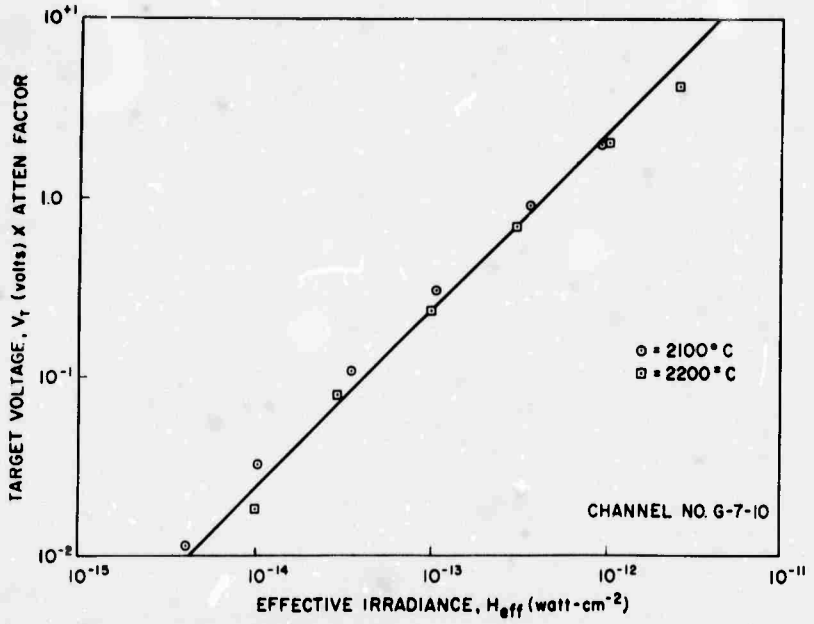

Figure B-13. $V_T G$ vs. Effective Irradiance

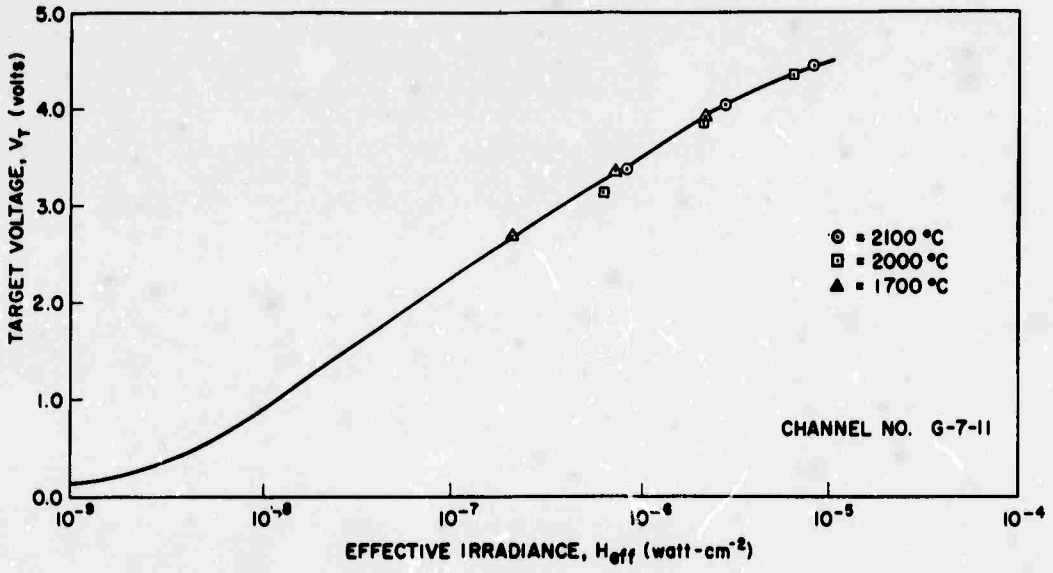

Figure B-14. V_T vs. Effective Irradiance

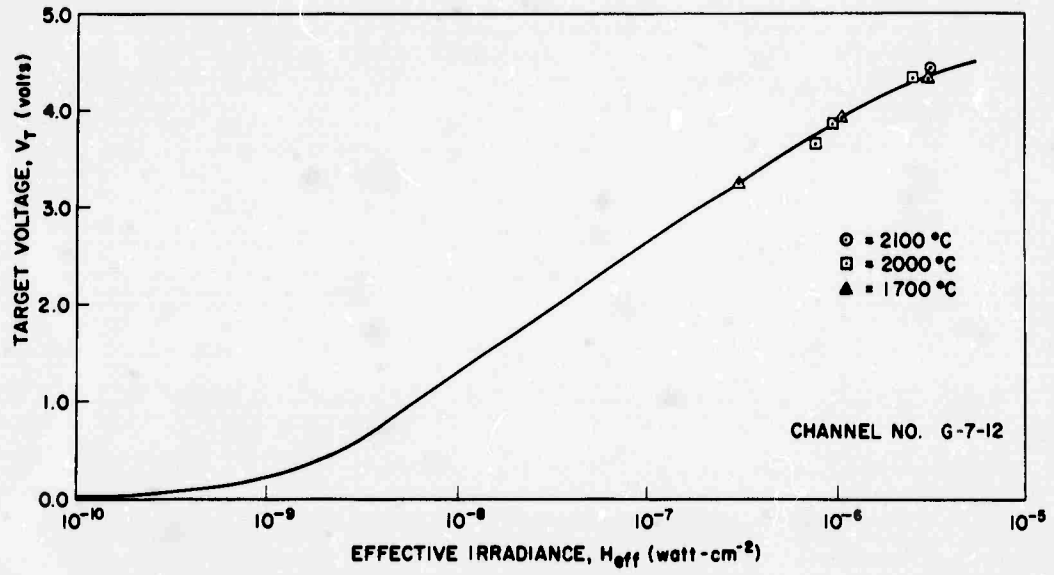

B-15. V_T vs. Effective Irradiance

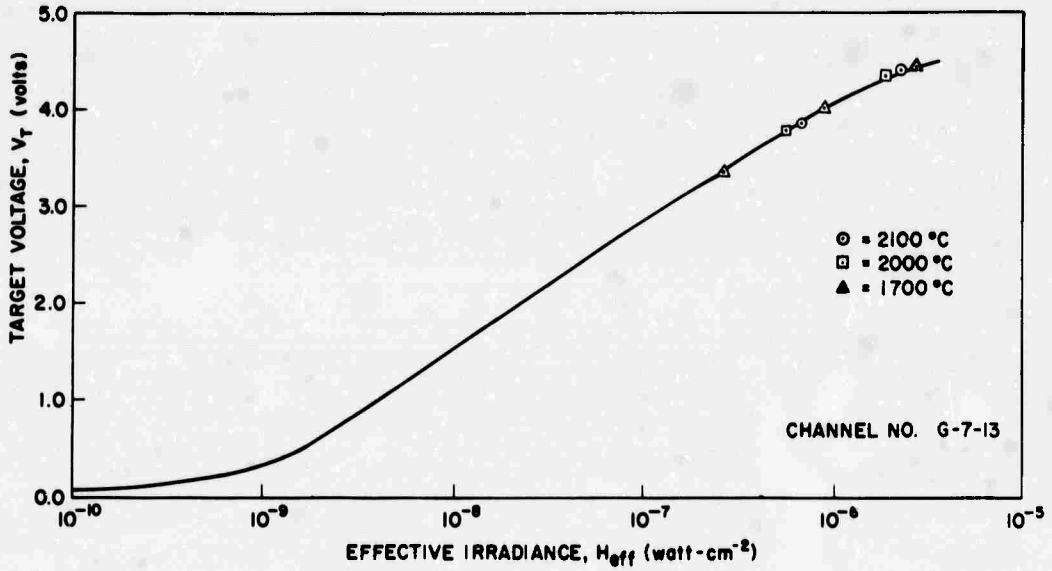

B-16. V_T vs. Effective Irradiance

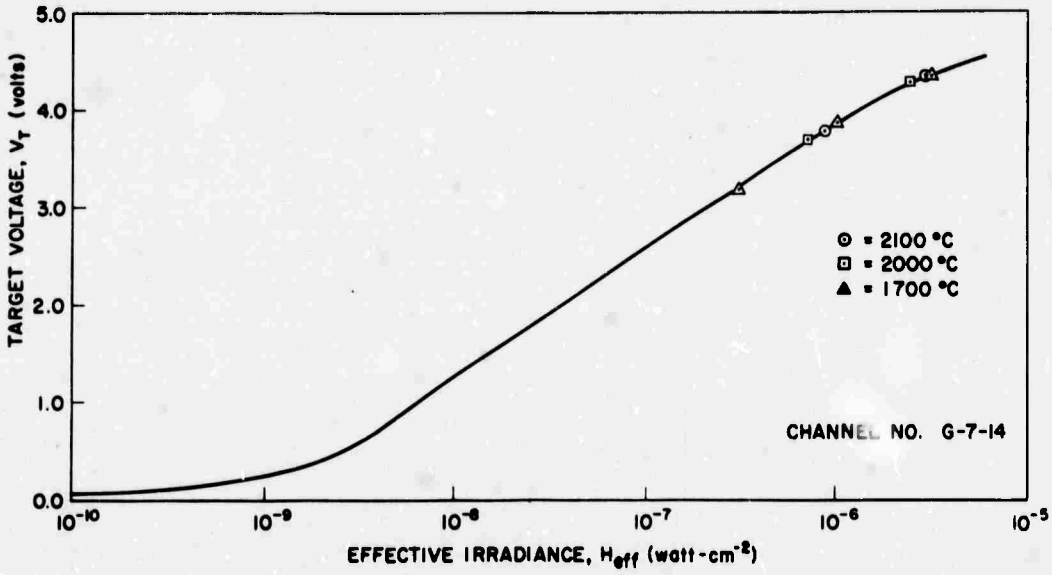

Figure B-17. V_T vs. Effective Irradiance

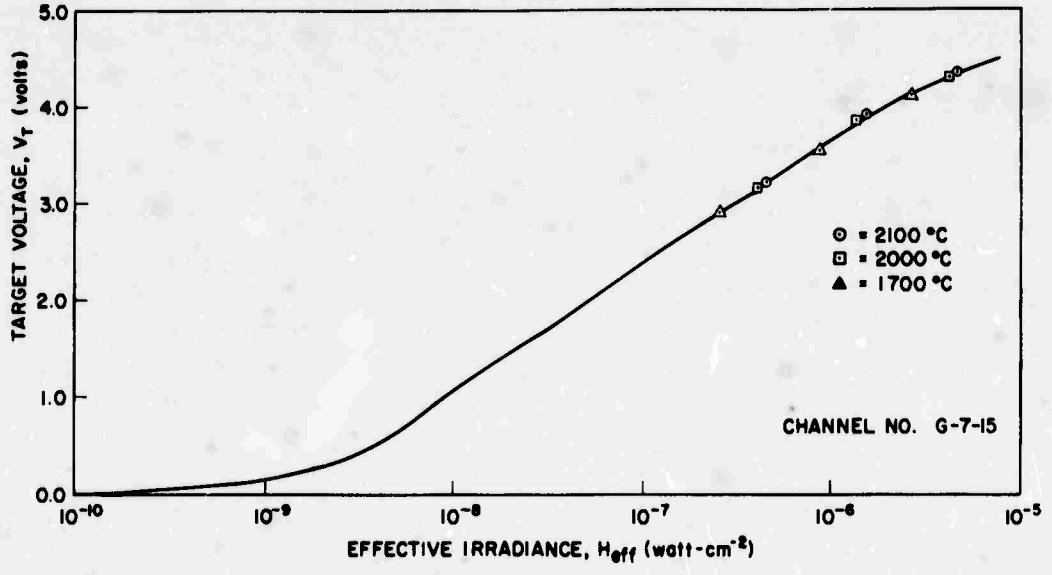

Figure B-18. V_T vs. Effective Irradiance

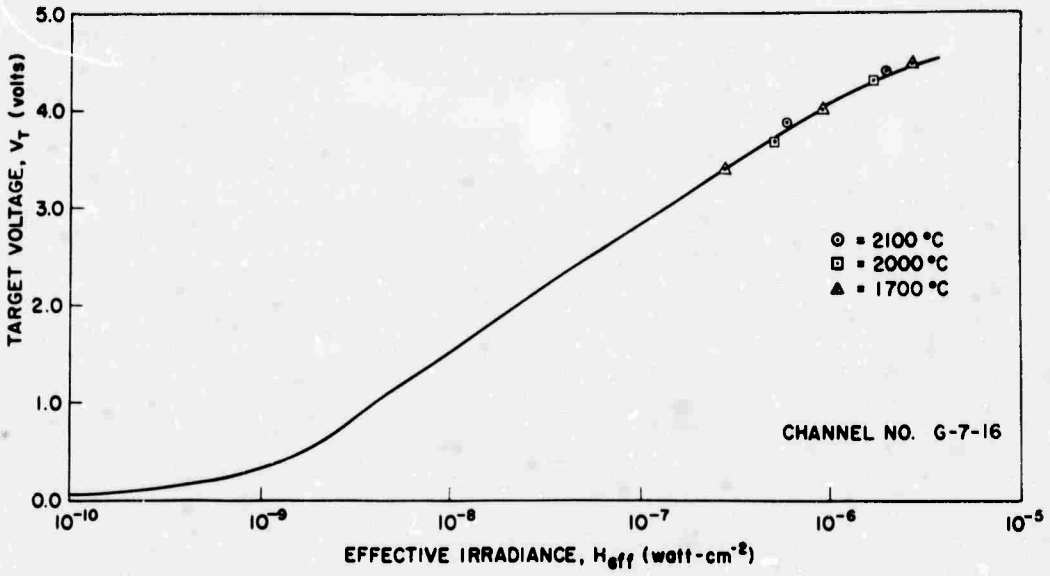

Figure B-19. V_T vs. Effective Irradiance

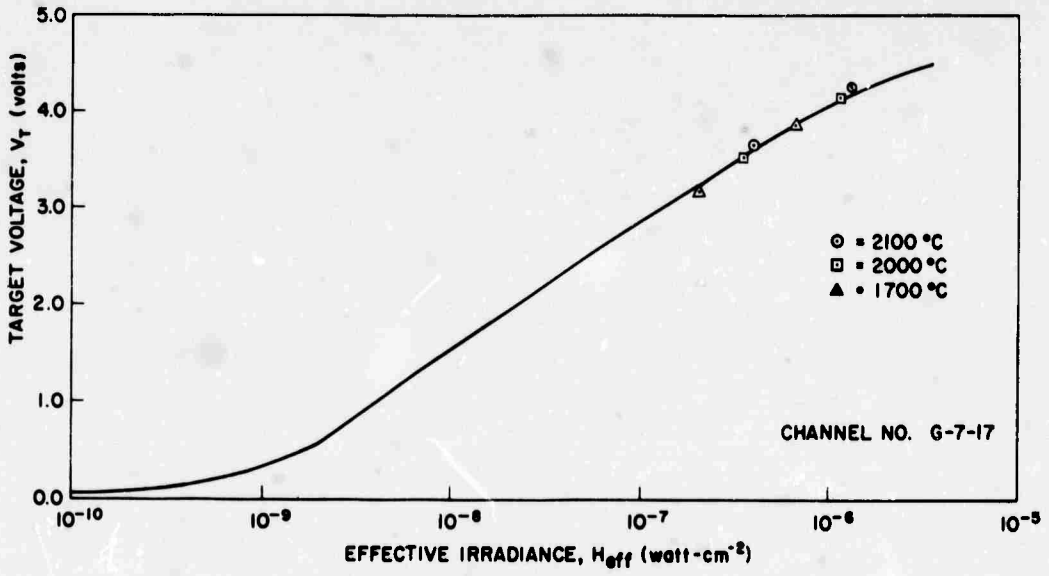

Figure B-20. V_T vs. Effective Irradiance

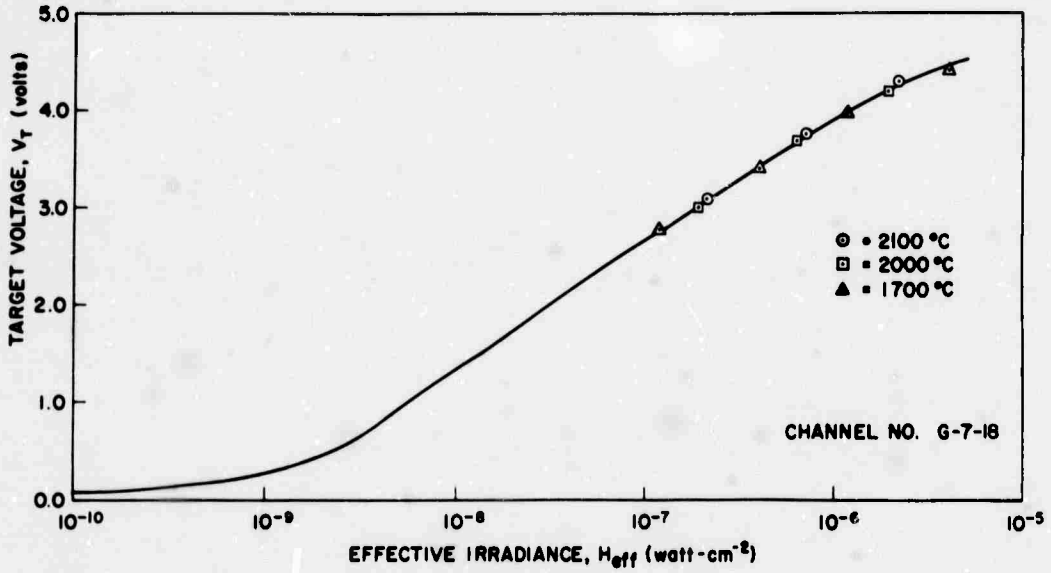

Figure B-21. V_T vs. Effective Irradiance

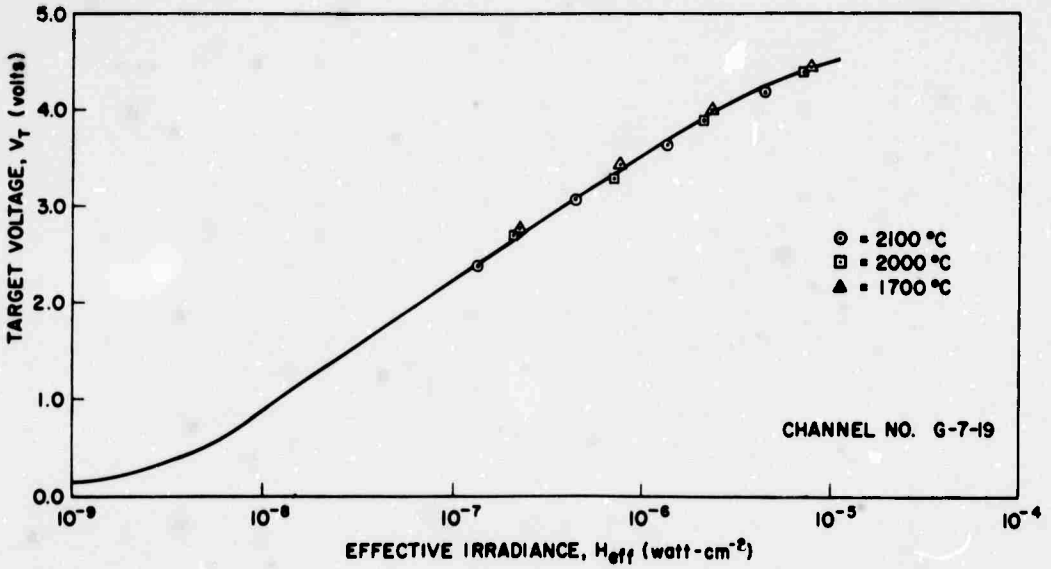

Figure B-22. V_T vs. Effective Irradiance

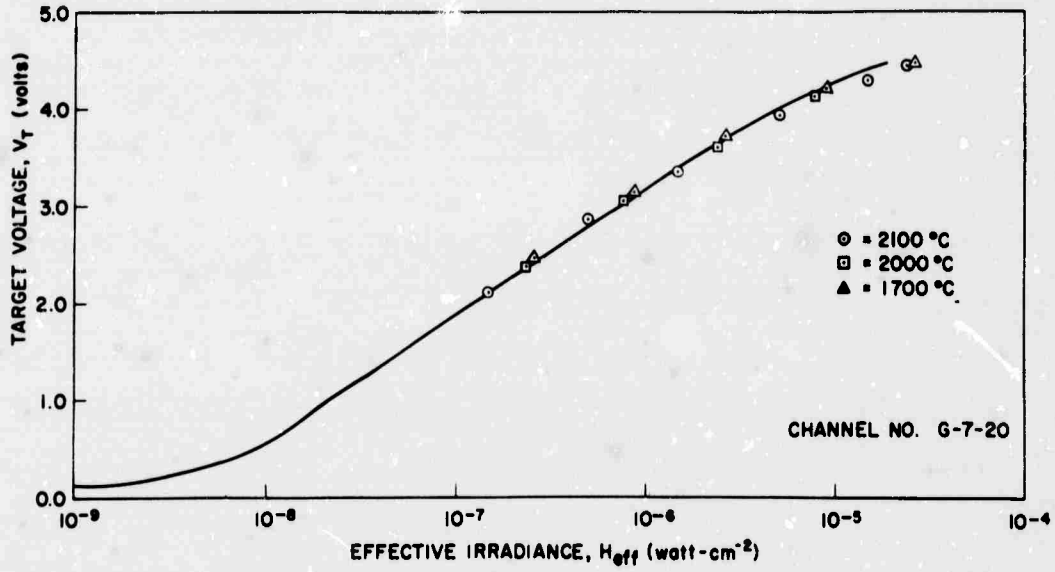

Figure B-23. V_T vs. Effective Irradiance

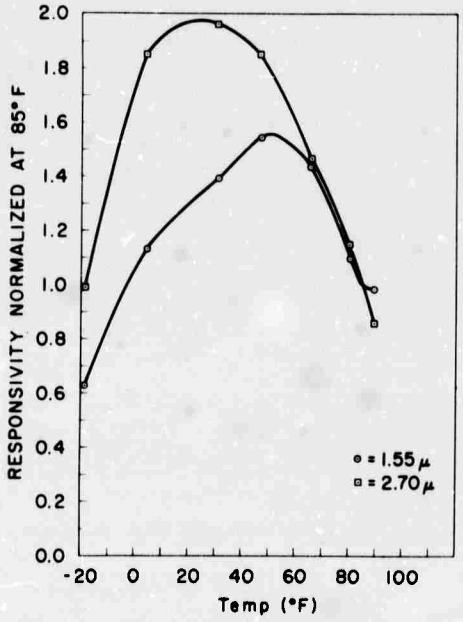

Figure B-24. Radiometer Responsivity vs. Temperature

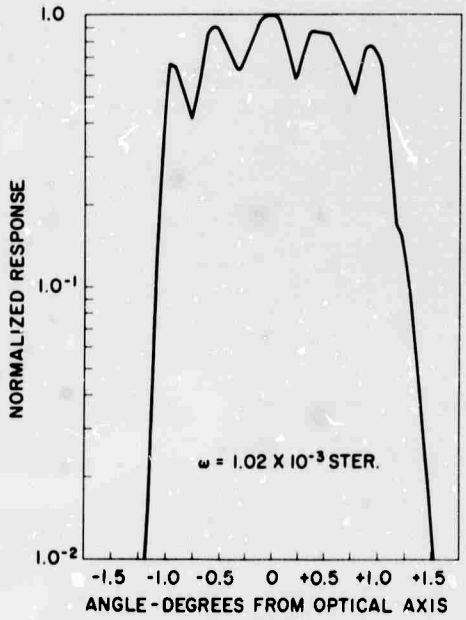

Figure B-25. Radiometer Field of View — Photomultiplier Section

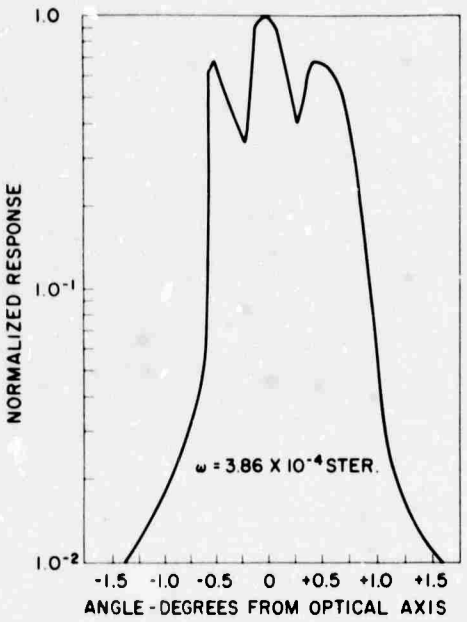

Figure B-26. Radiometer Field of View — PbS Section

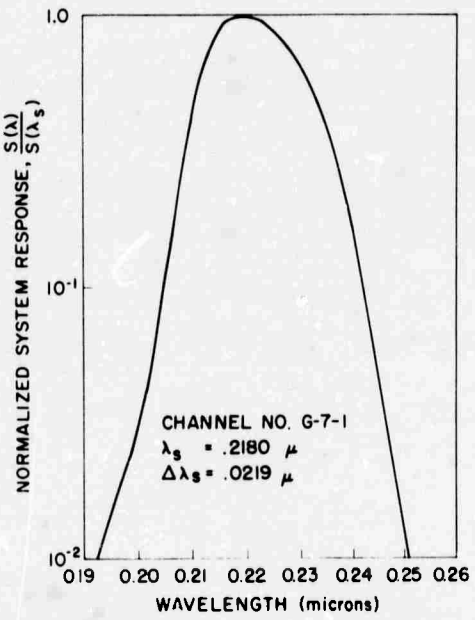

Figure B-27. System Response Curves — Photomultiplier Channels

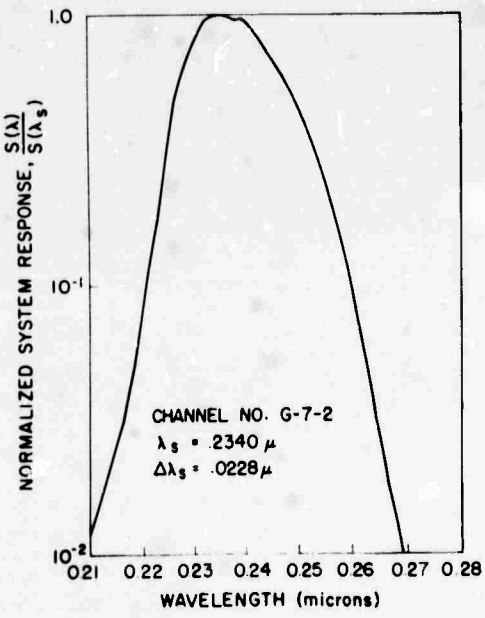

Figure B-28. System Response Curves — Photomultiplier Channels

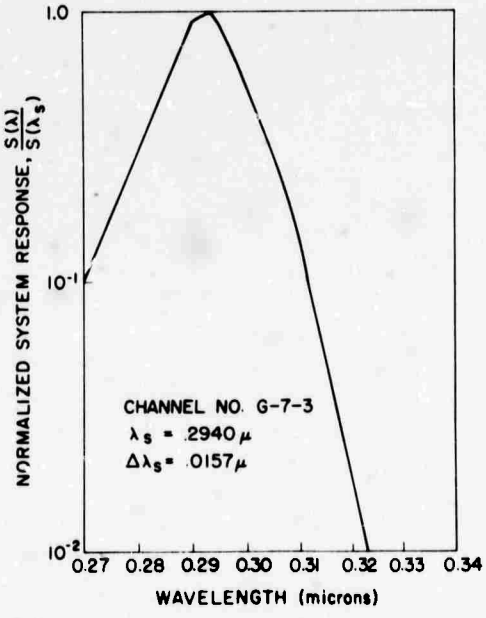

Figure B-29. System Response Curves — Photomultiplier Channels

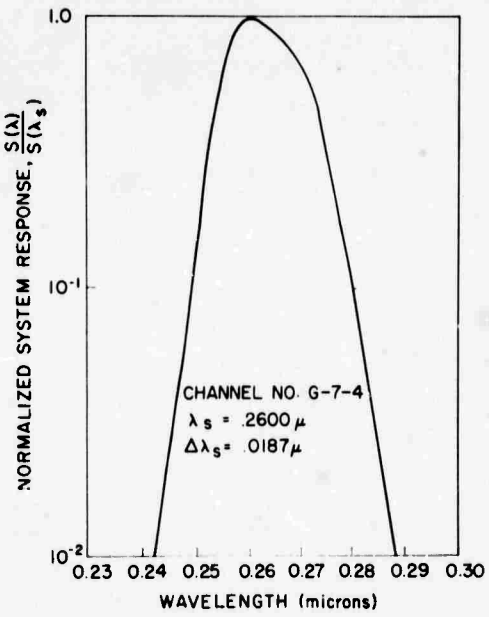

Figure B-30. System Response Curves – Photomultiplier Channels

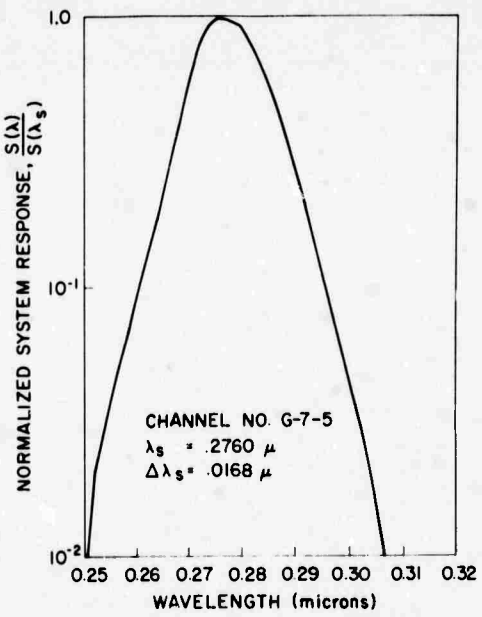

Figure B-31. System Response Curves – Photomultiplier Channels

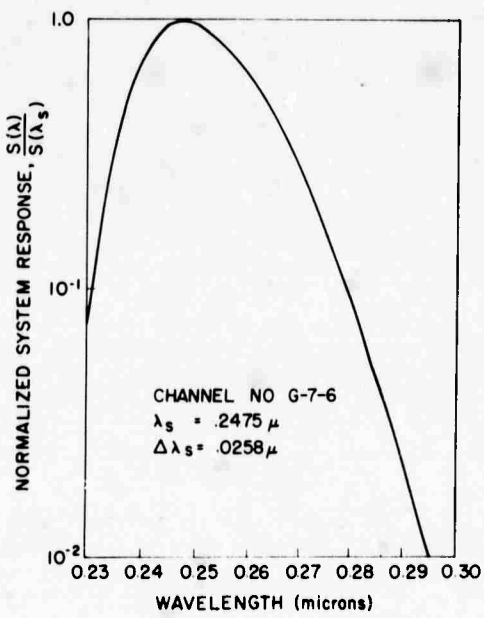

Figure B-32. System Response Curves – Photomultiplier Channels

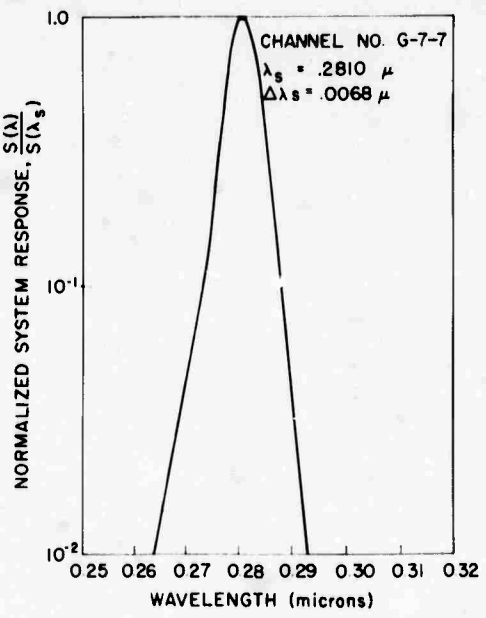

Figure B-33. System Response Curves – Photomultiplier Channels

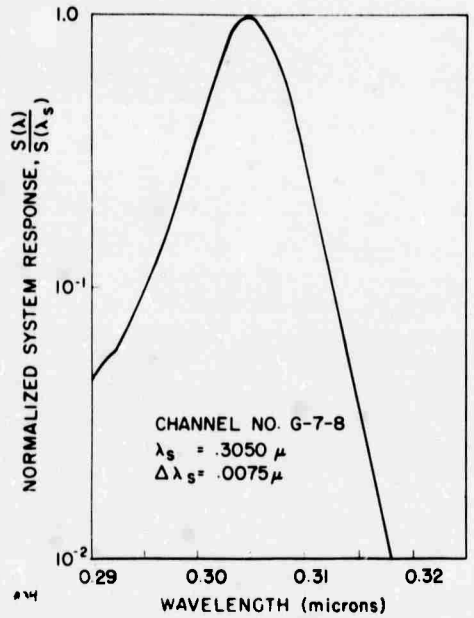

Figure B-34. System Response Curves – Photomultiplier Channels

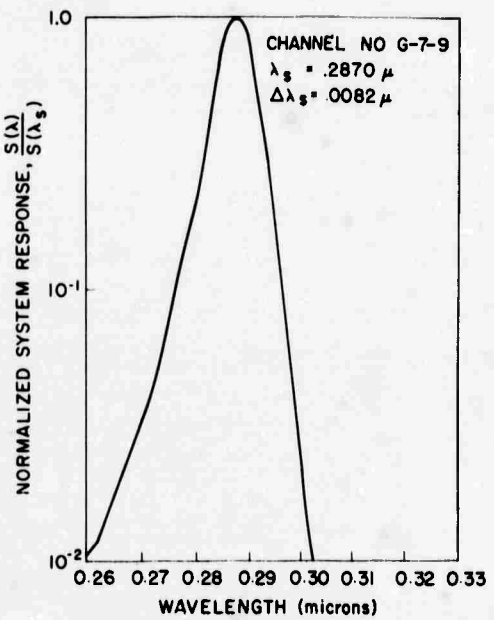

Figure B-35. System Response Curves – Photomultiplier Channels

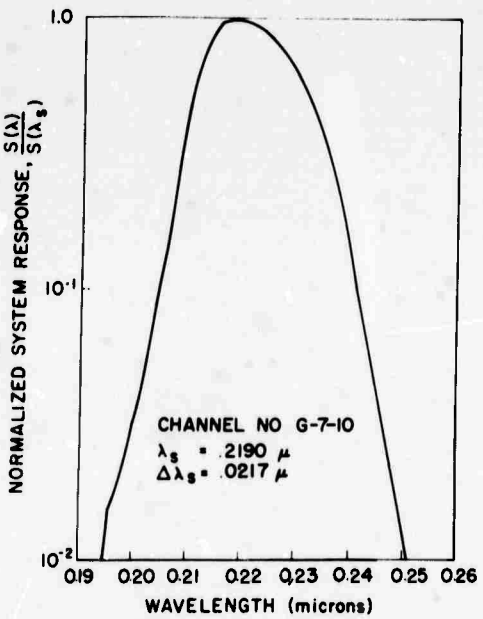

Figure B-36. System Response Curves – Photomultiplier Channels

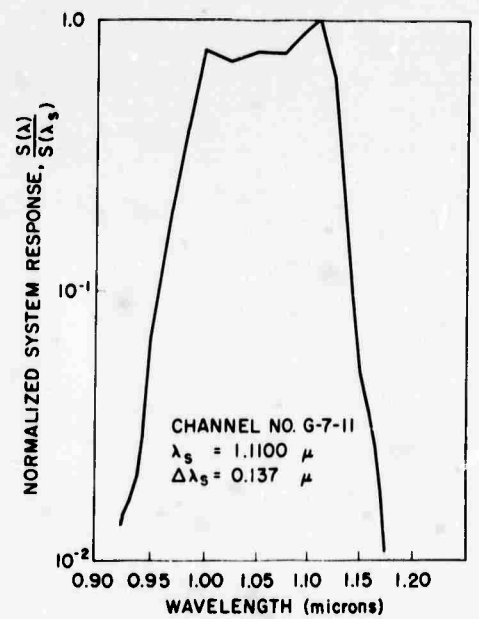

Figure B-37. System Response Curves – PbS Radiometer Channels

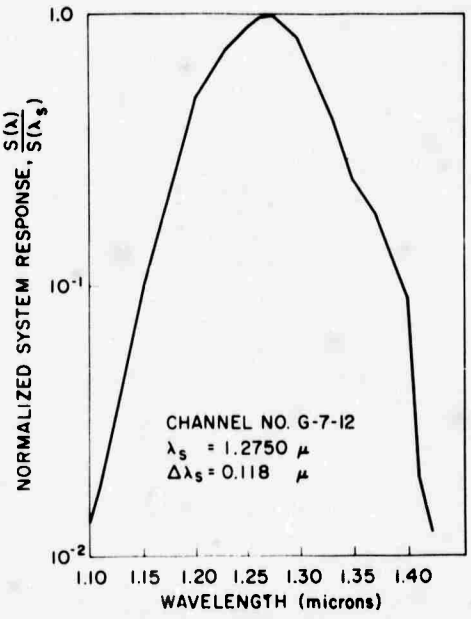

Figure B-38. System Response Curves — PbS Radiometer Channels

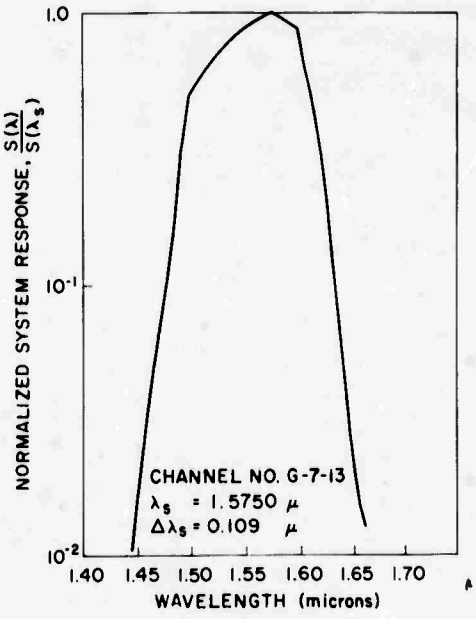

Figure B-39. System Response Curves — PbS Radiometer Channels

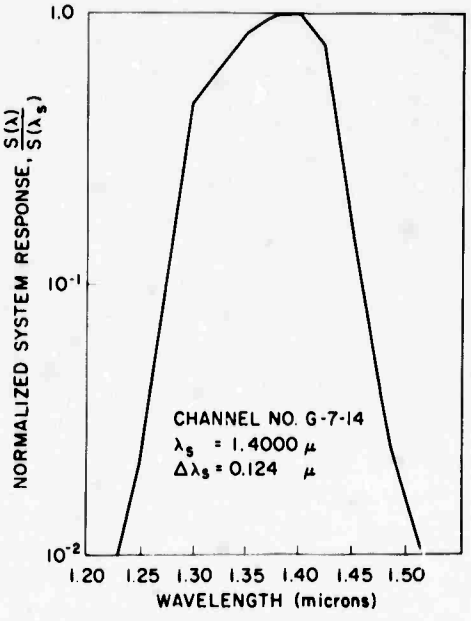

Figure B-40. System Response Curves — PbS Radiometer Channels

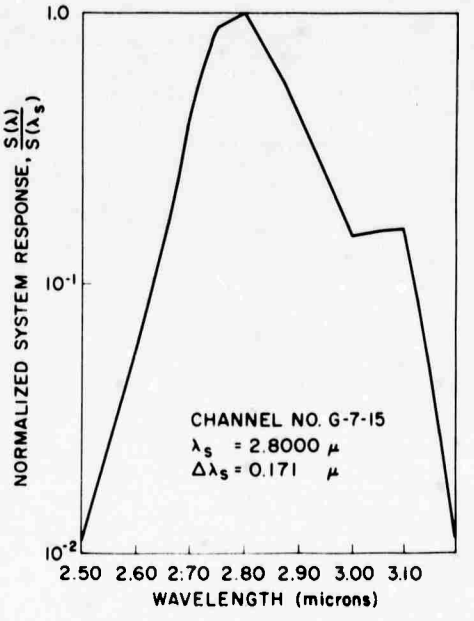

Figure B-41. System Response Curves — PbS Radiometer Channels

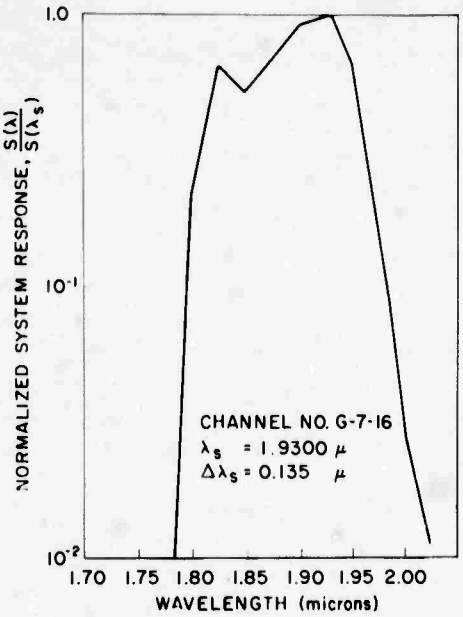

Figure B-42. System Response Curves — PbS Radiometer Channels

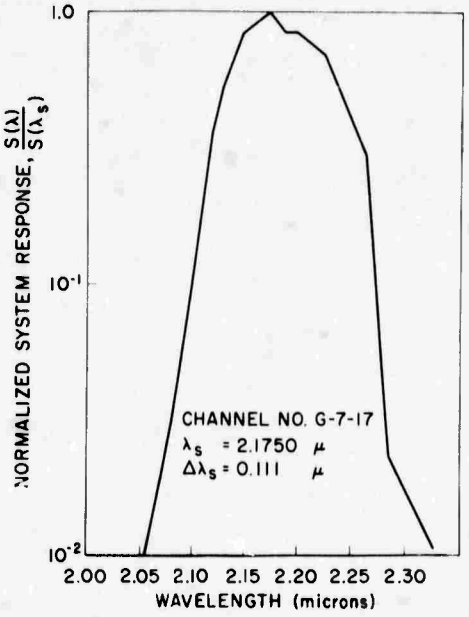

Figure B-43. System Response Curves — PbS Radiometer Channels

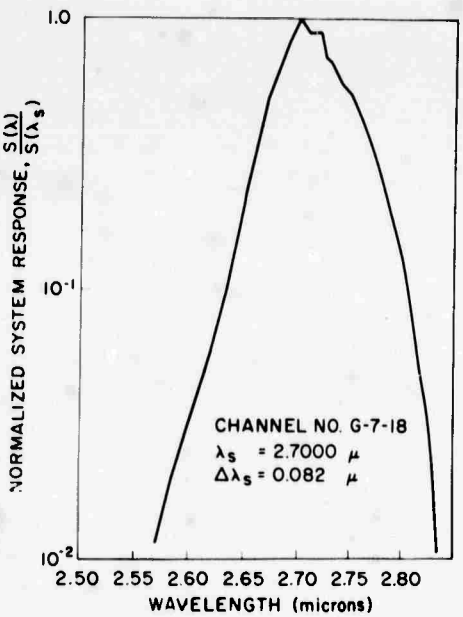

Figure B-44. System Response Curves — PbS Radiometer Channels

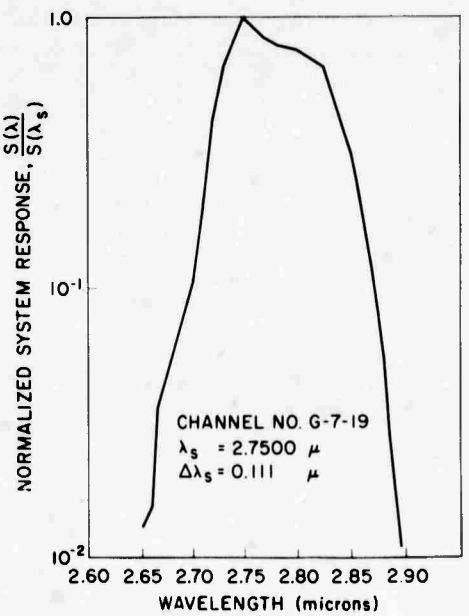

Figure B-45. System Response Curves — PbS Radiometer Channels

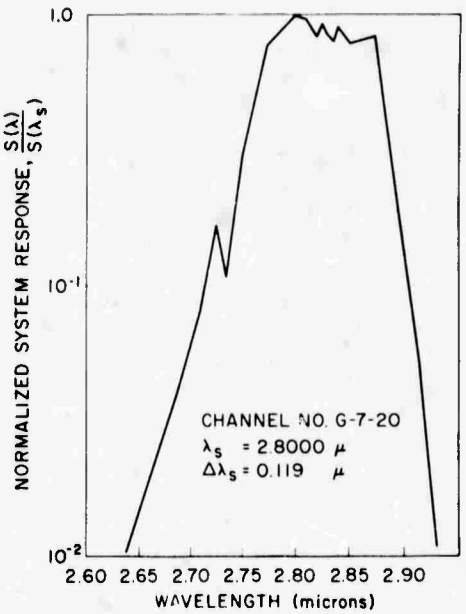

Figure B-46. System Response Curves — PbS Radiometer Channels

BLANK PAGE

Appendix C

Gemini 7 Interferometer Calibrations

I. DESCRIPTION OF I-14 INTERFEROMETER

The physical installation of the I-14 interferometer on the spacecraft required an optical axis that was at 90° with respect to the long dimension of the electronics package. This was accomplished by placing a plane front-surfaced aluminum mirror at a 45° angle behind the barium fluoride lens (Figure C-1). The mirror reflected the incident radiation through a barium fluoride transfer lens to the interferometer beamsplitter compensator which reflected one-half of the incident radiation to a fixed mirror and transmitted the other half to a moving mirror. The two signals were then recombined to produce an interference pattern on a dichroic beamsplitter that reflected 0.5 to 3.5 μ radiation to the PbS detector and transmitted the longer wavelength radiation to the bolometer. The outputs of both detectors were fed to linear amplifiers equipped with four output gain settings which were switched automatically to accommodate the recording equipment. The gain settings were set so that the interferograms would not saturate the recorder and would assure that the noise recorded on the tape would be the output noise of the interferometer. The latter objective was accomplished for the on-board FM recordings, but some of the real time telemetered data appeared on tapes that were extremely noisy.

Five year's experience with interferometers of the type flown on Gemini-7 has shown that an absolute calibration performed in the laboratory seldom yields accurate results when applied to data obtained in the field; this applies to both wavelength and amplitude. It has been found, however, that the relative spectral

response is stable; thus, the relative spectral radiance distribution of an unknown target based on laboratory calibration can be determined accurately provided that the frequency of the tonal component corresponding to a given wavenumber is measured in the field.

The ν/f factor used in converting sonic frequency (f) to wave-number (ν) has been observed to drift as much as 7 percent in 6 hours. This is a slow monotonic drift that seems to correlate to some degree with temperature. The problem is recognized by Block Associates, and they usually provide a low-level oscillator that was designed to monitor the gain of the system and to assure that the frequency corresponding to a given wavenumber will be known for the environment in which the measurements are made. The low-level oscillator has not been found particularly useful for either function since it does not monitor the optical components of the system. However, an oscillator tone was incorporated into the Gemini-7 interferometer as an aid in locating the source of the trouble if a malfunction occurred.

We seldom use an interferometer without a boresighted radiometer equipped with a narrow interference filter; although we calibrate the interferometer absolutely and reduce the data on the basis of this calibration, the usual procedure in the final analysis is to adjust the absolute level of interferometer spectrum to agree with the radiometer data.

Since we had no confidence that the instruments mounted on the Gemini-7 spacecraft would in fact be boresighted during the flight, and since our usual procedure of checking the responsivity and ν/f factor on the spot with a known standard could not be accomplished, a calibration light filtered by a narrow interference filter was installed behind an aperture in the interferometer mirror. This light was turned on for a period of 5 seconds at 71-second intervals.

When the Gemini-7 ON BOARD recorded tape was checked, it was found that the voltage obtained with the calibration light agreed with the value obtained at the time of calibration to within 1 dB (13 percent). It was also found that the oscillator tone appeared at a frequency of 1745 Hz, as compared to the laboratory value of 1790 Hz, amounting to a reduction of 2.5 percent, while the frequency corresponding to the calibration light changed from 642 to 659 Hz, amounting to an increase of 2.7 percent.

Interferometer spectra of earth background radiation taken during the flight showed that the O_2, CO_2, and H_2O absorption bands appeared at the correct wavelengths if the ν/f determined from the calibration light were used. The calibration light was used both for determining the wavelength and the absolute level in the data reduction; our usual procedure of adjusting the interferometric spectra in absolute level to agree with the radiometric data near 2.2 μ was not followed because the two instruments were not boresighted.

2. THE DICHROIC FILTER PROBLEM

The dichroic filter used in the Gemini-7 interferometer was a long wavelength, pass interference filter deposited on a barium fluoride substrate. Long wavelength, pass interference filters of this type invariably have "bumby" transmittance characteristics in their pass region; this is also true of very wide band pass interference filters.

A rise in the transmittance of the Gemini-7 interferometer dichroic filter near 1.4 μ caused a dip in the spectrum reflected to the PbS detector. Scheduling conditions made it impossible to change the filter in time to meet the delivery date for installation on the spacecraft for initial system check-outs; however, permission was obtained to change the instrument in Florida a few days before the scheduled flight. Consequently, the dichroic was replaced by a striped mirror in a spare instrument that was calibrated and taken to Florida; this instrument lost sensitivity just after the substitution was made and a decision was made to go with the dichroic.

The dichroic filter problem is the familiar one in which the data are either over-corrected, producing a false rise in the reduced spectrum, or under-corrected, leaving a residual false dip in the reduced spectrum. It is a problem, since the signal can be reduced sufficiently to be affected by the noise and, at best, the assumption of a random phase addition of signal and noise, which is used in our data reduction procedure, yields accurate results only if the signal-to-noise radio is 3 or more.

3. INTERFEROMETER CALIBRATION DATA

A plot of voltage versus spectral irradiance for the Gemini-7 interferometer PbS section is given in Figure C-2 for a wavelength of 2.2 μ. The circled points were obtained with collimated radiation, using the collimator described in Appendix B. The positions of the four lines on the figure indicate the changes in sensitivity corresponding to the four automatic attenuator settings used in the interferometer.

The triangles given in Figure C-2 represent the values obtained by irradiating the interferometer with a 12 x 12 inch, 200^{o}C blackbody source and a 4 x 4 inch, 300^{o}C extended blackbody source. This calibration was performed to check the effective field of view of the interferometer when used against targets filling the field of view. The spread in the extended source calibration points is partially due to error in setting the temperature of the blackbody. A small error in source temperature resulted in a much larger error in radiance at 2.2 μ for the temperatures used in the extended source calibration. In addition it was found that the

sources are not very uniform over their surfaces and that the emissivity varies with position; consequently the collimated irradiance calibration was used in the data reduction.

A plot of interferometer inverse irradiance responsivity versus wavelength based on the laboratory calibration is given in Figure C-3. The curve applies to a temperature of 82°F that was measured by the thermistor bead installed near the detector at the time of calibration. The dip in the responsivity indicated by the rise in inverse responsivity in Figure C-3 is due to the dichroic filter that was discussed earlier. The curve in the cut-off region near 2.7 μ is possibly too high by 25 percent due to water vapor in the optical path during calibration.

4. RESPONSIVITY VERSUS TEMPERATURE

We have never found as strong a dependence of responsivity on temperature in Block Associates' PbS interferometers as we have generally found in PbS radiometers, and the Gemini-7 instrument was no exception (Figure C-4). This response curve was made at a wavelength of 2.2 μ and is representative of the entire instrument bandwidth except for the 2.7 μ cut-off region where variation with temperature is more pronounced.

5. INTERFEROMETER FIELD OF VIEW

The field of view curve for the interferometer given in Figure C-5 was measured by irradiating the instrument with collimated radiation and rotating it while the collimator remained fixed; the target subtended an angle of approximately 0.005 radian.

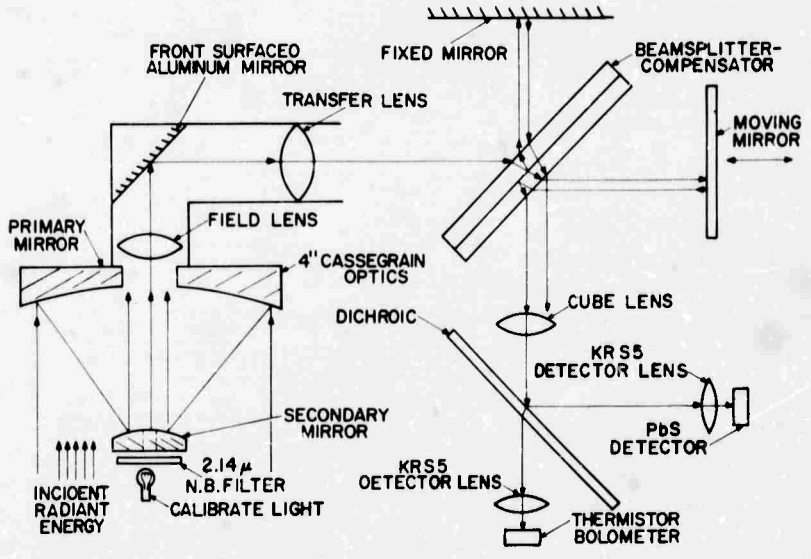

Figure C-1. Interferometer Schematic Diagram

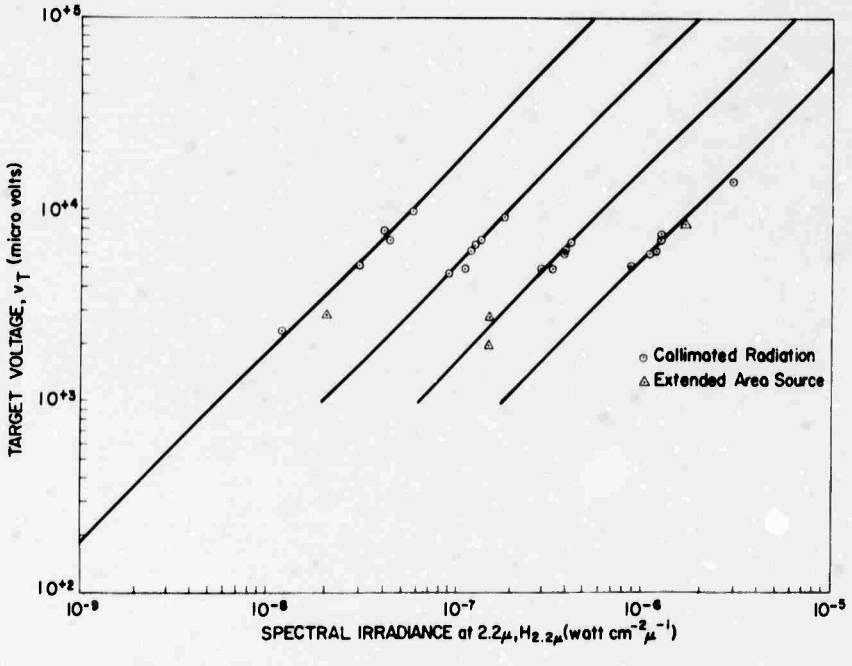

Figure C-2. Interferometer Output vs. Spectral Irradiance at 2.2 μ

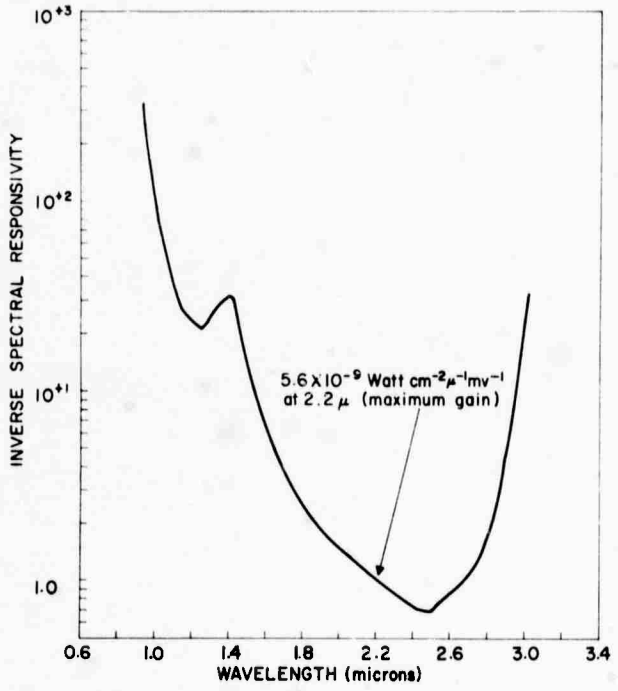

Figure C-3. Interferometer Inverse Spectral Irradiance Responsivity vs. Wavelength — PbS Section

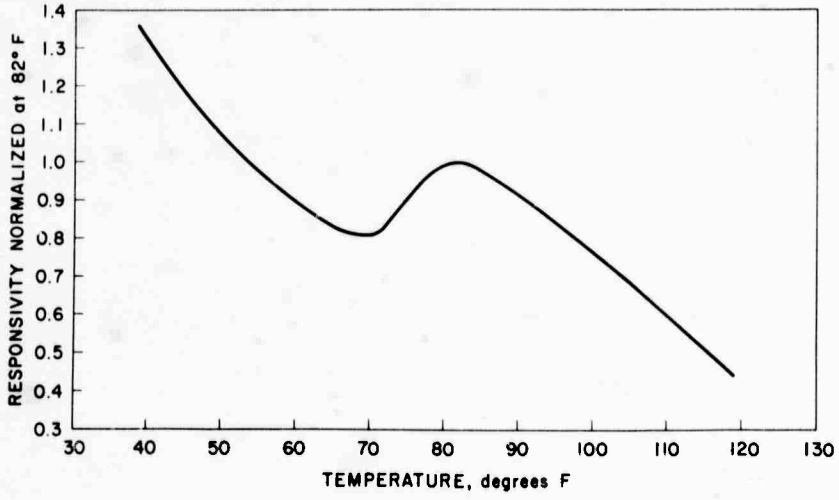

Figure C-4. Interferometer Responsivity vs. Temperature — PbS Section

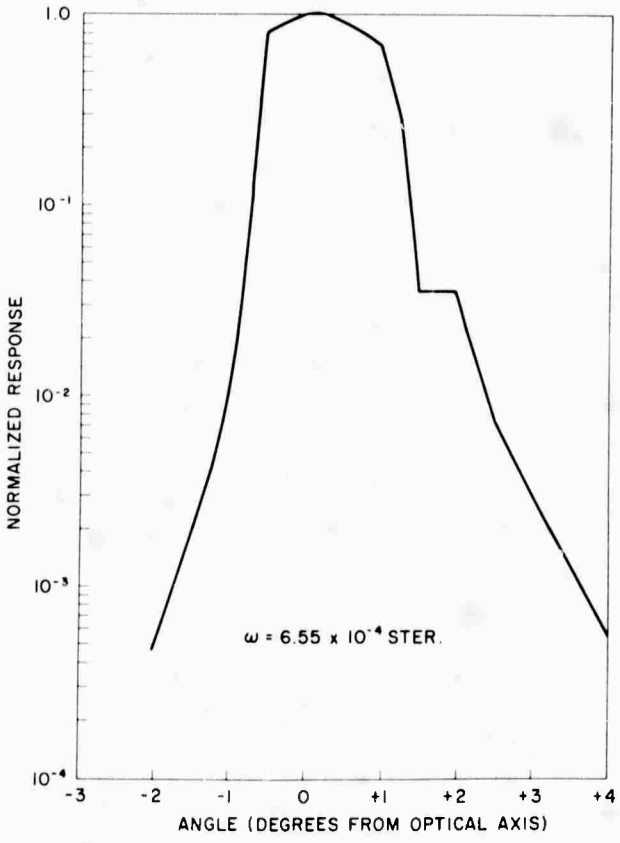

Figure C-5. Interferometer Field of View — PbS Section

DOCUMENT CONTROL DATA - R&D

(Security classification of title, body of abstract and indexing annotation must be entered when the overall report is classified)

1. ORIGINATING ACTIVITY *(Corporate author)*
Air Force Cambridge Research Laboratories (CRO)
L. G. Hanscom Field
Bedford, Massachusetts 01730

2a. REPORT SECURITY CLASSIFICATION
Unclassified

2b. GROUP

3. REPORT TITLE
GEMINI 7 LUNAR MEASUREMENTS

4. DESCRIPTIVE NOTES *(Type of report and inclusive dates)*
Scientific. Interim.

5. AUTHOR(S) *(First name, middle initial, last name)*
T. P. Condron
J. J. Lovett L. Marcotte
W. H. Barnes R. Nadile

6. REPORT DATE
September 1968

7a. TOTAL NO. OF PAGES
92

7b. NO. OF REFS
3

8a. CONTRACT OR GRANT NO. ARPA Order 363

b. PROJECT, TASK, WORK UNIT NOS. 8662

c. DOD ELEMENT 6250301R

d. DOD SUBELEMENT

9a. ORIGINATOR'S REPORT NUMBER(S)
AFCRL-68-0438

9b. OTHER REPORT NO(S) *(Any other numbers that may be assigned this report)*
ERP No. 291

10. DISTRIBUTION STATEMENT
1—Distribution of this report is unlimited. It may be released to the Clearinghouse, Department of Commerce, for sale to the general public.

11. SUPPLEMENTARY NOTES
Supported by SSD 631A and ARPA Order 363

12. SPONSORING MILITARY ACTIVITY
Air Force Cambridge Research Laboratories (CRO)
L. G. Hanscom Field
Bedford, Massachusetts 01730

13. ABSTRACT

Radiometric and interferometric measurements were made of the lunar surface during a penumbral eclipse from the Gemini 7 spacecraft. Data were obtained in the region from 0.25 to 2.6 microns. The bond albedo of the moon is computed for the spectral regions measured.

DD FORM 1 NOV 65 1473

14. KEY WOROS	LINK A		LINK B		LINK C	
	ROLE	WT	ROLE	WT	ROLE	WT
Gemini 7 Optical Measurements						
Moon Albedo Measurements						
Interferometer						